Development of Novel Polycrystalline Ceramics with Enhanced Magneto-Optical Performance

高機能磁気光学セラミックス多結晶体の創製

YAN LIN AUNG

Nagoya Institute of Technology

January 2021

Development of Novel Polycrystalline Ceramics with Enhanced Magneto-Optical Performance

高機能磁気光学セラミックス多結晶体の創製

YAN LIN AUNG

ヤン リン アウン

名古屋工業大学

2021 年 1 月

Development of Novel Polycrystalline Ceramics with Enhanced Magneto-Optical Performance

高機能磁気光学セラミックス多結晶体の創製

January 2021

YAN LIN AUNG

Contents

Chapter 1 Introduction

1-1. Background of this study -Magneto-optical ceramic isolator-

In recent years, laser processing machines have been widely used for precision processing, and the demand for lasers in the 1 μm band is more and more growing. For examples, fiber lasers are used for laser marking and fine processing of electronic parts, solid-state lasers with high output power are used for laser welding and cutting, and semiconductor lasers are used for optical communication via optical fiber network systems. The output power of various types of those lasers (e.g., solid-state, gas, semiconductor, fiber lasers, etc.) which are used as the light source is getting more and more powerful in these days, and laser equipment damage due to the returning wave of laser light becomes a critical problem [1]. Along with this progress, it is necessary to take measures to stabilize the light source and prevent the damage of laser equipment due to the reflected laser light back into the light sources. Similarly, in optical communication system using optical fiber cables, it is necessary to further stabilize the light source and prevent the damage of laser system especially for 5G network as the amount of transmitted information are increasing, and the reliability of transmitted information are improving gradually [2].

An optical isolator has a function of shutting down the return wave of incident laser light with a polarizer by the polarization technology applying a magnetic field [3]. A single crystal material is basically used for the key component of this Faraday device (i.e., Faraday rotating material). This is because it has been considered that single crystal has no scattering sources such as grain boundaries in polycrystalline ceramics and thus, its optical loss must be very small, and single crystals are capable of providing an accurate polarization angle. With an invention of laser ceramics by Dr. Ikesue in 1995 [4]; however, it is necessary to reconsider whether the established conventional theory and material science of the 19th and 20th centuries can be applied to the new materials born from the modern high-tech technology, and also important to examine the truthfulness of science and technology. Because it was firstly proved that optical amplification (laser) function was realized in polycrystalline ceramics, comparable to that of single crystal counterpart. Therefore, it is believed that similar innovation may occur in the field of magneto-optics as well.

1-2. Principle of optical isolation in a Faraday device

Thanks to the Faraday effect (magneto-optic effect) discovered by Michael Faraday in 1845 [5], it is well known that polarization of light can be rotated by an external magnetic field since light is a kind of electromagnetic wave. As shown in Figure 1.1, electromagnetic waves are composed of two different waves from electric and magnetic fields that oscillate perpendicular to each other and to the direction of propagation. Angle of rotation of polarized plane is directly proportional to the strength of the external magnetic field. Hence, the relationship between the angle of rotation of the polarization and the magnetic field in a transparent material can be expressed by the following equation,

$$\theta = VHL \qquad (1.1)$$

where θ is the Faraday rotation angle [rad], H is the magnetic flux density (T, [V s m^{-2}]), L is the length of optical path [m] where the light and magnetic field interact in the medium, and V is the Verdet constant [rad T^{-1} m^{-1}] of the material.

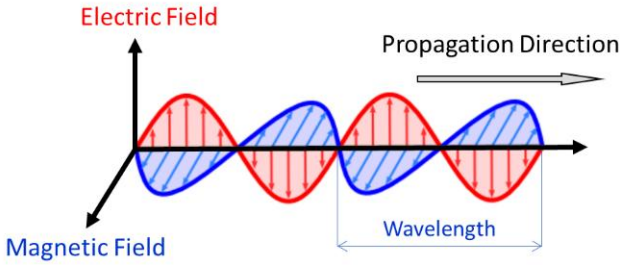

Figure 1.1 Light is an electromagnetic wave.

The most important optical element in an optical isolator is the Faraday rotator material. Specifically, for an optical isolator, the values in the above equation 1.1 are chosen to give a rotation angle of 45 degrees based on a calculation. Schematic diagram of an optical isolator is shown in Figure 1.2. A faraday rotator material and a magnet are sandwiched between two polarizing plates. Polarizer 1 is input polarizer and polarizer 2 is output analyzer. This Faraday device can pass the light in the forward direction, and it can block the light in the direction opposite to the propagation direction. Therefore, it is also named as optical diode. The principle is that when a laser light passes through a Faraday rotator which is placed under a magnetic field in the propagation direction, the passed light is rotated by 45 degrees in clockwise. Once the passed through laser light reaches the target, it certainly reflects back as a return wave. Similarly, the return light is also rotated by another 45 degrees in clockwise when it passes through the Faraday rotator as it is in the same magnetic field again, so that the return wave can be completely blocked by the polarizer plate 1 as illustrated in the figure.

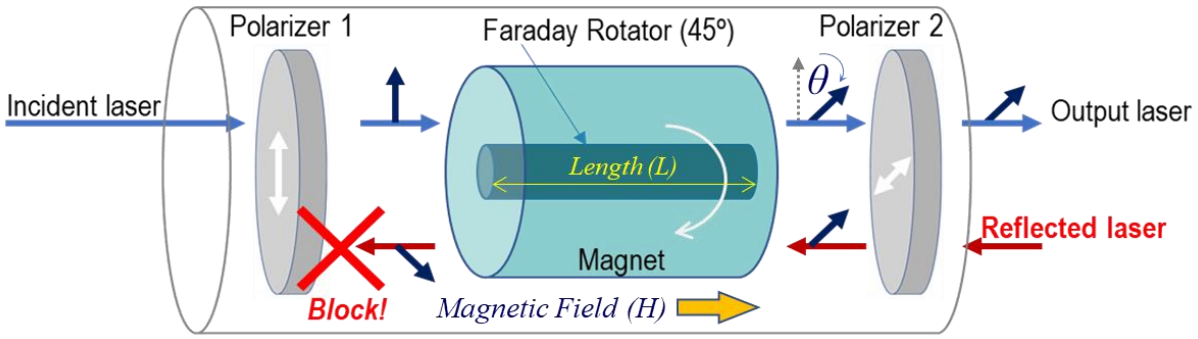

Figure 1.2 Principle of isolation of laser light in a Faraday optical isolator device.

Magnetic hysteresis images of paramagnetic and ferrimagnetic materials are illustrated in Figure 1.3. When an external magnetizing force is applied to a ferrimagnetic material such as YIG ($Y_3Fe_5O_{12}$), a saturated magnetic flux density is reached at a certain magnetizing force. Therefore, in the case of ferrimagnetic materials, the angle of rotation of polarization does not further increase once the saturated magnetic flux density is reached. Faraday rotation angle for a ferrimagnetic material is that the rotation angle per unit length of the medium obtained when the saturation magnetic flux density is reached. For example, the Faraday rotation angle of YIG material is 175 deg cm^{-1} for 1550 nm wavelength [6]. In contrast, when a magnetizing force is applied to a paramagnetic material, the change in the magnetic flux density inside the material is small, and the magnetic flux density increases in proportion to the applied magnetizing force. It does not form a hysteresis loop because there is no saturated magnetic flux density as seen in ferrimagnetic materials. The magnetic flux density only changes linearly. Thus, the angle of rotation in the unit length and unit magnetic flux in paramagnetic materials generated in the slope obtained by this straight line corresponds to the Verdet constant of the material. For example, the Verdet constant of TGG ($Tb_3Ga_5O_{12}$) material is 39 rad T^{-1} m^{-1} for 1064 nm wavelength [7]. In both cases, the applied magnetic field generates a magnetic flux inside the material, and hence a magneto-optical effect is also obtained with respect to the magnetic flux.

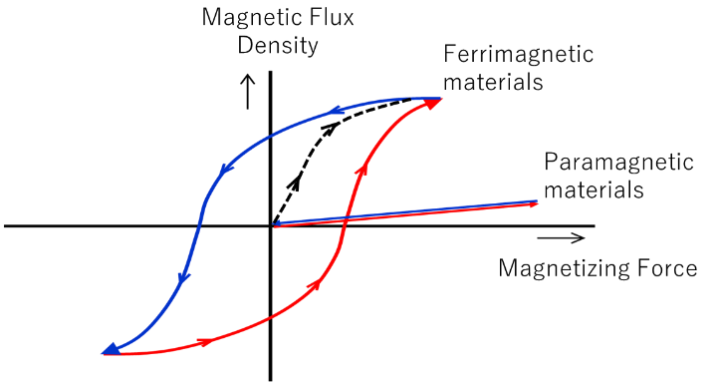

Figure 1.3 Image of hysteresis loop for ferrimagnetic and paramagnetic materials.

1-3. Technical issues of Faraday rotator materials

(a) Single crystals

Tb^{3+}-doped glass has been widely used as a Faraday rotator material but its thermal conductivity is low (0.8 $W.m^{-1}.K^{-1}$) and its Verdet constant is small. Therefore, paramagnetic TGG crystal has become a typical Faraday rotator material for high-power lasers. The Verdet constant of TGG single crystal (~39 rad T^{-1} m^{-1} at 1064 nm) is more than twice that of Tb-doped glass, and it has high thermal conductivity and is an excellent material. However, there is a problem that it is difficult to increase the aperture size required for a high-power laser, and it is not easy to control the homogeneity of optical quality such as extinction (isolation) characteristics. The extinction ratio correlates with the stress inside the crystal, and the smaller the internal stress, the higher the extinction ratio. This parameter that greatly affects the ability to block the return light in the optical isolator.

Schematic of garnet structure is shown in Figure 1.4. As an alternative to TGG materials, TAG ($Tb_3Al_5O_{12}$) crystals can be produced by replacing the Ga^{3+} sites with Al^{3+} ions. As shown in the transmission spectrum of

TAG in Figure 1.5, it also can be used for the wavelength regions of visible to near IR (shorter than 1.1 μm) as a Faraday rotator material; however, there are distinct problems in the crystal growth process of TAG.

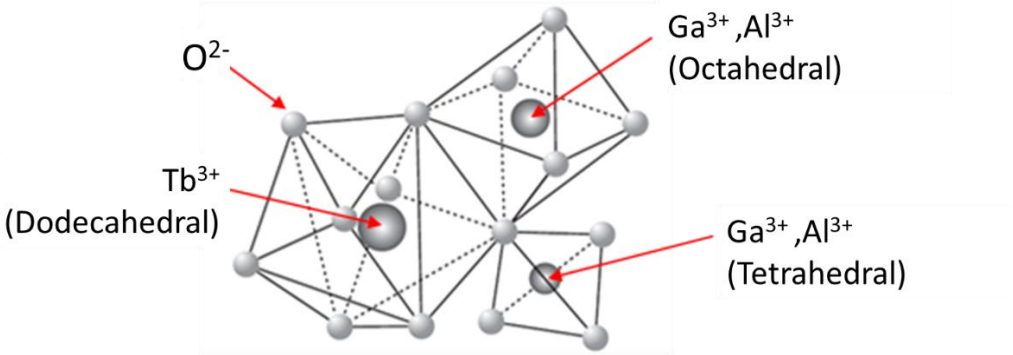

Figure 1.4 Schematic of garnet crystal structure.

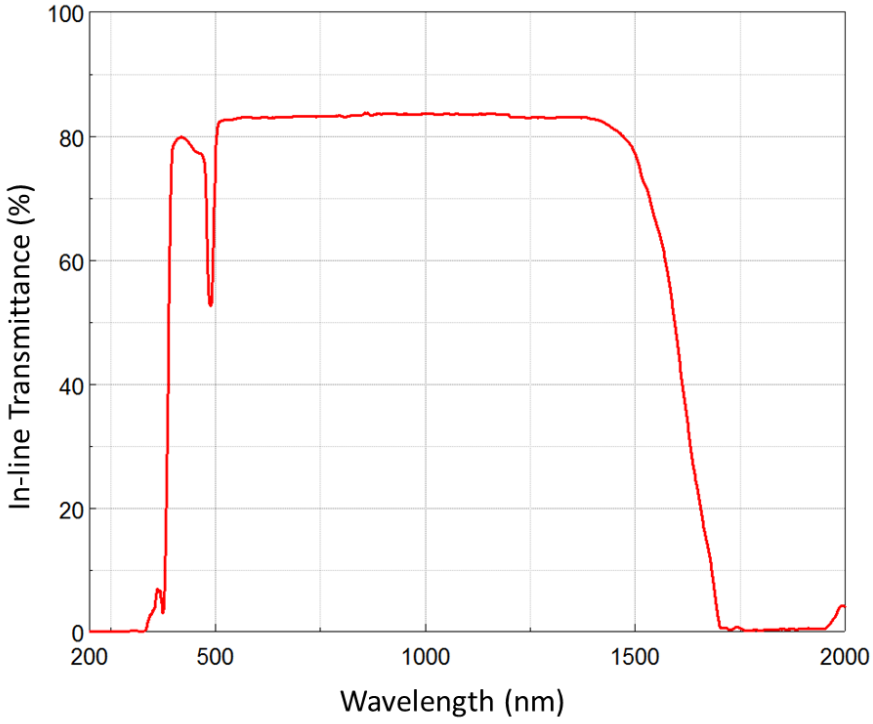

Figure 1.5 Transmission spectrum of TAG ceramics.

Generally, single crystals are grown by Czochralski (CZ) method. Since TAG is an incongruent melting compound as seen in the phase diagram of xTb_2O_3-$(1-x)Al_2O_3$ system indicated in Figure 1.6 (a) [8], it is more difficult to grow by using the CZ method. Laser assisted floating zone (FZ) method was reported to grow the TAG crystal as shown in Figure 1.6 (b) [8]. This fact limits the size of the crystal (diameter: up to a few mm, length: up to a few of tens mm) that can be grown.

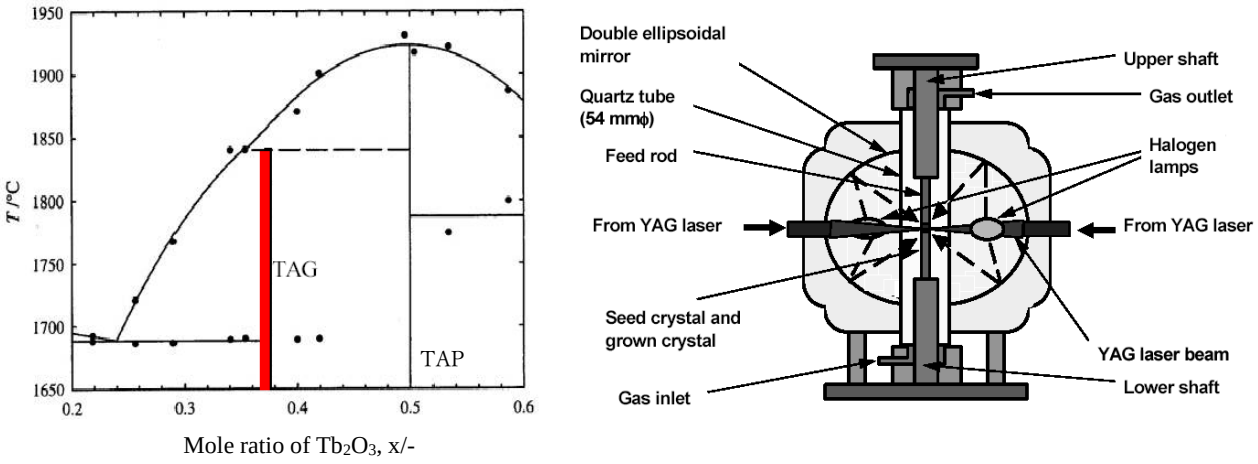

(a) (b)

Figure 1.6 (a) Phase diagram for xTb_2O_3-$(1-x)Al_2O_3$ system. (b) Schematic of floating zone method. [8]

In optical telecommunication, a 1.5 μm band semiconductor laser is usually used as a light source, and large-capacity of information is transmitted through optical fiber networks and finally delivered to for example personal PCs or smart phone terminals. Optical isolators are used as protection devices for semiconductor lasers in optical fiber systems. An iron-based magnetic garnet thin film single crystal (typically Bi-substituted iron garnet) has been mainly used as Faraday rotator. The ferrimagnetic material has a larger Faraday rotation characteristic than the paramagnetic material and has an optical polarization rotation function at a low magnetic field, but it can operate only at wavelengths longer than 1.2 μm because of the strong absorption of Fe^{3+} ions as shown in the transmission spectrum of YIG materials in Figure 1.7 [9].

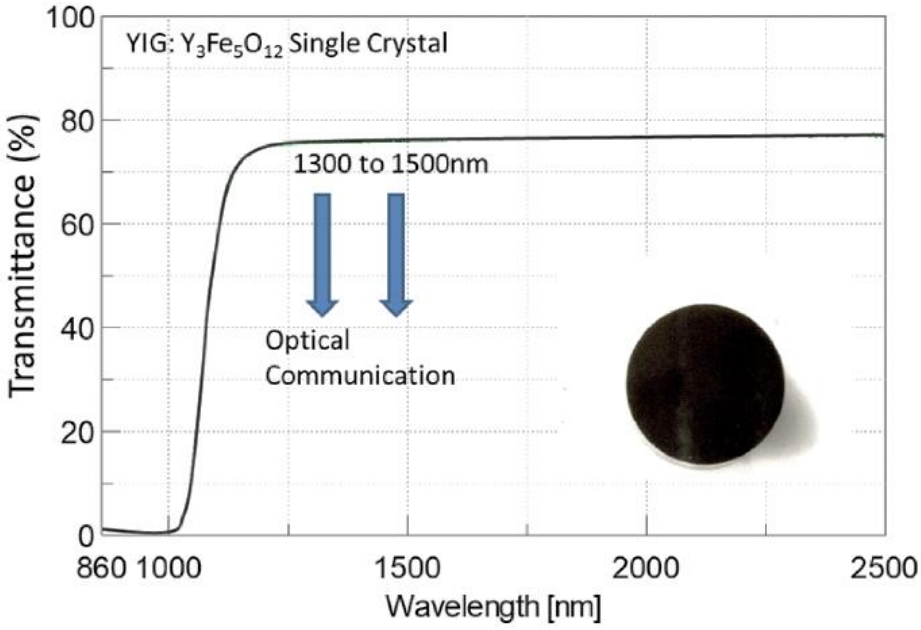

Figure 1.7 Transmission spectrum for YIG materials [9].

However, there have been problems such as deterioration of the thin film single crystal due to high output power of the laser light source and a narrow wavelength band through which light is transmitted, which limits the wavelength range that can be used. In particular, in the wavelength band of 1 μm used for laser processing machines, the transparency of iron-based magnetic garnet thin film single crystals is not sufficient, and it has been necessary to expand the wavelength range that can be used as an optical isolator. To enhance the magneto-optical performance, Bi-substituted iron garnet (Bi:$Re_3Fe_5O_{12}$, Re = lanthanide rare earth) single crystals have been produced by the LPE (Liquid Phase Epitaxial) method from the 1970s to the present day, and only single crystals have been used as Faraday rotator materials due to the same reason as written in the above paramagnetic material. Other than the LPE method, it is difficult to synthesize the Bi-substituted iron garnet single crystals, and furthermore there is no synthetic example of transparent ceramics with the same composition as the single crystal. The LPE method is the only feasible method for synthesizing Bi-substituted iron garnet single crystals with high Faraday rotation performance, which limits the usable size of grown crystal. Actually, a larger size of Faraday rotator is required for high output power laser applications. However, the manufacturing method requires a very expensive GGG ($Gd_3Fe_5O_{12}$) single crystal substrate, which causes an economic problem in industrial production. There are also problems of low productivity due to extremely slow crystal growth rate (only several tens of μm/h), hence the crystal growth period to achieve 1 mm thickness is about one week. In addition, it is well-known that the growth crystal includes numbers of crystal defects. Another concerning issue is related to health problems due to the evaporation of lead-based flux and Bismuth. However, since there is no alternative method, it is still produced in the same method until today [10].

(b) Ceramics

Microstructure of polycrystalline ceramics is illustrated in Figure 1.8, and it is composed of fine grains with random crystal orientations. Since traditional ceramics include numerous scattering sources as shown in the figure, the internal scattering is very high, and the intensity of incident light is attenuated to almost zero after passing through it. According to the classical scattering theory, Mie scattering [11] occurs by (b) residual pores and (e) inclusions which are relatively large defects with respect to the visible wavelength. Other scattering sources such as (a) grain boundaries, (c) secondary (grain boundary) phases, and (d) double refractions due to crystal twin-domains etc. are considered to cause Rayleigh scattering [12] because they are sufficiently smaller than the visible wavelengths.

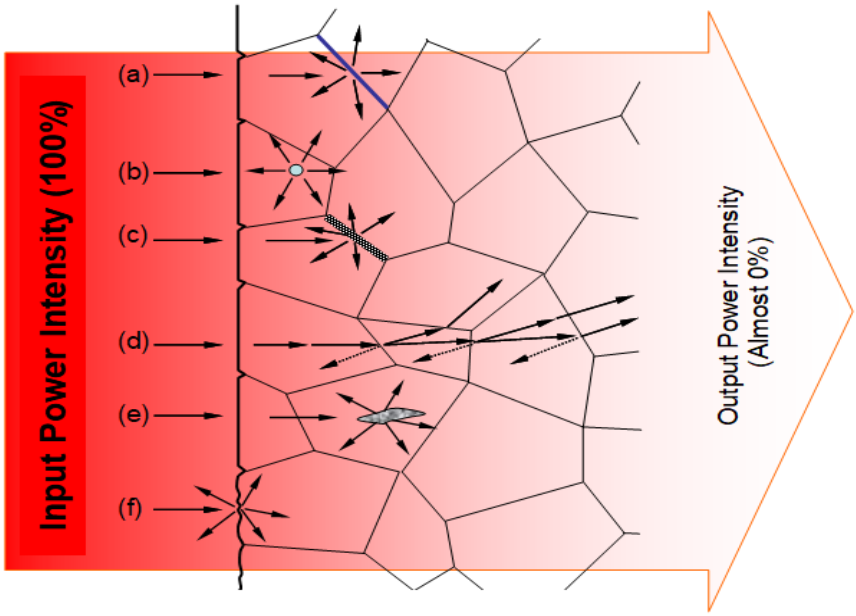

Figure 1.8 Image of strong scattering in traditional ceramics owing to (a) a grain boundary, (b) residual pore, (c) secondary phase, (d) double refraction, (e) inclusion and (f) surface roughness in ceramics which prohibits applications in optics.

Nevertheless, by the development of transparent ceramics with high optical quality for laser oscillation in 1995 [4], such scattering sources in ceramics can be effectively eliminated by improving the fabrication technology and optical loss in the materials can be significantly lowered to the level that is comparable to the single crystal counterparts. Ultimately one technological issue that is remained unsolved in optical ceramics is the existence of grain boundary, which is assumed as crystal defect (dislocation) in atomic level. However, it was also verified that as long as the clean grain boundaries are formed in optical ceramics, the optical loss due to scattering at the grain boundaries is almost negligible, and it has been already demonstrated that ceramic laser materials can contribute laser generation with high lasing efficiency, high output power, and high laser beam quality comparable or superior to the counterpart single crystal laser materials [13]. When a He-Ne laser (wavelength: 633 nm) was irradiated into a normal transparent ceramic and an optical grade ceramic, scattered line was not detectable in optical grade ceramics which is as an evidence that clean grain boundary is formed. (Figure 1.9 is presented as an evidence of scattering.)

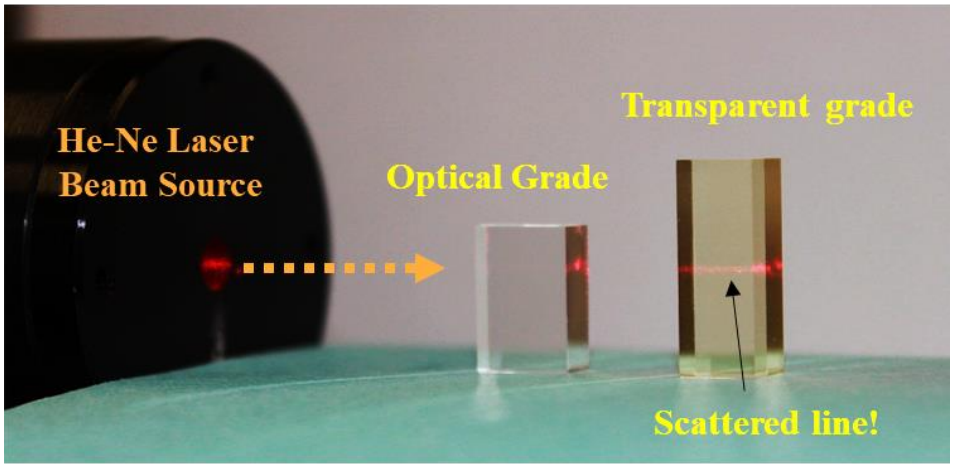

Figure 1.9 Optical scattering in normal transparent ceramics and optical grade ceramics irradiated with a visible He-Ne laser (wavelength: 633 nm).

In this study, the target application of magneto-optical ceramic materials is for Faraday optical isolator device. Hence the materials must have low insertion loss, high extinction ratio and high laser damage threshold. For instance, insertion loss must be low (normally less than 1 dB), and extinction ratio must be larger than 30 dB and it must be resistant to 30 W class CW (continuous wave) laser. Here, the insertion loss corresponds to the transmission loss when an incident light passes through the materials. Principally, it is possible to produce transparent polycrystalline ceramic materials, but the critical issue is to minimize the insertion loss and maximize the extinction ratio to be able to practically use in an optical isolator. Figure 1.10 (a) shows an illustration of optical isolation in the case of single crystal materials with a certain orientation. In the conventional theory, Faraday effect depends on the orientation of grown crystal [14], that is the magneto-optical characteristics such as Verdet constant, magnetization and extinction ratio vary with the orientation even for the single crystals with same chemical composition. A Faraday rotator crystal has an axis of easy magnetization (normally <111> orientation for cubic system), and a strong magnetic field is applied to obtain polarization of the incident laser beam exactly at a certain angle of rotation.

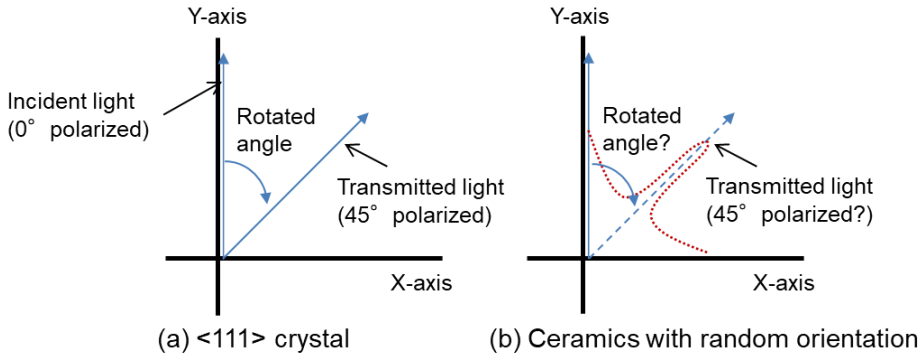

Figure 1.10 (a) Faraday rotation angle in the case of crystal under magnetic field, and (b) possible distribution of Faraday rotation angle in the case of ceramic isolator.

However, in the case of ceramic isolator, each grain of ceramics has random crystal orientation, and each crystallite may show an individual Faraday rotation angle. Therefore, a certain distribution of rotation angles can be estimated as shown in Figure 1.10 (b). Here, the interesting questions from the viewpoint of materials science and technology are whether the polycrystalline ceramic isolator will give an accurate Faraday rotation angle (45 °) and a high extinction ratio as in the case of crystal isolator; or will its rotation angle show a kind of distribution depending upon the random orientation of each grain of ceramics? Accordingly, it is necessary to verify the characteristics of ceramic isolators in this study.

1-4. Objective of this study

Faraday rotator materials are classified into iron-free paramagnetic materials and iron-containing ferrimagnetic materials. Paramagnetic materials are applied in the 1 μm wavelength band to the visible range of fiber lasers and YAG lasers. Currently TGG single crystal is commercially available as the main material for Faraday rotator. Since the Verdet constant of TGG is small, the required length of the Faraday rotator must be approximately 20 mm or longer when it is used in an optical isolator. In addition, a strong magnetic field is required to obtain a desired Faraday rotation. Many studies have been performed on polycrystalline TGG ceramic materials and improved optical qualities were also reported [15]; however, their magneto-optical performances were merely compatible with that of the TGG crystal. Therefore, it is still necessary to search for new types of ceramic materials with high Verdet constant exceeding the TGG material.

In the case of ferrimagnetic materials such as YIG, they are used in the wavelength band longer than 1.3 μm (mainly in optical communication). In particular, the Bi-substituted iron garnet single crystal has high performance and therefore occupies most of the market. As described in the above section 1-3, the synthesis of this single crystal is extremely difficult and only the LPE (Liquid Phase Epitaxial) method is available. However, the LPE method has economic problems such as the need of an expensive GGG ($Gd_3Ga_5O_{12}$) single crystal substrate for lattice matching, low productivity such as an extremely slow growth rate of several tens of μm/h, and health problems due to evaporation of lead-based flux and Bi. To date there has been no report of the synthesis of polycrystalline transparent ceramics having the same composition. Moreover, it still has many technical problems that cannot be solved, therefore it is required to develop and put into practical use new approaches of production that can replace this method. Conventional polycrystalline ceramic technology has made it possible to synthesize the same substance as a single crystal, but it has not been able to exceed the basic characteristics of a single crystal. In this study, the targets are paramagnetic materials and ferrimagnetic materials through an exploratory synthesis of novel materials and evaluation and analysis of their functions, and the objective was to develop an advanced polycrystalline Faraday rotator material composed of fine grains with random orientation having performance comparable or superior to the performance of the conventional Faraday rotator materials.

1-5. Outlines of achievements of this study

In this study, regarding the paramagnetic polycrystalline ceramics focusing on Tb, which is a magnetically active ion it was successful to develop with high magneto-optical performance in the 1 μm to visible range, specifically $(Tb_xY_{1-x})_3Al_5O_{12}$ ceramics with garnet structure, $Tb_2Hf_2O_7$ ceramics with pyrochlore structure, and $(Tb_xY_{1-x})_2O_3$ (abbreviated as TYO), Tb_2O_3 (abbreviated as TO), and Dy_2O_3 (abbreviated as DO) with bixbyite structure.

In Chapters 2 and 3, the insertion loss of polycrystalline ceramics (optical loss when the incident laser light is polarized by applying a magnetic field) was compared to that of a commercially available TGG ($Tb_3Ga_5O_{12}$, current main material of isolator) single crystal. An extremely low insertion loss up to 1/5 of a single crystal was achieved by optimizing the synthesis conditions. The biggest concern for the use of ceramic materials in optical isolator is certainly its polarization characteristics because ceramic is an aggregate of fine grains in random crystal orientations, but there was no problem with the plausible inaccurate polarization due to the difference in the Verdet constant of each grain. In addition, it was also proved that the extinction ratio (the ability to shut down the laser light using polarizers) completely exceeded that of single crystal. These results not only completely overturn the conventional understanding in material science, but also mean that the Faraday rotating material has entered a period of transition from “single crystals” to “ceramics”.

In Chapter 4, among the developed magneto-optical ceramics, especially TO and TYO ceramics have the world’s largest Verdet constant which cannot be obtained with the existing single crystal technologies. Moreover, a prototype of compact isolator device was built and also commercialized. Garnet-based Faraday rotating materials are also suitable for high-power laser applications because of their extremely low insertion loss, high extinction ratio, high laser damage threshold, and excellent thermal lens and thermal birefringence characteristics. In this work, the world’s first isolator device was developed for high output that does not require a specific cooling and licensing this technology has been negotiated for mass production. It should be noted that only the paramagnetic materials are viable for the 1μm ~ visible wavelength region. Next to the Tb_2O_3, a high Verdet constant is expected for Dy_2O_3, and an optical grade Dy_2O_3 polycrystalline ceramics was developed as described in Chapter 5.

Regarding the ferrimagnetic materials for wavelength bands longer than 1.3 μm (mainly for optical communication), rare-earth iron garnet ceramics were developed. In Chapters 6 and 7, it was successful to obtain a transparent YIG ($Y_3Fe_5O_{12}$) and TIG ($Tb_3Fe_5O_{12}$) ceramics without addition of Bi for the first time in the world by the solid-state reactive sintering process. Then, also Bi-substituted iron garnet transparent ceramics were successively developed, and details are described in Chapter 8. Both ceramics showed similar magneto-optical properties to their single crystal counterparts. This fact suggests that the Bi-substituted iron garnet ceramics produced by the sintering method can be an effective approach for solving the current problems of the LPE method and, suggests that it can become a mass production technology suitable for future 5G network

telecommunication. The main reasons why the production of transparent Bi-substituted iron garnet ceramics was successful by the sintering method are; (1) formation of ultra-high-density sintered body without scattering defects, and (2) without Bi segregation since sintering is a non-melting process.

This study examined whether further innovation is possible from an academic and industrial perspective in this field. In Chapter 9, it was confirmed that the Ce-substituted iron garnet ceramics far exceeded the magneto-optical properties of the materials that have been industrially applied so far. There was a report of trial production of this single crystal material by the FZ (Floating Zone) method, but since the segregation coefficient of Ce with respect to iron garnet is very small and almost no solid solution is possible in the base garnet material. Due to this reason, the synthesis of this material was discarded in the 1980s. Indeed, thin film synthesis technology can provide this material with a high Faraday rotation angle, there is still no successful example of production of bulk ceramics because it is very difficult to transmit light (make transparent) in this material. In this work, the synthesis of highly transparent Ce-substituted iron garnet was successful by the simplest reactive sintering method followed by HIP (hot isostatic pressing) process for the first time. It is to be noted that the degree of change in Faraday rotation angle per 1 at.% Ce is 144 deg cm^{-1} (about 5 times larger than that with Bi added iron garnet), which is the highest performance in worldwide. Owing to the high Faraday rotation performance, even a very thin medium thickness enables the construction of a compact high-performance isolator for optical communication, and a technical innovation has also occurred in the optical isolator using a ferrimagnetic Faraday rotator material. If this innovative technology can be industrially applied in the future, it is believed that its contribution will be for more than 5 billion people using 5G network telecommunication in worldwide as it will be available in the near future. Once this is realized, a huge number of optical isolators will be essential for the optical fiber system in telecommunication field, therefore it is highly demanded to develop new production methods that can replace the LPE method, but the fact is that no one has achieved it yet.

References

1. R. Yasuhara, I. Snetkov, A. Starobor, E. Mironov, O. Palashov, “Faraday rotator based on TSAG crystal with <001> orientation”, Opt. Express, **24**, 15486-15493 (2016).

2. Y. Shoji, T. Mizumoto, “Silicon Waveguide Optical Isolator with Directly Bonded Magneto-Optical Garnet”, Appl. Sci., **9** [3], 609 (2019).

3. B. E. A. Saleh, M. C. Teich, Chap.6, in Fundamentals of Photonics, Second Edition, Wiley-Interscience, (2007).

4. A. Ikesue, T. Kinoshita, K. Kamata, K. Yoshida, “Fabrication and Optical Properties of High-Performance Polycrystalline Nd:YAG Ceramics for Solid-State Lasers”, J. Am. Ceram. Soc., **78**, 1033-1040 (1995).

5. M. Faraday, “Faraday’s Diary, Vol. 4, Nov. 12, 1839 - June 26, 1847”, edited by. T. Martin, George Bell and Sons Ltd. (1933).

6. A. Ikesue, Y. L. Aung, “Development of Optical Grade Polycrystalline YIG Ceramics for Faraday Rotator”, J. Am. Ceram. Soc., **101** [11], 5120-5126 (2018).

7. K.T. Stevens, W. Schlichting, G. Foundos, A. Payne, E. Rogers, “Promising Materials for High Power Laser Isolators”, Laser Tech. J., **13,** 18-21 (2016).

8. T. Fujii, M. Geho, “Crystal growth and optical properties of $Tb_3Al_5O_{12}$ with Faraday-effect”, New Glass 71 **18** [4], p.32 (2003).

9. Unpublished work.

10. T. Fujii, Y. Sakabe, “Growth and Magnetic Properties of YIG Films”, pp. 3666-3670 in Encyclopedia of Materials: Science and Technology, edited by Subhash Mahajan, K.H.J. Buschow, Robert Cahn, Merton C Flemings, Bernhard Ilschner, Edward J Kramer and Patrick Veyssiere, Elsevier (2001).

11. G. Mie, “Beiträge zur Optik trüber Medien, speziell kolloidaler Metallösungen”, *Annalen der Physik*. **330** [3], 377-445 (1908).

12. L. Rayleigh, “On the transmission of light through an atmosphere containing small particles in suspension, and on the origin of the blue of the sky”, Philos. Mag. Ser. **47** [287], 375-384 (1899).

13. A. Ikesue, Y. L. Aung, “Ceramic Laser Materials”, Nat. Photonics, **2**, 721-727 (2008).

14. Y. Kagamitani, D.A. Pawlak, H. Sato, A. Yoshikawa, H. Machida, T. Fukuda, “Dependence of Faraday effect on the orientation of terbium-scandium-aluminum garnet single crystal”, J. Mater. Res., **19**, 579-583 (2004).

15. H. Yoshida, K. Tsubakimoto, Y. Fujimoto, K. Mikami, H. Fujita, N. Miyanaga, H. Nozawa, H. Yagi, T. Yanagitani, Y. Nagata, H. Kinoshita, “Optical Properties and Faraday Effect of Ceramic Terbium Gallium Garnet for a Room temperature Faraday Rotator”, Opt. Express, **19** [16], 15181-15187 (2011).

Chapter 2 Development of Optical Grade $(Tb_xY_{1-x})_3Al_5O_{12}$ Ceramics as Faraday Rotator Material

2-1. Introduction

Faraday rotator materials developed for visible to near infrared wavelength regions are TGG ($Tb_3Ga_5O_{12}$) and TAG ($Tb_3Al_5O_{12}$) [1-8]. The TGG material mainly occupies the market because it can be produced with high optical quality by CZ (Czochralski) method and its Verdet constant is relatively high. On the other hand, the TAG material possesses higher Verdet constant than the TGG; however, as described in Chapter 1, section 1-3, it is difficult to grow TAG crystal by the CZ method because of the peritectic reaction during melt-growth process. Even though it can be grown by modified FZ (floating zone) method, there is size limitation and actually it is difficult to be applied for industrial applications.

Highly efficient laser oscillation by using polycrystalline ceramics was demonstrated in 1995 [9,10]. After this achievement, transparent ceramics were being developed for various types of polycrystalline optics such as laser gain media [11,12], scintillators [13,14], etc. Recently, transparent TGG [15-17] and TAG [18-23] ceramics have been reported. The former one has high optical quality and similar Faraday rotation property as commercial TGG crystal, but its weak point is large transmission loss, about 5 dB was measured when it was placed in magnet house to provide 45 º Faraday rotation angle [15]. The latter one was reported with about laser damage by 300 W laser input power but the details about optical properties of the materials were not described. In these literatures, the thickness of the prepared samples was only about 1~2 mm and the transmittance was approximately 78 %. The optical losses can be roughly estimated to be higher than 40 % cm^{-1}, which is extremely high to be used in practical devices because target optical loss for practical application as optics must be as low as 0.1 % cm^{-1}. In this research work, high-quality TAG ceramics with partial substitution of terbium (Tb) sites with yttrium (Y) were developed by reactive sintering method.

2-2. Experimental Procedure

High purity raw materials, Tb_4O_7 (particle size: 3 μm, commercially available) with 99.999 % purity, Y_2O_3 (particle size: 0.6 μm, commercially available) with 99.999 % purity and Al_2O_3 (particle size: 0.4 μm, commercially available) with 99.99 % purity were used as starting materials. These raw powders were weighed to have garnet composition of $(Tb_xY_{1-x})_3Al_5O_{12}$ (x=0.5~1.0). Then colloidal silica (ca.100 wt. ppm) was added as sintering aids and mixed in ethanol solvent for 15 hours by ball milling. A spray dryer (TRS-4W, Sakamoto Engineering, Kawasaki, Japan) was used to dry the slurry and granulate the premixed powders (ca. 30 μm). These granulated powders were pressed into disk or rod shape by using metal molds and then applied CIP (cold isostatic press, P200, Kobe Steel, Ltd., Tokyo, Japan) at 147 MPa. Next, the obtained powder compacts were heated at various temperatures (1000~1800 ºC) in a vacuum furnace (W-heater, Special ordered furnace, Futek Furnace Inc., Yokohama, Japan) and their apparent densities of the heat-treated compacts were measured. In order to obtain optical grade samples, the powder compacts were presintered at 1500 ºC for 2 hours under

vacuum ($1x10^{-3}$ Pa) and then, HIP (hot isostatic pressing, SYS50X-SB, Kobe Steel, Ltd., Tokyo, Japan) treatment was performed at 1690 ºC for 3 hours with argon gas pressure of 176 MPa.

Transmitted polarized optical microscope (BX-50, Olympus Co., Tokyo, Japan) and SEM (scanning electron microscope, SU8000, Hitachi Co., Tokyo, Japan) were used to observe the microstructure of prepared ceramics. Spectro-photometer (V670, JASCO Co., Tokyo, Japan), macro polarizer (SVP-200, Toshiba Co., Tokyo, Japan) and interferometer (GPI-XP, ZYGO Ltd., Middlefield, USA) were used to evaluate the optical quality of prepared ceramics.

An experimental setup to measure the Verdet constant and Faraday rotation property was shown in Figure 2.1. A continuous wave (cw) laser diode (FPLD-1060-24, FiberLabs Inc., Saitama, Japan) was used as the incident laser source of which the wavelength was 1064 nm, and the maximum output power was 10 mW. Laser was irradiated into the sample, which is placed between input polarizer and output analyzer made of Glan Thompson prism (GTP, SIGMA KOKI, Tokyo, Japan). The extinction ratio of the prism was 50 dB. The produced $(Tb_{0.6}Y_{0.4})_3Al_5O_{12}$ ceramics (5 mm in diameter by 23 mm length) and TAG ceramics (5 mm in diameter by 13 mm length) and commercial TGG single crystal (5 mm in diameter by 20 mm length, Electro-Optics Technology Inc., Traverse, USA) with <111> orientation as a reference were used to compare their insertion loss and extinction ratio. For the measurement of Faraday rotation property, the produced $(Tb_{0.6}Y_{0.4})_3Al_5O_{12}$ ceramics (5 mm in diameter by 20 mm length) was used. Faraday rotator sample was clamped in copper holder, and a commercially available Faraday rotator magnetic housing was used. Neodymium-iron-boron permanent magnets (Shin-Etsu Chemical Co., Ltd., Tokyo, Japan) were used to generate high axial magnetic field. Magnetic flux density calculated for the 20 mm length of $(Tb_{0.6}Y_{0.4})_3Al_5O_{12}$ ceramic was 0.98 Tesla. A polarization plane of laser light was rotated by the Faraday effect because of the applied magnetic field. The transmitted laser output power was measured by using a power meter (PM400K1, Thorlabs Japan Inc., Tokyo, Japan) against the rotation angle of the output analyzer.

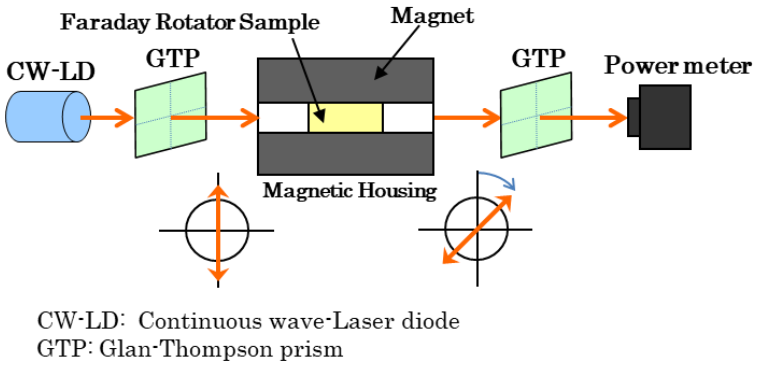

Figure 2.1 Experimental setup to evaluate the Faraday properties.

2-3. Results and discussion

Relationship between the sintering temperatures and density change of Tb_4O_7-Al_2O_3 powder compact with TAG composition when it was heated at 5 ºC min^{-1} in air was shown in Figure 2.2(a), and their appearances after heating were shown in Figure 2.2(b). Density increase due to sintering shrinkage was observed above 1200 ºC and it got saturated above 1500 ºC. Apparent density sintered at 1500 ºC was 6.30 g cm^{-3}. There was no further increase in the apparent density of materials even after sintering at temperatures higher than 1500 ºC. The color of powder compact at initial stage was brown color due to the presence of Tb_4O_7, and it became white color after heating at 1100 ºC. It was due to oxygen dissociation reaction as follows: $Tb_4O_7 \Rightarrow 2Tb_2O_3 + 1/2O_2$, but cracking did not occur inside the material due to gas generation during heating process. After sintering this sample at 1720 ºC for 5 hours in vacuum furnace, it became transparent, but some voids (scattering sources) were remained inside the sample. Therefore, it was treated in HIP (hot isostatic pressure) furnace after presintering and high optical quality ceramics were obtained.

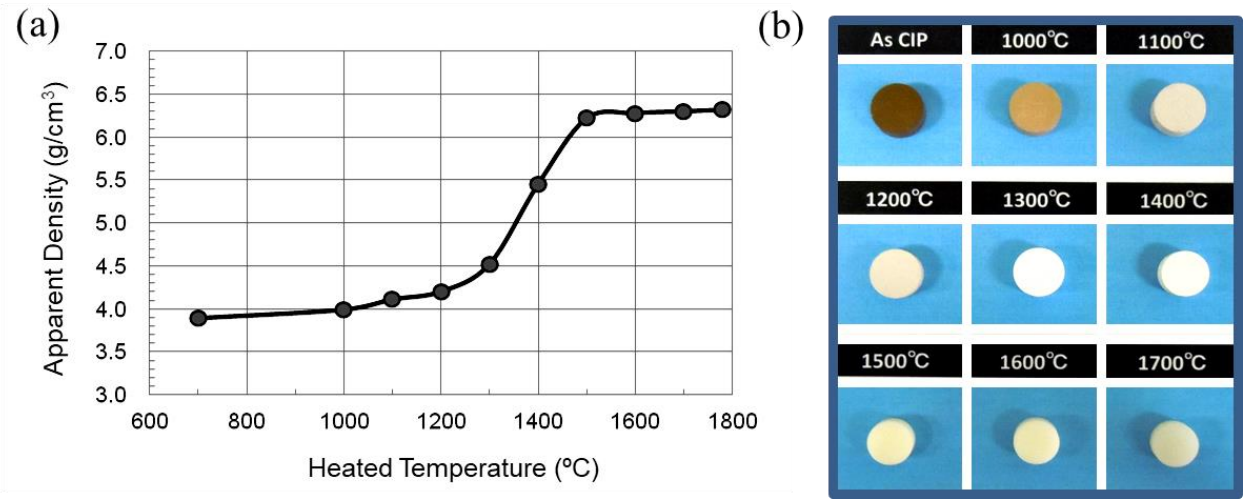

Figure 2.2 (a) Density change of $Tb_4O_7 – Al_2O_3$ powder compact. (b) Appearance of compact sample before and after heating at 1000 to 1700ºC.

SEM images of HIP treated $(Tb_{0.6}Y_{0.4})_3Al_5O_{12}$ and TAG ceramics were shown in Figure 2.3. As seen in these images, fracture surfaces were found to be mostly grain boundary fracture. Their grain sizes were approximately 10~20 μm and found to be uniform. Also, voids and grain boundary phases were not observed.

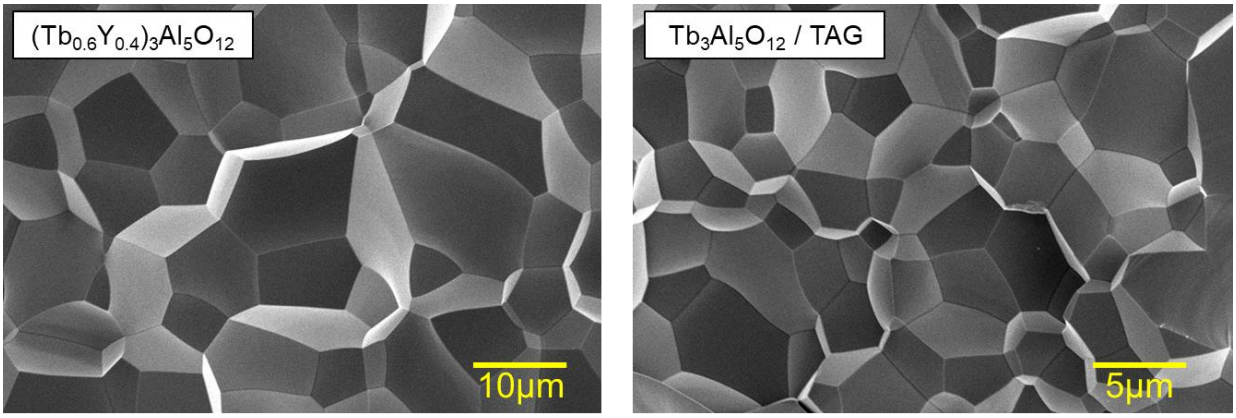

Figure 2.3 SEM image (fracture surface) of $(Tb_xY_{1-x})_3Al_5O_{12}$ (x=0.6 and 1.0) ceramics after HIP treatment at 1690 ºC for 2 hours under 176 MPa Ar gas pressure.

Transmitted polarized optical microscopic images of internal microstructure were shown in Figure 2.4. There were almost no residual pores and also, optically inhomogeneous parts (birefringence due to crystal phases other than cubic phase) such as secondary phases or grain boundary phases were not detected.

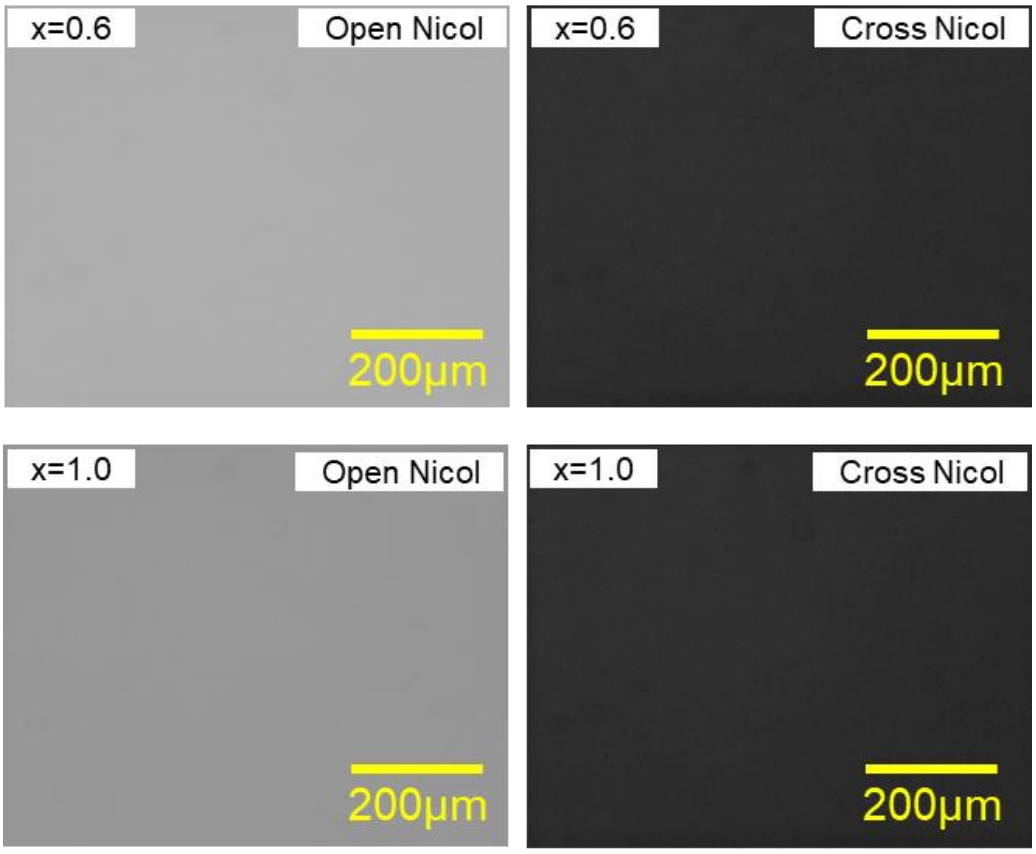

Figure 2.4 Transmission and polarizing microscopy of transparent $(Tb_xY_{1-x})_3Al_5O_{12}$ (x=0.6 and 1.0) ceramics.

Relationship between the transmittance of $(Tb_xY_{1-x})_3Al_5O_{12}$ ceramics (thickness: 11 mm with optical polished surfaces) and x value (Tb content) was shown in Figure 2.5. Vertical axis is in-line transmittance measured by a spectro-photometer. Refractive indices of YAG ($Y_3Al_5O_{12}$) and TAG for 1064 nm were n_{YAG}=1.802 and n_{TAG}=1.845, respectively. Accordingly, their theoretical transmissions calculated from Fresnel equation were 83.6 % and 82.4 %, respectively. Dash line represents the theoretical transmittance calculated by Fresnel's correction depending upon the Tb content in the garnet composition. Actual measured values of transmittances for samples (t=11 mm) with x=0, 0.5, 0.6, 0.8 and 1.0 were plotted in this figure. These values were in good accordance with the ones calculated from Fresnel equation. This suggested that the optical loss of these ceramics were extremely low (less than 0.1 % cm^{-1}). The transmittance of TAG crystal (t=3 mm) grown by FZ method reported by M. Geho et al. was about 80 % [7], and it can be estimated that the optical loss of TAG crystals reported so far were not smaller than 8~10 % cm^{-1} at minimum. From this fact, it can be said that the optical loss of the $(Tb_xY_{1-x})_3Al_5O_{12}$ ceramics in this work was able to reduce to approximately 10^{-2} times than their TAG crystal. Zheleznov et al. and Chen et al. reported transparent TAG ceramics [18-23] but the transmittance of these ceramics was greatly affected by the thickness of the materials and measuring wavelengths. This suggested that these ceramics includes numerous scattering sources, and the optical losses of these ceramics are 10^2 ~ 10^4 times higher than that of the current work. In the previously reported literatures about TAG crystal and ceramics, there were no data about the transmittance actually measured from the length which is required for practical use as Faraday rotator (i.e., 10~20 mm).

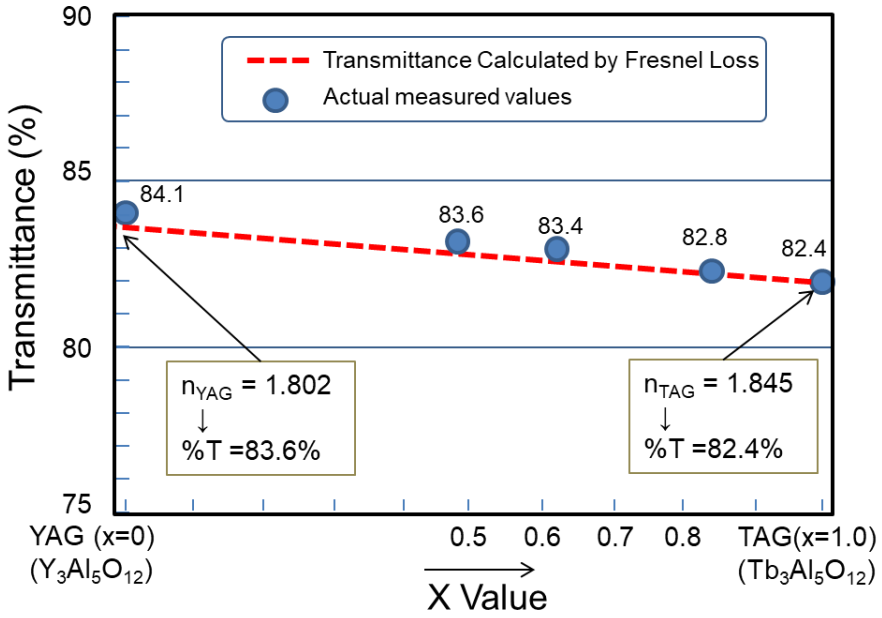

Figure 2.5 Transmittance calculated from Fresnel loss and in-line transmittance of $(Tb_xY_{1-x})_3Al_5O_{12}$ ceramic samples (x=0, 0.5, 0.6, 0.8, and1.0) with 12 mm thickness at 1064 nm.

Therefore, it was difficult to directly compare the current results with the previously reported data but from the transmission spectra of those samples, Mie scattering and Rayleigh's scattering can be suggested. It is not too much to say that solid-state reaction route is a very sensitive process because similar solid-state reaction conditions were applied in this work, but superior optical properties were achieved. It can be considered that selection of starting materials with good sinterability and mixing the raw powders materials with very good homogeneity etc. are very important parameters that can drastically change the properties of the produced materials.

Transmission spectra for $(Tb_{0.6}\ Y_{0.4})_3Al_5O_{12}$ and TAG ceramics (each sample thickness: 11 mm) were shown in Figure 2.6. Refractive indices of $(Tb_{0.6}\ Y_{0.4})_3Al_5O_{12}$ and TAG for 1064 nm were 1.834 and 1.845, respectively. Hence, their theoretical transmissions calculated from Fresnel equation were 82.7 % and 82.4 %, respectively. Measured transmissions were in good accordance with the ones calculated from Fresnel equation. It is to be noted that lowering of transmittance at shorter wavelength regions was not observed, which implies that Rayleigh's scattering did not occurred inside the materials.

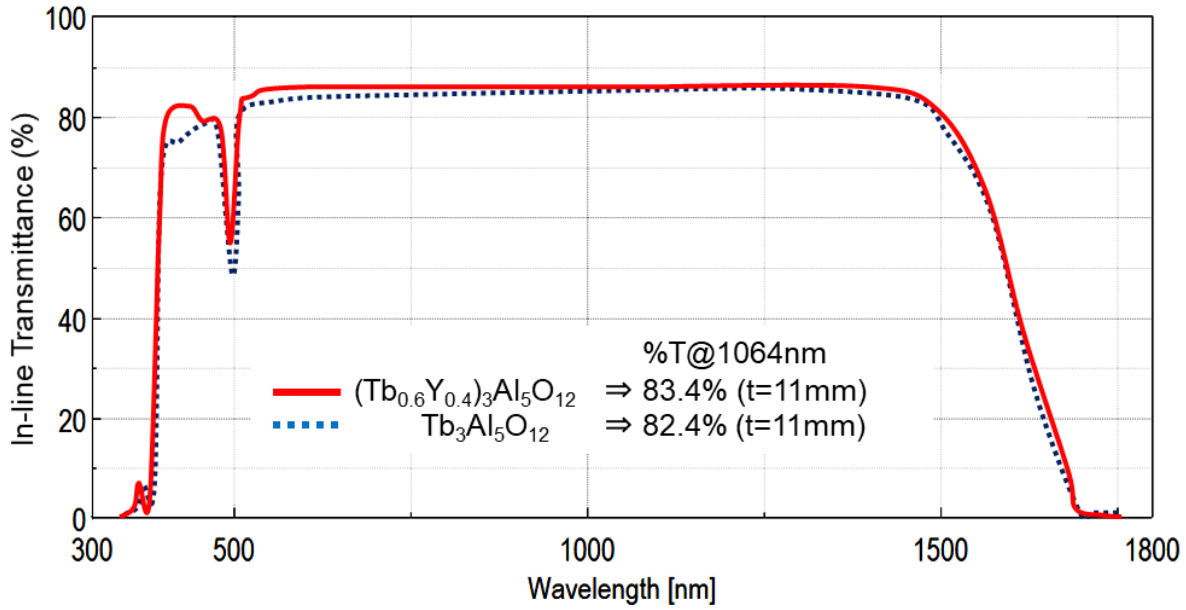

Figure 2.6 Transmission spectra for $(Tb_{0.6}\ Y_{0.4})_3Al_5O_{12}$ and TAG ceramics (each sample thickness: 11mm).

External views of TAG ceramics with long length (Φ10xL40, 25, 12 mm) produced in this work were shown in Figure 2.7(a) and, large aperture samples (t5xΦ10, 23, 45 mm) were shown in Figure 2.7(b). One of these samples was machined to have a dimension with Φ10xL11 mm, and then Φ10 mm double faces were optically polished. The internal optical quality of this sample was inspected by a polarizer and an interferometer

was used to view the wavefront image. These results were shown in Figure 2.7(c) and Figure 2.7(d), respectively. Birefringence was not observed inside the sample, and its transmitted wavefront distortion (TWD value) was as good as λ/12 (t=11 mm). As shown in Figure 2.7(e), when a Gaussian mode laser beam (1064 nm) was irradiated into this sample without AR coating, the transmitted laser beam pattern was very similar to the original beam pattern although the intensity of laser beam was somewhat decreased due to the reflecting optical loss at surfaces (about 17.6 %). This result suggested that this Faraday rotator material possesses a performance that laser light can be transmitted through it without deteriorating the beam quality.

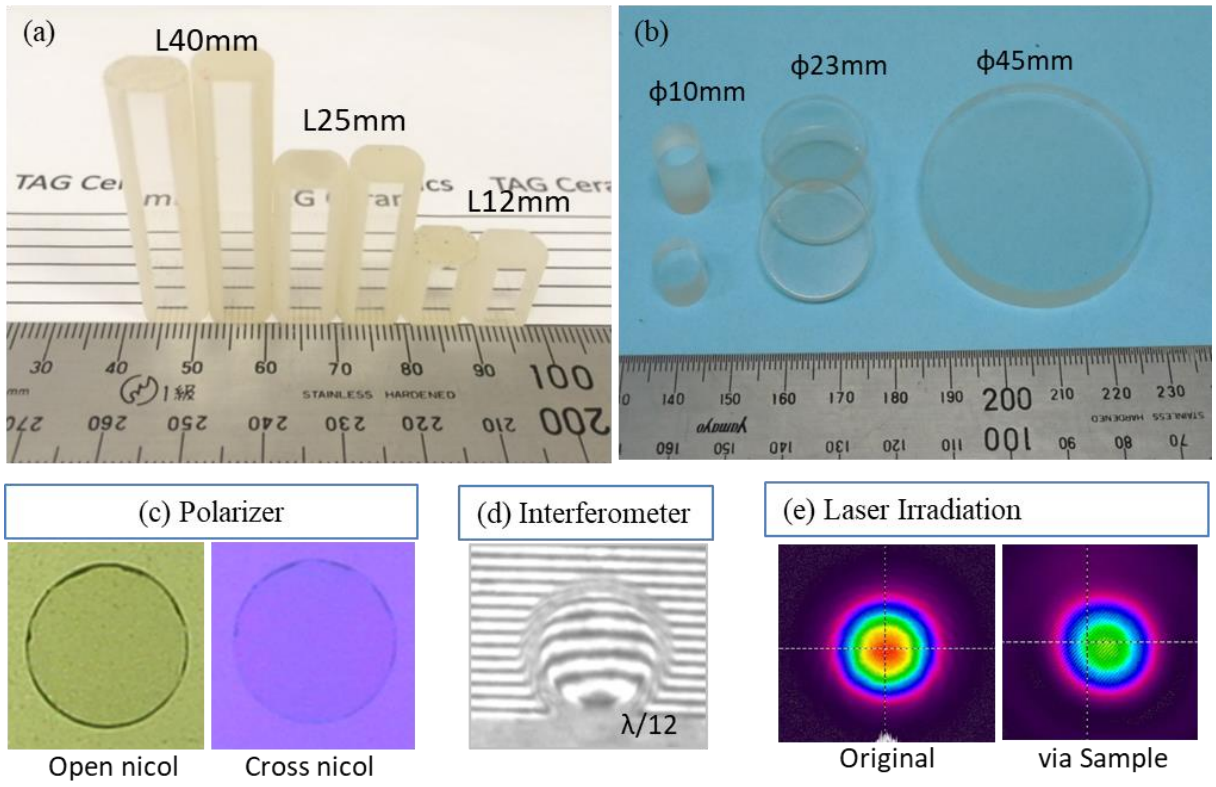

Figure 2.7 (a) Appearance of rod shaped ceramics, (b) disk shaped TAG ceramics, (c) image of TAG ceramics under polarizing plate, (d) transmitted wavefront distortion, (e) Gaussian mode original beam pattern and after passing sample.

Wavelength dependency of Verdet constant for $(Tb_xY_{1-x})_3Al_5O_{12}$ (x=0.5, 0.6, 0.8 and 1.0) ceramics was summarized in Table 2.1 for wavelengths at 532, 633 and 1064 nm. Verdet constants were high when the Tb content (x value) was high and measuring wavelength was shorter. The Verdet constant of TAG ceramics was about 1.5 times higher than that of TGG crystal at any measuring wavelengths. According to the Eq. 1.1 shown in Chapter 1, Verdet constant is inversely proportional to the length of the Faraday rotator material under the same magnetic field to obtain 45 ^{o} rotation angle. Therefore, the length of TAG ceramics which is required to

have similar Faraday rotation properties as TGG can be as short as 13 mm, which is about 40 % shorter than the required length of TGG crystal.

Table 2.1 Measured Verdet constant at wavelengths of 532, 633, and 1064 nm

Materials: $(Tb_xY_{1-x})_3Al_5O_{12}$	**Verdet Constant [rad T^{-1} m^{-1}] at:**		
	532nm	**633nm**	**1064nm**
x =0.5	142	91	30
x =0.6	178	114	36
x =0.8	242	155	49
x =1.0 (TAG)	307	194	60
TGG Crystal	---	133	39

Generally, TGG material needs 20 mm length to provide 45 ° Faraday rotation angle. Measured data of insertion loss and extinction ratio for the prepared $(Tb_{0.6}Y_{0.4})_3Al_5O_{12}$ and TAG ceramics, and commercial TGG crystal were summarized in Table 2.2. It was noted that the extinction ratio of TAG ceramics was higher than that of TGG crystal. Especially the insertion loss of $(Tb_{0.6}Y_{0.4})_3Al_5O_{12}$ ceramics was as low as 0.01 dB, which is an extremely small optical loss under applied magnetic field.

Table 2.2 Insertion loss and extinction ratio of each material measured at 1064nm

	TGG Crystal (t=20mm)	**$(Tb_{0.6}Y_{0.4})_3Al_5O_{12}$ (t=23mm)**	**$Tb_3Al_5O_{12}$ (t=13mm)**
Insertion Loss (dB)	0.05	0.01	0.05
Extinction Ratio (dB)	35.0	39.5	40.3

Faraday rotation property of the prepared $(Tb_{0.6}Y_{0.4})_3Al_5O_{12}$ ceramics (AR coated) was shown in Figure 2.8. X-axis is rotation angle of output analyzer and Y-axis is transmission loss (in dB expression) of transmitted laser light at each rotation angle of output analyzer. Since the length of this sample was only 20 mm, the Faraday

rotation angle achieved was 38.5 degree because its Verdet constant was slightly smaller than that of TGG. However, it was confirmed that the irradiated laser beam was polarized exactly at a certain degree depending upon the length of the Faraday rotator and magnitude of applied magnetic field due to Faraday effect.

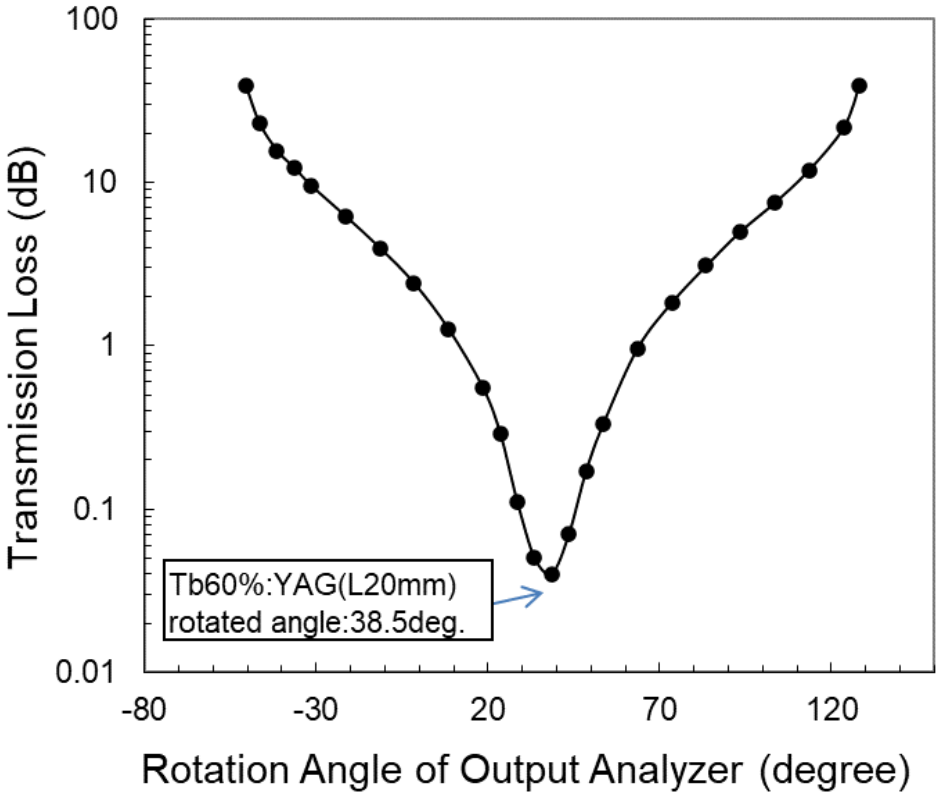

Figure 2.8 Faraday rotation property of $(Tb_{0.6}Y_{0.4})_3Al_5O_{12}$ ceramics.

Only FZ (floating zone) method can produce TAG crystal with limited crystal size (approx. ϕ3xL25 mm) but the optical quality is inferior to that of the TGG crystal grown by CZ method. [7] Compared to TGG, TAG has superior performance in terms of Faraday rotation property but TGG has mostly occupied the market because TGG can be produced in mass production scale although they are same garnet family materials. If TAG can replace TGG, expensive Ga_2O_3 raw material is not necessary, and ceramic fabrication process is usable for mass production with low production cost. Therefore, economic advantages can be expected compared to single crystal production. Another advantage of using TAG ceramics as Faraday rotator materials is downsizing the optical isolator device because (1) length of Faraday rotator material can be shortened, and (2) magnetic volume can be reduced. In this work, not only the optical loss but also other important optical properties such as wavefront distortion, polarization, and laser irradiation test on the produced polycrystalline $(Tb_xY_{1-x})_3Al_5O_{12}$ ceramics showed better results than that of the commercially available TGG crystal or TAG crystal.

2-4. Summary

Results of this work were summarized as below.

(1) Full dense $(Tb_xY_{1-x})_3Al_5O_{12}$ (x=0.5~1.0) ceramics with optical grade were successfully produced by solid-state reaction between (Y_2O_3+Tb_4O_7) and Al_2O_3 raw powders.

(2) By additional HIP treatment on the above (1) sintered bodies, optical transmittance could be further increased, and ultralow optical loss ceramic samples without any birefringence and refractive index variation were achieved. The scattering loss of the obtained $(Tb_xY_{1-x})_3Al_5O_{12}$ (x=0.5~1.0) including TAG ceramics was about 10^{-2} times compared to the TAG single crystal grown by the FZ (floating zone) method, and lower than 10^{-2} ~ 10^{-4} times compared to the TAG ceramics which have been reported in the literatures.

(3) Verdet constant of $(Tb_xY_{1-x})_3Al_5O_{12}$ (x=0.5~1.0) ceramics increased with an increase of x value (Tb content). When x=1.0 ($Tb_3Al_5O_{12}$), the Verdet constant was 307, 196 and 60 rad T^{-1} m^{-1} for 532, 633 and 1064 nm, respectively at each measuring wavelength. These values were about 1.5 times higher than that of the commercially available TGG ($Tb_3Ga_3O_{12}$) crystal.

(4) Faraday rotation characteristics of the obtained ceramics for 1064 nm wavelength were very analogous to that of the commercial TGG crystal. Superior performances of this $(Tb_xY_{1-x})_3Al_5O_{12}$ ceramics were high extinction ratio and low insertion loss.

(5) Large scaled $(Tb_xY_{1-x})_3Al_5O_{12}$ ceramic samples with sizes such as ϕ10xL40 mm or ϕ45xt10 mm could be successfully produced by using this ceramic process demonstrated in this work. It will be able to use in high power laser application (over kW class) in the future.

Accordingly, it was concluded that fundamental properties of the prepared $(Tb_xY_{1-x})_3Al_5O_{12}$ ceramics were superior to that of the commercial high quality TGG single crystal. In addition to advantages such as downsizing, cost performance can be expected when TAG is used as Faraday rotator in practical device because the Verdet constant of TAG is higher than that of TGG.

References

1. E. Khazanov, N. Andreev, O. Palashov, A. Poteomkin, A. Sergeev, O. Mehl, D. H. Reitze, “Effect of Terbium Gallium Garnet Crystal Orientation on the Isolation Ratio of a Faraday Isolator at High Average Power”, Appl. Opt., **41** [3], 483-492 (2002).

2. N. P. Barnes, “Variation of the Verdet Constant with Temperature of Terbium Gallium Garnet”, J. Opt. Soc. Am. B, **9** [10], 1912-1915 (1992).

3. A. Yoshikawa, Y. Kagamitani, D. A. Pawlak, H. Sato, H. Machida, T. Fukuda, “Czochralski Growth of $Tb_3Sc_2Al_3O_{12}$ Single Crystal for Faraday Rotator”, Mater. Res. Bull., **37** [1], 1-10 (2002).

4. M. Geho, T. Sekijima, T. Fujii, “Growth of Terbium Aluminum Garnet ($Tb_3Al_5O_{12}$: TAG) Single Crystals by the Hybrid Laser Floating Zone Machine”, J. Cryst. Growth, 267, 188-793 (2004).

5. S. Ganschow, D. Klimm, P. Reiche, R. Uecker, “On the Crystallization of Terbium Aluminum Garnet”, Cryst. Technol., **34** [5-6], 615-619 (1999).

6. N. P. Barnes, L. B. Petway, “Variation of the Verdet Constant with Temperature of Terbium Gallium Garnet”, J. Opt. Soc. Am., B **9** [10], 1912-1915 (1992).

7. M. Geho, T. Takagi, S. Chiku, T. Fujii, “Development of Optical Isolators for Visible Light using Terbium Aluminum Garnet ($Tb_3Al_5O_{12}$) single crystals”, Jpn. J. Appl. Phys., **44** [7A], 4967-4970 (2005).

8. T. Fujii, M. Geho, “Crystal Growth and Optical Properties of $Tb_3Al_5O_{12}$ with Faraday-Effect”, J. New Glass 71, **18** [4], 32-36 (2003).

9. A. Ikesue. T. Kinoshita, K. Kamata, K. Yoshida, “Fabrication and Optical Properties of High-Performance Polycrystalline Nd:YAG Ceramics for Solid State Lasers” J. Am. Ceram. Soc., **78** [4], 1033-1040 (1995).

10. A. Ikesue, Y. L. Aung, “Ceramic Laser Materials”, Nat. Photonics, **21**, 721-726 (2008).

11. L. Wang, H. Huang, D. Shen, J. Zhang, H. Chen, Y. Wang, X. Liu, D. Tang, “Room Temperature Continuous-Wave Laser Performance of LD pumped Er:Lu_2O_3 and Er:Y_2O_3 Ceramics at 2.7μm”, Opt. Express, **22** [16], 19495-19505 (2014).

12. J. Sanghera, W. Kim, G. Villalobos, B. Shaw, C. Baker, J. Frantz, B. Sadowski, I. Aggarwal, “Ceramic Laser Material”, Mater., **5**, 258-277 (2012).

13. T. Yanagida, A. Yoshikawa, A. Ikesue, K. Kamada, Y. Yokota, “Basic Properties of Ceramic Pr:LuAG Scintillator”, IEEE Trans. Nuc. Sci., **56** [5], 2955-2959 (2009).

14. T. Yanagida, Y. Fujimoto, M. Koshimizu, K. Watanabe, H. Sato, H. Yagi, T. Yanagitani, “Positive Hysteresis of Ce:-doped GAGG Scintillator”, Opt. Mater., **36**, 2016-2019 (2014).

15. H. Yoshida, K. Tsubakimoto, Y. Fujimoto, K. Mikami, H. Fujita, N. Miyanaga, H. Nozawa, H. Yagi, T. Yanagitani, Y. Nagata, H. Kinoshita, “Optical Properties and Faraday Effect of Ceramic Terbium Gallium Garnet for a Room Temperature Faraday Rotator”, Opt. Express, **19** [16] 15181-15187 (2011).

16. R. Yasuhara, S. Tokita, J. Kawanaka, T. Kawashima, H. Kan, H. Yagi, H. Nozawa, T. Yanagitani, Y. Fujimoto, H. Yoshida, M. Nakatsuka, “Measurement of Magneto-Optical Properties and Thermal Conductivity on TGG Ceramic for Faraday Material of High-Peak and High Average Power Laser”, Rev. Laser Eng., **35**, 806-810 (2007).

17. R. Yasuhara, I. Snetkov, A. Starobor, D. Zheleznov, O. Palashoz, E. Khazanov, T. Yanagitani, “Terbium gallium garnet ceramic Faraday rotator for high-power laser application”, Opt. Lett., **39** [5], 1145-1148 (2014).

18. D. Zheleznov, A. Atarobor, O. Palashov, C. Chen, S. Zhou, “High Power Faraday Isolators based on TAG Ceramics”, Opt. Express, **22** [3], 2578-83 (2014).

19. D. Zheleznov, A. Atarobor, O. Palashov, H. Lin, S. Zhou, “Improving Characteristics of Faraday Isolator based on TAG Ceramics by Cerium Doping”, Opt. Lett. **39** [7], 2183-2186 (2014).

20. H. Lin, S. Zhou, H. Teng, “Synthesis of $Tb_3Al_5O_{12}$(TAG) Transparent Ceramics for Potential Magneto-

Optical Application", Opt. Mater., **33**, 1833-36 (2011).

21. C. Chen, X. Yi, S. Zhang, Y. Feng, Y. Tang, H. Lin, S. Zhou, "Vacuum Sintering of $Tb_3Al_5O_{12}$ Transparent Ceramics with combined TEOS + MgO Sintering Aid Aluminum", Ceram. International, **41**, 12823-12827 (2015).

22. C. Chen, X. Li, Y. Feng, H. Lin, X. Yi, Y. Tang, S. Zhang, S. Zhou, "Optimization of CeO_2 as Sintering Aid for $Tb_3Al_5O_{12}$ Faraday Magneto-Optical Transparent Ceramics", J. Mater. Sci., **50**, 2517-2521 (2015).

23. H. Furuse, R. Yasuhara, K. Hiraga, S. Zhou, "High Verdet Constant of Ti-doped Terbium Garnet (TAG) Ceramics", Opt. Mater. Expr., **6** [1] 191-196 (2016).

Chapter 3 Development of Optical Grade $Tb_2Hf_2O_7$ Pyrochlore Ceramics

3-1. Introduction

The paramagnetic TGG ($Tb_3Ga_5O_{12}$) single crystal can be synthesized by the Czochralski method and is mainly used as an optical isolator for shutting down the reflected light of a 1μm band fiber laser. As described in Chapter 2, the author has successfully developed optical grade polycrystalline $(Tb_xY_{1-x})_3Al_5O_{12}$ ceramics [1] for Faraday rotator materials although it is very difficult to synthesize the TAG single crystal materials with high optical quality using the melt growth method [2,3]. In paramagnetic materials, one of the important parameters involved in the Faraday rotation function is the Tb concentration in the material. In the case of TGG, the Tb occupancy in all cation sites is 37.5 %, and the Verdet constant remains at 36 rad T^{-1} m^{-1}. But in the case of pyrochlore (general chemical formula $A_2B_2O_7$) structure, Tb can occupy up to 50 % of all cation sites, and a larger Verdet constant can be further expected. Pyrochlore is a substance that has a high melting point and is difficult to synthesize by the melt growth method, but it is possible to synthesize this single crystal by the conventional methods. Most of Tb-based pyrochlore materials that can be used as Faraday rotator materials until now are only single crystals [4-6], and there were no pyrochlore polycrystalline ceramics produced by general ceramic production (sintering) technology that can be applied to optical isolators. As a matter of fact, there is almost no ceramics that can be evaluated as applicable product quality. The main reason is that the ceramics synthesized to date are simply transparent, and they are not at the appropriate optical grade for practical applications. Therefore, objective of the present study is to synthesize optical grade $Tb_2Hf_2O_7$ (THO) ceramics using terbium oxide (Tb_4O_7) and hafnium oxide (HfO_2) as starting materials by the simplest reactive sintering and HIP treatment, which will be advantageous in upcoming practical applications.

3-2. Experimental Procedure

As starting materials, approximately 10 μm Tb_4O_7 powder (purity 99.99 %, commercially available) in which 0.2 μm primary particles were aggregated and secondary particle approximately 5 μm HfO_2 powder (> 99.9 % in total of HfO_2 and ZrO_2, commercially available) in which 0.3 μm primary particles were aggregated were used. These powders were weighed to have a stoichiometric composition of $Tb_2Hf_2O_7$ and mixed in ethanol solvent with PVA-based binder for 15 hours using Zirconia balls. The resulting slurry was put into a glass beaker and the solvent was evaporated while stirring on a hot plate with a magnetic stirrer. The dried powder was molded with a mold of Φ8 to 20 mm and then treated CIP (cold isostatic press, P200, Kobe Steel, Ltd., Tokyo, Japan) at a pressure of 146 MPa. The preformed body was calcined at 900 °C, then pre-sintered in a vacuum furnace (W-heater, Special ordered furnace, Futek Furnace Inc., Yokohama, Japan) at 1550 °C for 2 hours followed by HIP (hot isostatic pressing, SYS50X-SB, Kobe Steel, Ltd., Tokyo, Japan) treatment at 1650 °C for 3 hours (Ar gas pressure, 176 MPa). Some of these HIP-treated samples were heat-treated (annealed) at 1700 °C for 10 hours in H_2 gas for the purpose of improving the optical homogeneity.

The HIP-treated sample and the HIP & annealed sample were mirror-polished on both sides and their transmission spectra were measured. Using a Schlieren visualization device (SLM-10S, Mizojiri Kogaku, Tokyo, Japan), the uniformity of the refractive index inside the material was observed. The change in beam shape before and after passing through the material was recorded on a beam profiling camera (SP620U, Ophir-Spiricon, LLC, Logan, USA) by irradiating a 5 mW output of the Gaussian mode Nd:YAG laser at 1064 nm (DPSSL, Sanctity Laser, Shanghai, China). Microstructure observation was performed using a reflection and transmission polarization microscope（BX-50, Olympus Co., Tokyo, Japan), and SEM (Scanning Electron Microscope), and the composition was analyzed by SEM-EDS (Energy Dispersive Spectroscopy, SU8000, Hitachi Co., Tokyo, Japan). In order to evaluate the magneto-optical properties of the material, the surface of the material was optically polished (flatness λ/4, parallelism 30 sec, microroughness R_a = 0.3 nm) and then AR coated on both sides (Anti-Reflection coating at 1064 nm). The magneto-optical properties were measured with the same measuring devices shown in Figure 2.1 described in the previous Chapter 2.

3-3. Results and Discussion

Figure 3.1(a) shows an external view of the produced THO ceramics (Φ6 x L15 mm) with mirror polished surfaces on both ends and (b) shows a view of the outside scenery seen through this sample. The outer periphery of the sample shows green color due to the deposition of Mo and W from the vacuum furnace materials onto the surface of the sample during sintering, but the inside of this ceramics is colorless and transparent. Since the optical loss of the material is very small, it is possible to clearly observe the far-away scenery through this 15 mm long sample.

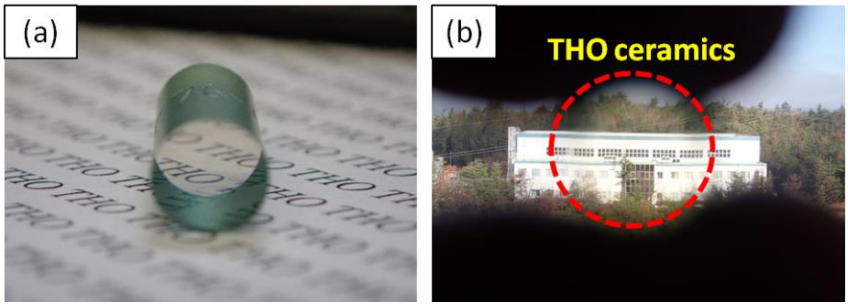

Figure 3.1 (a) Appearance of the produced THO ceramics (Φ6xL15 mm) and (b) a clear view seen through this ceramic (outside building is about 1 km far).

Figure 3.2 shows a reflection, transmission (open nicol) and transmission polarization (cross nicol) micrographs of the THO ceramics. The sample is composed of grains of approximately 3~5 μm, and no residual pores can be observed inside the material. Since it is a dark field under transmission polarization observation, there is no secondary phase other than the cubic phase in the material, and no birefringence component is detected.

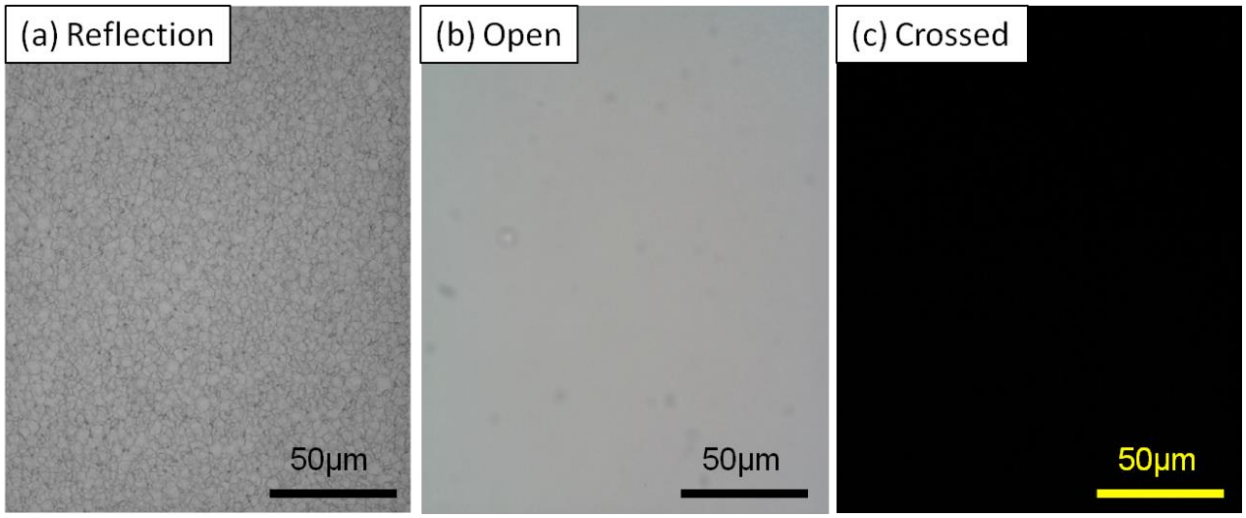

Figure 3.2 (a) reflection, (b) transmission (open nicol) and (c) transmission (crossed nicol) microphotograph of THO ceramics.

Figure 3.3 shows a SEM photograph (back scattered electron image) and elemental mapping (Tb, Hf and O) of thermal etched THO ceramics. Both Tb and Hf are uniformly distributed, and segregation at grain boundaries is not detected. In addition, since the sintering aids are not added in this ceramic fabrication, there is no segregation problem of sintering aids at grain boundaries.

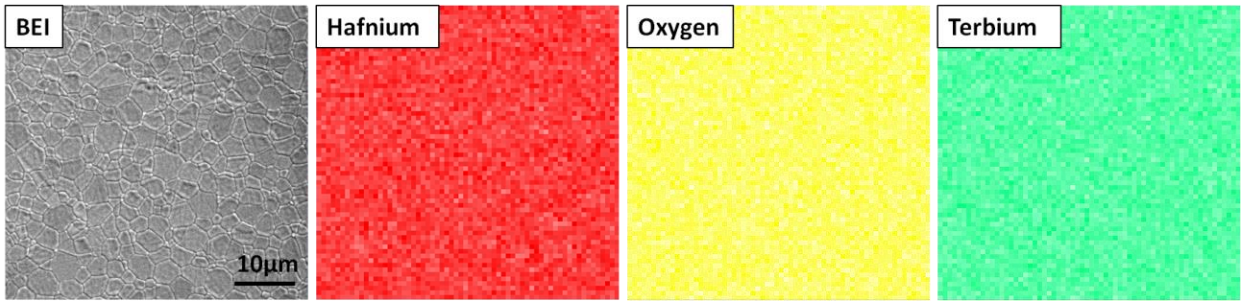

Figure 3.3 BEI (back scattered electron image) and element mapping of THO ceramics by SEM-EDS system.

Figure 3.4 shows transmission spectra of two THO ceramic samples (thickness: 15 mm) from 200 to 1800 nm wavelength ranges. One is as-HIP sample, and another one is a sample annealed in hydrogen at 1700 °C for 10 hours after HIP processing. In the as-HIP sample, an absorption band of up to around 5 % is observed at 600 to 1000 nm, but this absorption has disappeared by the additional heat treatment (annealing). Since the annealing process is performed at a temperature higher than the HIP temperature and for a long time, diffusion inside the material is promoted, which contributes to optical (chemical composition) homogeneity. The absorption in the 600 to 1000 nm region is presumed to be due to the color center (point defect) of the material, and it is considered

that the light absorption disappeared because the point defect decreased during annealing. When Tb occupies the pyrochlore structure, both Tb^{3+} and Tb^{4+} can be formed. The prepared ceramics are colorless and transparent, and the optical loss (light absorption) associated with Tb^{4+} formation is extremely small because it may show brown color even when a small amount of Tb^{4+} is formed. Therefore, the chemical formula of the synthesized ceramics is $Tb^{3+}_2Hf^{4+}_2O_7$. The transmittance of 0.5 mm thick sample was also measured to calculate the optical loss of this ceramics. The estimated optical loss is approximately <0.1 % cm^{-1} because the difference of transmittance in the wavelength ranges (500 to 1400 nm) from the 15 mm thick sample is 0.12 %.

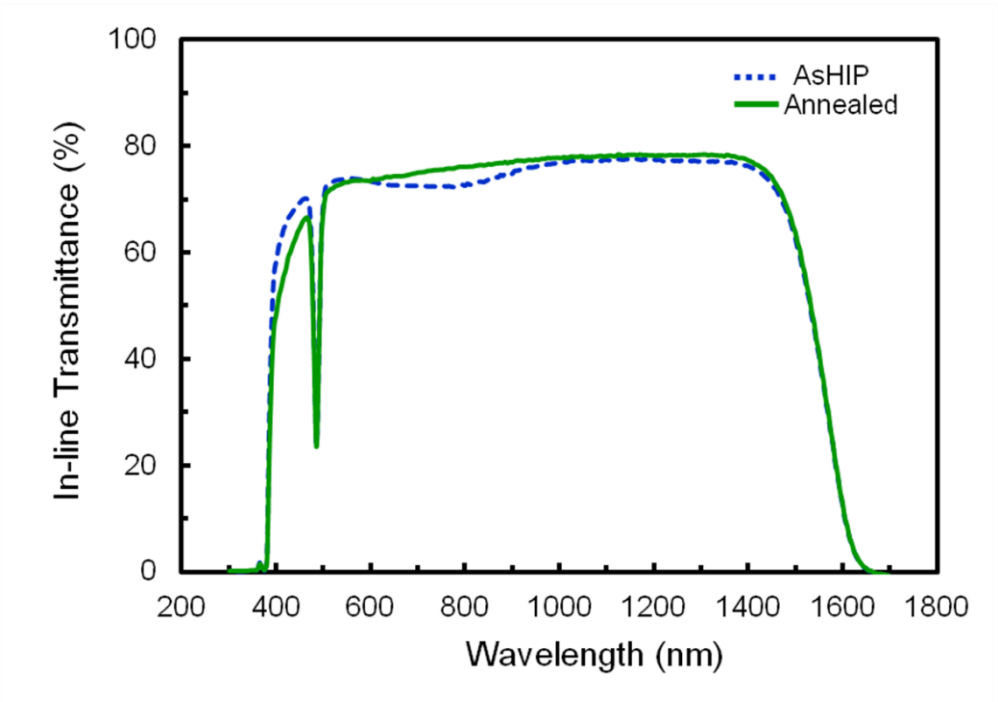

Figure 3.4 Transmission spectra of as-HIP sample (dash line) and annealed sample (solid line) at high temperature after HIP treatment.

L. An et al. [7] have attempted to synthesize $La_2Zr_2O_7$ ceramics using reactive sintering and SPS (Spark Plasma Sintering) method. Their obtained material has difficulty in transmitting light in the visible region even with a thickness of 1 mm and has only a 68 % transmittance in the wavelength range of 4 to 6 μm even in the infrared region, so the optical loss is extremely large. Z. Wang et al. [8] summarized the transmission characteristics of many translucent pyrochlore ceramics reported in the past, such as $La_2Hf_2O_7$, $Y_2Zr_2O_7$, $Lu_2Ti_2O_7$, etc. There is no ceramics showing high transmittance (especially in the visible range) although their thickness is as thin as 1 mm. In most of the pyrochlore ceramics developed up to date, significant Mie and Rayleigh scatterings occur inside the materials, and it is hopeless to use those materials in practical applications as optics because of very high scattering inside the materials.

We have successfully developed a transparent polycrystalline ceramic material with pyrochlore crystal structure with an optical quality that has not been reported up to now, which has an optical loss of <0.1 % cm^{-1} especially in the visible wavelength to near-infrared isolator application wavelength range. Without being limited to pyrochlore structure, we have also succeeded in the development of YAG ($Y_3Al_5O_{12}$) and RE_2O_3 (RE=Y, Lu, Sc, etc.) ceramic laser gain media previously, which have extremely low optical scattering properties [9-11]. In the 1950s, R. L. Coble [12] developed translucent alumina ceramics in which residual pores were reduced. In this work, we have minimized Mie scattering by removing residual pores completely in ceramics. Furthermore, mixing, and sintering method of the raw powders were optimized to improve optical homogeneity based on reactive sintering, and hence the homogeneity of the refractive index inside the material was improved to the highest level. As a result, clean grain boundary was formed where Rayleigh scattering hardly occurs. These facts are difference from the conventional technology and unique to our advanced process.

Figure 3.5 (a-1) shows an appearance of a sample of which the outer periphery of THO ceramics colored in green was removed by grinding and followed by optical polishing on both sides. Then the sample was observed between the polarizing plates which are being orthogonal to each other. No optical distortion is detected in the material, and there is no light (leakage of light) passing through the material when the two polarizing plates are orthogonal to each other. Figure 3.5 (a-2) and 3.5 (b) show the beams before and after irradiation of YAG laser light with a wavelength of 1064 nm on As-HIP and HIP & annealed are observed with a beam profiler, respectively. When the As-HIP sample is irradiated with a laser, the beam is distorted, but the distortion can hardly detect in the annealed one. This is the fact that the homogeneity of Tb and Hf inside the material is further improved by the annealing, and the improvement is also seen in the Schlieren image. In the transmittance measurement result shown in Figure 3.4, an absorption band was found in the 600 to 1000 nm region of the As-HIP sample, which is caused by some defect structure because the homogeneity of Tb and Hf is insufficient. The homogeneity of the material was improved by the annealing treatment, and the contribution of the annealing to the homogeneity can be easily understood from the improvement of the beam quality of the transmitted laser beam profile and the disappearance of the absorption band in the 600 to 1000 nm region.

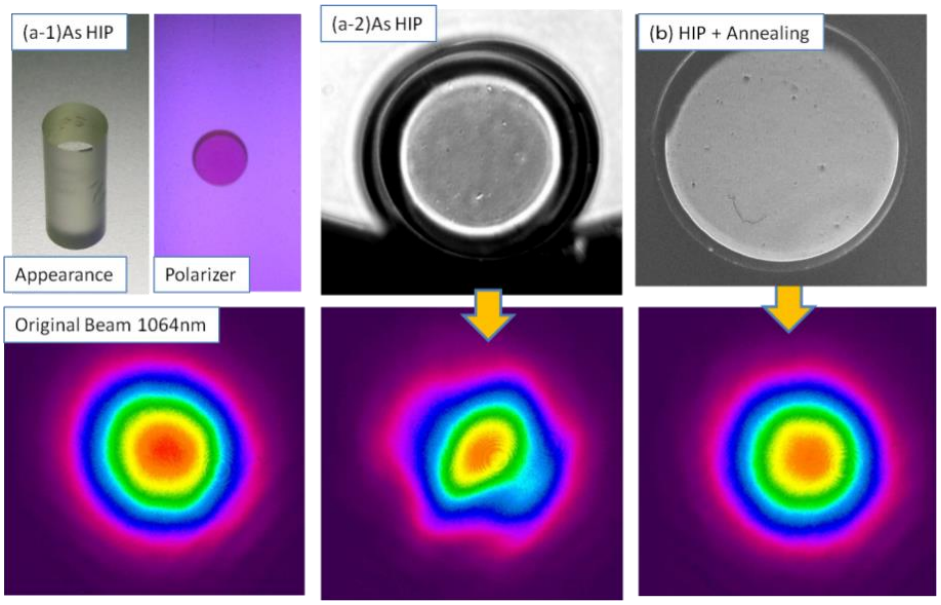

Figure 3.5 (a-1) Appearance after optical grade polishing and observation under polarizer. Schlieren image of (a-2) as HIP sample and (b) HIP plus annealed sample and laser beam pattern passed through each specimen and original beam by beam profiler.

Figure 3.6 shows the wavelength dependence of the Verdet constant of THO ceramics of this work and TGG single crystals which is currently used for fiber laser isolators. The Verdet constant of THO ceramics is about 40 % larger than that of TGG single crystals in any wavelength range. In the 1 μm band for fiber laser processing, in order to obtain Faraday rotation angle at 45 degrees for the TGG single crystal, the crystal length is required approximately 20 mm under a magnetic field of 1 T, but in the case of the THO ceramics, it can be shortened to 15~16 mm.

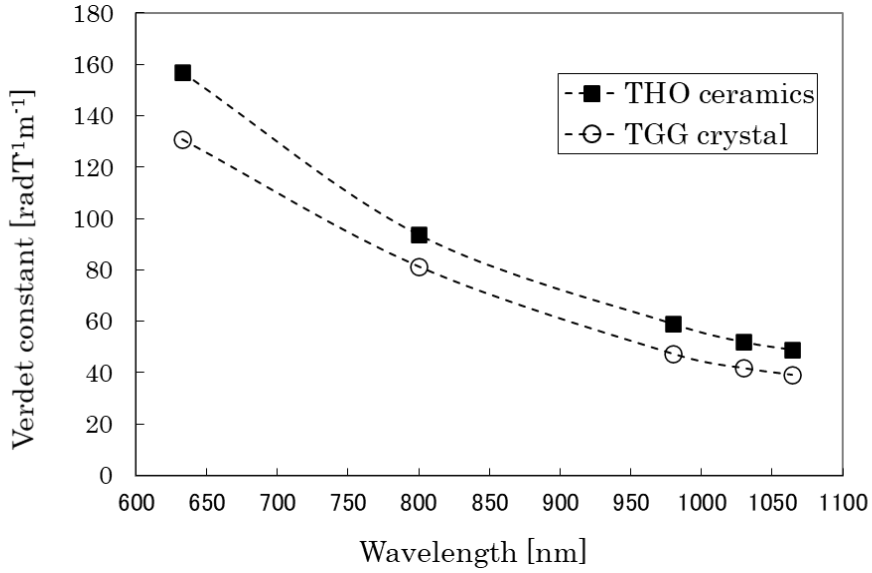

Figure 3.6 Wavelength dependence of Verdet constant of THO ceramics and TGG single crystal.

Table 3.1 shows comparison data on magneto-optical characteristics of the produced THO ceramics and TGG single crystal for a wavelength of 1064 nm. The measurement was performed with the conditions (magnetic field of 1 T) similar to the magneto-optical characteristic of TAG ceramics as described in Chapter 2. THO ceramics has a Verdet constant 40 % higher than TGG single crystal, and it also has a lower insertion loss and a higher extinction ratio.

Table 3.1 Comparative data of opto-magnetic properties for THO ceramics and TGG single crystal

	THO Ceramics	**TGG Single Crystal**
*Verdet Constant (rad T^{-1} m^{-1})	50	36
Insertion Loss (dB)	0.03	0.05
Extinction Ratio (dB)	38	34

*Measured at 1064 nm, magnetic field at 1 T, dimension of THO ceramics and TGG single crystal is Φ4 x 15.5 mm and Φ4 x 20.0 mm, respectively. (Both faces are with laser grade polishing and anti-reflection coating.)

3-4. Summary

By reactive sintering and HIP process, it was successful to produce THO ceramics with low optical loss comparable to single crystal for optical isolator application. The results obtained are summarized below.

1) Since residual pores and grain boundary phases cannot be detected in the THO ceramics and the distribution of Tb and Hf in the material is very good, and the optical loss is as good as approximately 0.1 % cm^{-1}.

2) The as-HIP material has insignificant absorption and small inhomogeneity in the wavelength region of 600 to 1000 nm. Long-time heat treatment at a high temperature of 1700 °C solved these absorption problems, and the distortion of the beam quality of the laser beam transmitted through the inside of the material is eliminated.

3) The Verdet constant, insertion loss, and extinction ratio of the THO ceramics at 1064 nm were 50 rad T^{-1} m^{-1}, 0.03 dB and 38 dB, respectively, exceeded the characteristics of commercially available TGG single crystals.

References

1. Y. L. Aung and A. Ikesue, “Development of Optical Grade $(Tb_xY_{1-x})_3Al_5O_{12}$ Ceramics as Faraday Rotator Material”, J. Am. Ceram. Soc. **100** [9], 4081-4087 (2017).

2. M. Geho, T. Takagi, S. Chiku, T. Fujii, “Development of Optical Isolators for visible light using Terbium Aluminum Garnet ($Tb_3Al_5O_{12}$) Single Crystals”, Jpn. J. Appl. Phys., **44**, 4967-4970 (2005).

3. M. Geho, T. Sekijima, T. Fujii, “Growth of Terbium Aluminum Garnet ($Tb_3Al_5O_{12}$; TAG) Single Crystals by the Hybrid Laser Floating Zone Machine”, J. Cryst. Growth, 267, 188-193 (2004).

4. R. Sibille, E. Lhotel, M. Ciomaga Hatnean, G. J. Nilsen, G. Ehlers, A. Cervellino, E. Ressouche, M. Frontzek, O.Zaharko, V. Pomjakushin, U. Stuhr, H. C. Walker, D. T. Adroja, H. Luetkens, C. Baines, A. Amato, G.Balakrishnan, T. Fennell, M. Kenzelmann, “Coulomb spin liquid in anion-disordered pyrochlore $Tb_2Hf_2O_7$”, Nat. Commun., **8** [1], 892 (2017).

5. V. K. Anand, L. Opherden, J. Xu, D. T. Adroja, A. D. Hillier, P. K. Biswas, T. Herrmannsdörfer, M. Uhlarz, J.Hornung, J. Wosnitza, E. Canévet, B. Lake, “Evidence for a dynamical ground state in the frustrated pyrohafnate $Tb_2Hf_2O_7$”, Phys. Rev. B, **97** [9], 094402 (2018).

6. F. Guo, Y. Sun, X. Yang, X. Chen, B. Zhao, N. Zhuang, J. Chen, “Growth, Faraday and inverse Faraday characteristics of $Tb_2Ti_2O_7$ crystal”, Opt. Express, **24** [6], 5734-5743 (2016).

7. L. An, A. Ito, T. Goto, “Fabrication of Transparent $La_2Zr_2O_7$ by Reactive Spark Plasma Sintering”, Key Eng. Mater., **484**, 135-138 (2011).

8. Z. Wang, G. Zhou, D. Jiang, S. Wang, “Recent Development of $A_2B_2O_7$ System Transparent Ceramics”, J. Adv. Ceram., **7** [4] 289-306 (2018).

9. A. Ikesue, Y. L. Aung, “Ceramic Laser Materials”, Nat. Photonics, **21**, 721-726 (2008).

10. S. Sattayaporn, G. Aka, P. Loiseau, A. Ikesue, Y. L. Aung, “Optical spectroscopic properties, 0.946 and 1.074 μm laser performances of Nd^{3+} - doped Y_2O_3 transparent ceramics”, J. Alloys Compd., **711 [**15], 446-454 (2017).

11. A. Ikesue, Y. L. Aung, “Origin and Future of Polycrystalline Ceramic Lasers”, *IEEE J. Selected Topics in Quantum Electronics,* **24** [5], 1-7, (2018).

12. R. L. Coble, “Preparation of transparent ceramic Al_2O_3”, Am. Ceram. Soc. Bull., **38,** 507 (1959).

Chapter 4 Enhanced Magneto-Optical Performance of Terbium Oxide Ceramics with Bixbyite Structure

4-1. Introduction

Basically, the Faraday rotation angle of an optical isolator is determined by the Verdet constant of the Faraday rotator material. According to the results obtained in the previous Chapters 2 and 3, in the case of paramagnetic materials, the Verdet constant is determined by the concentration (or occupancy) of magneto-active terbium (Tb) ions in the materials. From this point of view, it can be assumed that the material with the highest occupancy of Tb^{3+} is terbium (III) oxide (i.e., Tb_2O_3) in order to maximize the performance of the Faraday rotator materials. Since the Tb_2O_3 possesses a bixbyite structure and belongs to the cubic crystal system, it can be an optically isotropic body; that is, it does not cause double refraction or birefringence.

In 1995, highly efficient laser oscillation using a polycrystalline Nd:YAG ($Y_3Al_5O_{12}$) ceramic material was reported for the first time [1]. Since then, research and development on various types of transparent ceramic materials and their laser oscillation have been successively reported [2]. Generally, ceramic materials are easily influenced by Mie scattering and Rayleigh scattering [3–6] as they contain many grain boundaries which degrade the laser oscillation efficiency and laser beam quality when they are used as a laser gain medium. However, recent studies have revealed that certain types of ceramic materials can provide novel characteristics that cannot be achieved in single crystals [7–9]. Polycrystalline ceramics are anticipated to be widely applied to the field of photonics in addition to laser applications.

The melting point of Tb_2O_3 is very high as 2400 °C. And as seen in the phase diagram shown in Figure 4.1, it appears to undergo phase transitions from an orthorhombic ⇔ cubic crystal system near 1400 °C to an orthorhombic ⇔ hexagonal crystal system near 2100 °C [10,11]. These phase transitions cause volumetric changes in the material and induce mechanical stress, causing cracking problem.

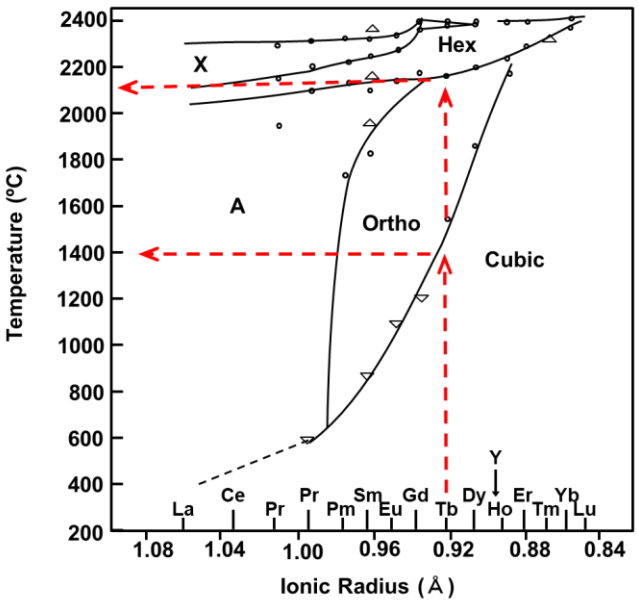

Figure 4.1 Phase diagram for various lanthanide rare earth oxide materials.

Since Tb_2O_3 is not stable at room temperature, when Tb_4O_7 is used as a starting material, oxygen gas is released during the sintering process, i.e., $Tb_4O_7 \rightarrow 2Tb_2O_3 + 1/2O_2$. Due to this reaction, the sintered powder compact is finally broken into pieces. There is almost no possibility to produce this type of material using a conventional fabrication method such as melt growth or sintering technologies. Therefore, in this work, based on the findings obtained in Chapter 2, the synthesis of optical grade $(Tb_xY_{1-x})_2O_3$ (x = 0.5–1.0) (hereafter abbreviated as TYO) ceramics in which the Tb^{3+} site was partially substituted with Y^{3+} was explored, and their magneto-optical characteristics relating to their use in practical application as a Faraday rotator device were extensively studied.

4-2. Experimental procedure

Tb_4O_7 (1 μm, 99.99%, Shin-Etsu Chemical Co., Ltd., Tokyo, Japan) and Y_2O_3 (1 μm, 99.999 %, Shin-Etsu Chemical Co., Ltd., Tokyo, Japan) powders were used as starting materials. Tb_2O_3 (yellowish white color) powders were prepared by heat treating the dark brown Tb_4O_7 raw powders under a hydrogen atmosphere. Ethanol (analytical grade reagent) was used as the solvent. A small amount (0.5–1.5 mass %) of ZrO_2 (TZ-0, 99.9%, TOSOH Corporation, Tokyo, Japan) was used as a sintering aid.

Tb_2O_3 powder was mixed with Y_2O_3 powder in ethanol solvent for 10 hours by a conventional ball-milling process. The obtained slurry was dried and granulated by using a spray-dryer (TRS-4W, Sakamoto Engineering, Kawasaki, Japan). The premixed Tb_2O_3-Y_2O_3 powders were made into tablets using a metal mold (internal diameter: 8 mm) by uniaxial pressing (CDM-5PA, Institute of Physical and Chemical Research (RIKEN), Wako, Japan). Then, the tablets were isostatically pressed in a CIP machine (cold isostatic press, P200, Kobe Steel, Ltd., Tokyo, Japan) with a pressure of 196 MPa. Depending on the Tb doping level, these powder compacts were sintered in a vacuum furnace (W-heater, Special ordered furnace, Futek Furnace Inc., Yokohama, Japan) under a vacuum level of 1×10^{-3} Pa at 1500–1680 °C for 3 hours. Then, the pre-sintered tablets were treated in a HIP (hot isostatic press, SYS50X-SB, KOBE Steel, Ltd., Tokyo, Japan) machine at a temperature range from 1500 to 1700 °C for 2 hours under Ar gas pressure at 176 MPa. The sintering temperature and pressure were adapted in accordance with the Tb content. Transparent ceramics were obtained after the HIP treatment. Their basic optical properties and magneto-optical properties were investigated. The microstructures of the $(Tb_{0.6}Y_{0.4})_2O_3$ and Tb_2O_3 ceramics after HIP treatment were observed by TEM (transmission electron microscopy, ARM-200F, JOEL, Tokyo, Japan). The crystal structure was identified by XRD (X-ray diffraction, X'PERT PRO MPD, Malvern Panalytical, Almelo, Netherland).

To evaluate the Faraday rotation performance, the similar experimental setup reported in the Chapter 2 (see Figure 2.1) was used. Samples of $(Tb_{0.6}Y_{0.4})_2O_3$ ceramics (5 mm in diameter by 8 mm length) and TGG single crystal (5 mm in diameter by 20 mm length, Electro-Optics Technology Inc., Traverse City, MI, USA) with <111> orientation were used. Each sample was clamped in a copper holder and put in a commercial Faraday

rotator magnetic housing. The average magnetic field exerted on the TGG crystal and $(Tb_{0.6}Y_{0.4})_2O_3$ ceramics was 1 T. A polarization plane of laser light was rotated by the Faraday effect due to the magnetic field. The transmitted laser output was measured using a power meter as described in the previous chapters.

4-3. Results

A ceramic fabrication process was applied to produce sintered bodies with a $(Tb_{0.6}Y_{0.4})_2O_3$ composition. Initially, Tb_4O_7 (Shin-Etsu, RU, 99.99 %) and Y_2O_3 (Shin-Etsu, RU, 99.999 %) powders were used as starting materials; they were mixed in ethanol solvent for 10 hours, then the dried premixed powders were pressed in a CIP (Cold Isostatic Press) machine at 196 MPa. The color of the obtained powder compacts was dark brown. Then, the powder compacts were sintered (1) under hydrogen atmosphere and (2) under vacuum (1×10^{-3} Pa) at 1600 °C for 2 hours, separately. In both processes, almost all samples were broken into pieces after sintering in hydrogen, and many cracks occurred after sintering in vacuum.

From the TG-DTA (Thermogravimetry Differential Thermal Analysis, Thermo plus EVO TG8120, RIGAKU Corporation, Tokyo, Japan) analysis result, it was concluded that the following oxygen dissociation reactions occurred during the heating of Tb_4O_7 due to the release of oxygen inside the material when the samples cracked or were crushed into pieces.

$$7Tb_4O_7 \Leftrightarrow 4Tb_7O_{12} + 1/2O_2 \text{ at } 540\ ^\circ C$$

$$2Tb_7O_{12} \Leftrightarrow 7Tb_2O_3 + 3/2O_2 \text{ at } 940\ ^\circ C$$

In order to avoid this cracking problem, Tb_2O_3 (yellowish white color) powders were prepared in advance by heat treating the dark brown Tb_4O_7 raw powders under a hydrogen atmosphere. The fabrication process for TYO ceramics derived from Tb_2O_3 is shown in Figure 4.2 (a). Then, the Tb_2O_3 powder was mixed with Y_2O_3 powder in ethanol solvent for 10 hours by a ball-milling process. The obtained slurry was dried and granulated using a spray-dryer. The premixed Tb_2O_3-Y_2O_3 powders were made into tablets using a metal mold (Φ 8 mm) by uniaxial pressing and a CIP machine with a pressure of 196 MPa. The obtained powder compacts are shown in Figure 4.2 (b). Depending on the content of Tb, these power compacts were sintered under vacuum (1×10^{-3} Pa) conditions at 1500–1680 °C for 3 hours. Then, the pre-sintered tablets were treated by HIP at a temperature range from 1500 to 1700 °C for 2 h under Ar gas pressure at 176 MPa. The sintering temperature and pressure were adapted in accordance with the Tb content. After the HIP treatment, yellowish transparent ceramics were achieved (see Figure 4.2 (c)). The color of the transparent ceramic samples varied with the content of Tb ions. The higher the Tb content was, the deeper the color of the sample. However, when pure Tb_2O_3 was produced, it was colorless and transparent. If there were no sintering aids used, the grain growth was accelerated during sintering, and the sintered sample showed poor translucency or crack formations occurred inside the samples, or it ended up being broken to pieces in the worst case (see Figure 4.2 (d)).

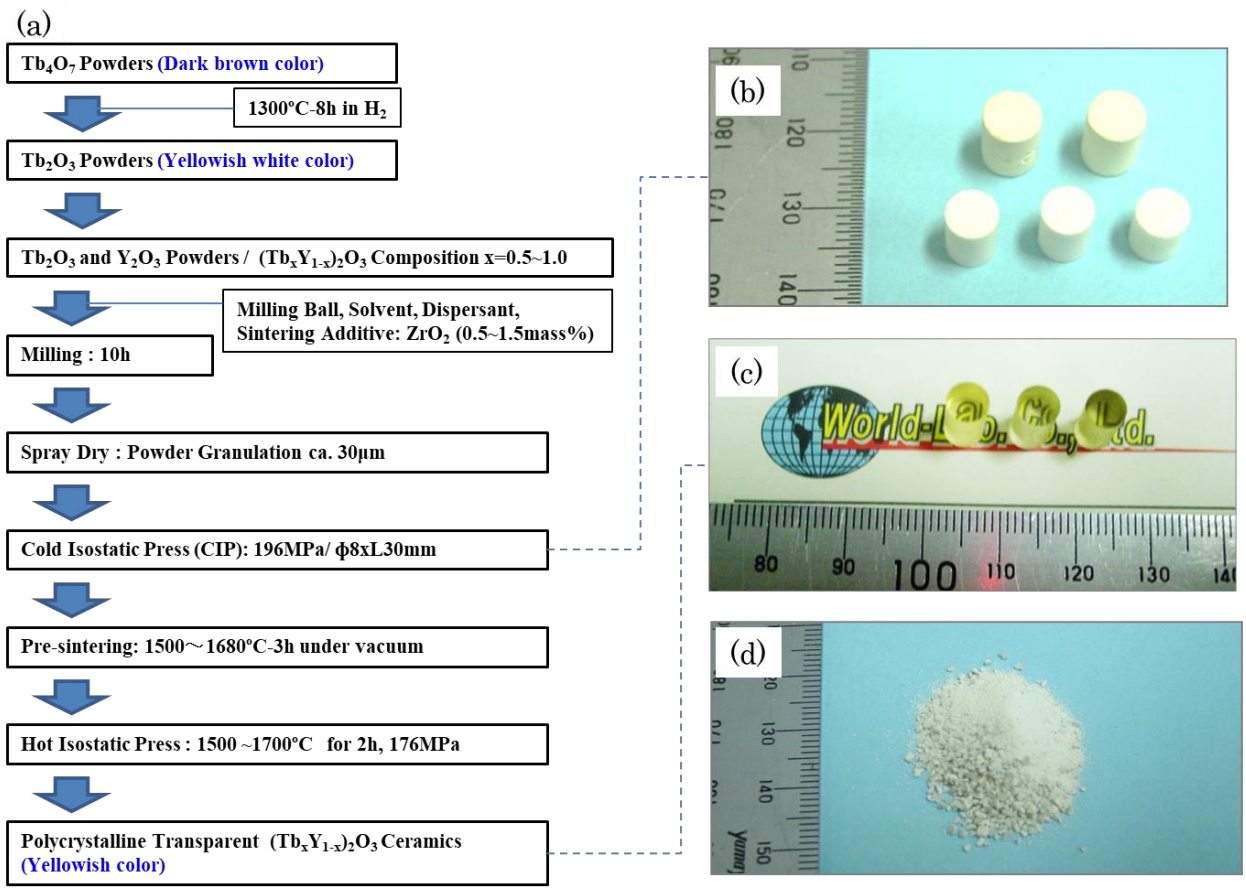

Figure 4.2 (a) Fabrication process for $(Tb_xY_{1-x})_2O_3$ ceramics derived from Tb_2O_3 and Y_2O_3 raw powders; (b) powder compacts after the cold isostatic press (CIP) process; (c) transparent sintered bodies with ZrO_2 additives after hot isostatic press (HIP) treatment; (d) crushed sintered bodies without ZrO_2 additives after sintering.

TEM images of the $(Tb_{0.6}Y_{0.4})_2O_3$ and Tb_2O_3 ceramics after HIP treatment are shown in Figure 4.3 (a). It was confirmed that both ceramics were composed of fine grains of several micrometers with different crystal orientations, and neither secondary phases nor grain boundary phases were observed. A lattice structure of bixbyite and a clean grain boundary structure were observed. Figure 4.3 (b) shows the transmission polarized optical microscopic images of the $(Tb_{0.6}Y_{0.4})_2O_3$ and Tb_2O_3 ceramics. There was no birefringence, and they were optically homogeneous. No residual pores, the main factor in optical scattering, were detected inside the materials. Results of XRD analysis revealed that the crystal system was only cubic phase and there were no other phases. When these ceramics were heat treated above 1400 °C, an orthorhombic ⇔ cubic phase transition occurred and the general optical quality was degraded. As seen in the above TEM images, the microstructures of the developed TYO ceramics were of a high-quality finished form.

It was anticipated that the added ZrO_2 would play an important role in inhibiting grain growth during the sintering of TYO ceramics; hence, the sintered bodies were composed of fine grains. Accordingly, (1) damage

due to phase transition was effectively reduced by forming numerous grain boundaries, or (2) ZrO_2 itself possibly inhibited the phase transition. In the case of TYO ceramics without the addition of ZrO_2, the optical quality of the sample was very poor due to the significant grain growth during the sintering process or the sample got to be broken into pieces.

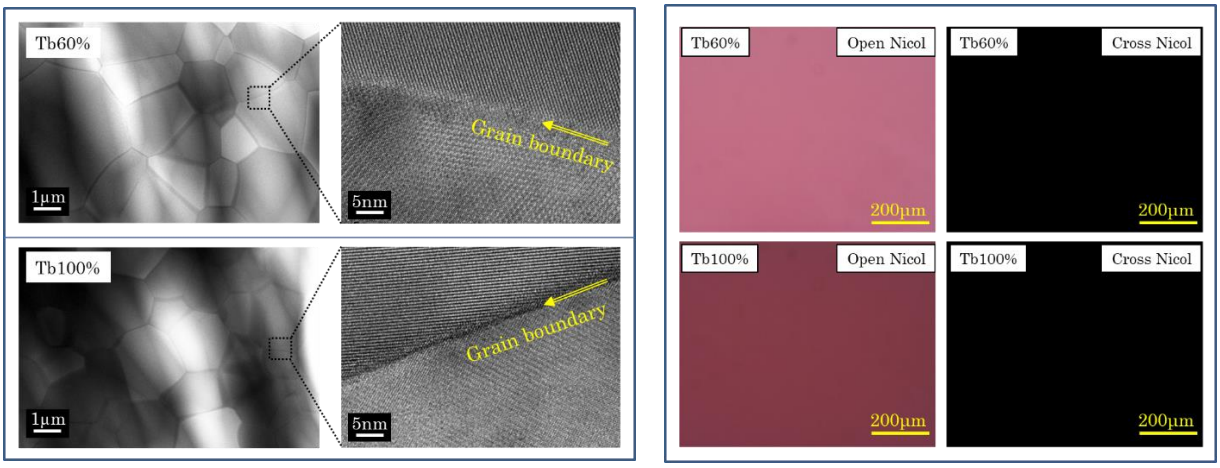

(a) **(b)**

Figure 4.3 (a) TEM images, and (b) transmission polarized optical microscopic images of $(Tb_{0.6}Y_{0.4})_2O_3$ and Tb_2O_3 ceramics after HIP treatment.

The in-line transmittance curves of the $(Tb_{0.6}Y_{0.4})_2O_3$ (Tb 60%) and Tb_2O_3 (Tb 100%) ceramics from the visible to near-infrared wavelength regions are shown in Figure 4.4. The thickness of each sample was 5 mm, and the surfaces were optical polished but without AR (anti-reflective) coating. Only absorption due to Tb^{3+} ions can be confirmed around 480 nm, and the absorption of Tb 100% was stronger than that of Tb 60%. Wavelength dependency of the transmission lines was not detected for both ceramics, suggesting no Rayleigh scattering inside the materials. The refractive indices of Tb 60% and Tb 100% materials at a 1μm wavelength are 1.920 and 1.940, respectively. The surface reflection loss (Fresnel loss) at a surface against air can be calculated by the following equation:

$$\beta(\lambda) = [(n(\lambda) - 1)^2]/[(n(\lambda) + 1)^2], \quad (4.1)$$

where $\beta(\lambda)$ is a reflection loss and n is a refractive index. Accounting for both sides of a sample, this Fresnel loss value is doubled to obtain theoretical transmittance. Their measured transmittance values, especially at a 1 μm wavelength, were very close to the theoretical values calculated by subtracting the Fresnel loss due to surface reflection. This result indicates that their optical losses are very low. An external view, polarized image, Schlieren image, and wavefront image by interferometry of the $(Tb_{0.6}Y_{0.4})_2O_3$ and Tb_2O_3 ceramics are shown in Figure 4.5 (a). The thickness of each sample was 11 mm. No optical inhomogeneity was observed in any inspection methods. The wavefront distortion was less than λ/10, suggesting that the ceramics are well suited for use as optical materials.

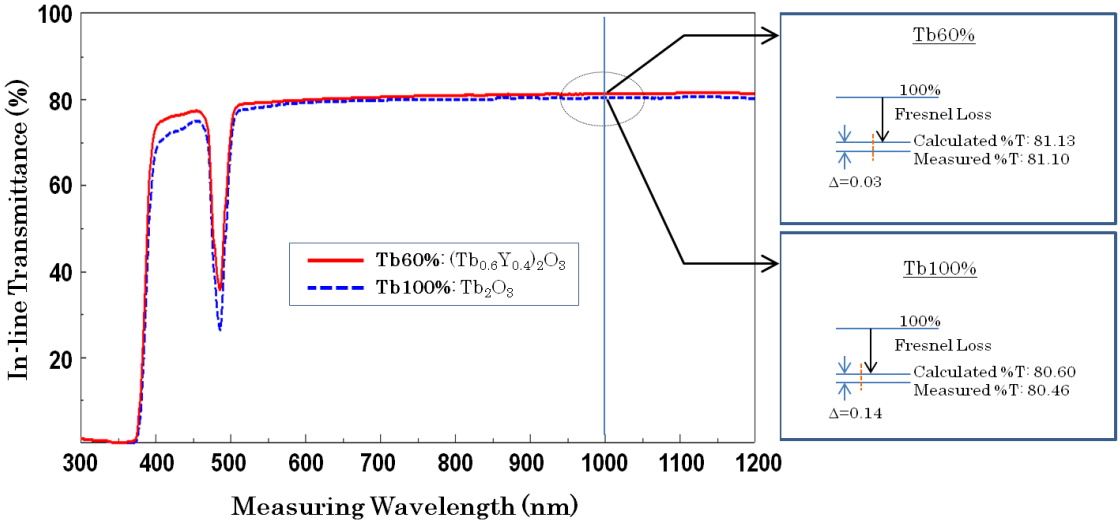

Figure 4.4 In-line transmittance curves of the $(Tb_{0.6}Y_{0.4})_2O_3$ and Tb_2O_3 ceramics (Sample thickness = 5 mm, optical-polished surfaces).

(a)

	External view	Polarized Image	Schlieren Image	Wavefront Image
Tb60%	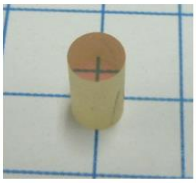	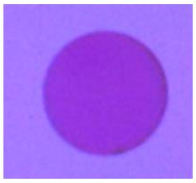	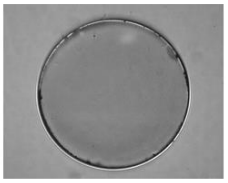	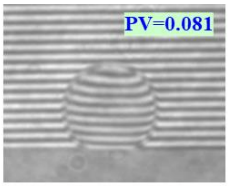
Tb100%	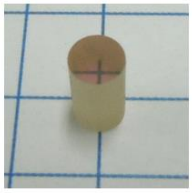	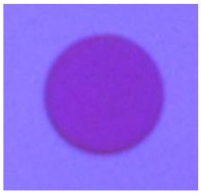	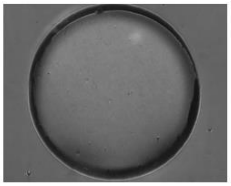	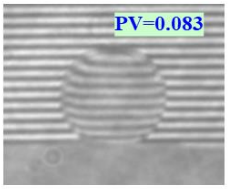

(b)

Original Beam Pattern 1064nm (30mW)	After passing samples (AR coated)		
	Via. TGG Single crystal	Via. $(Tb_{0.6}Y_{0.4})_2O_3$ ceramics	Via. Tb_2O_3 ceramics
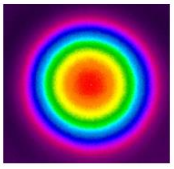	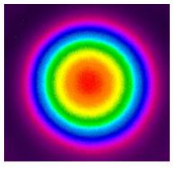	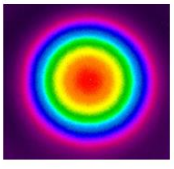	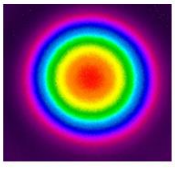

Figure 4.5 (a) External view, polarized image, Schlieren image, and wavefront image by interferometry of the $(Tb_{0.6}Y_{0.4})_2O_3$ and Tb_2O_3 ceramics. (The thickness of each sample was 11 mm.) (b) Original beam pattern and beam patterns after passing through the TGG single crystal and the produced $(Tb_{0.6}Y_{0.4})_2O_3$ and Tb_2O_3 ceramics.

A laser with an output power of 30 mW (1064 nm wavelength, beam spot size: 2 mm) and with a TEM_{00} mode was used as a light source to evaluate the beam quality after passing through the sample. For comparison, a commercially available TGG single crystal was also measured as a reference. The original beam pattern and those after passing through the TGG single crystal and the produced $(Tb_{0.6}Y_{0.4})_2O_3$ and Tb_2O_3 ceramics are compared and summarized in Figure 4.5 (b). The original beam pattern was in the Gaussian mode, and the beam patterns that passed through the TGG single crystal, $(Tb_{0.6}Y_{0.4})_2O_3$, and Tb_2O_3 ceramics were almost unchanged. This result suggested that the variation of the refractive index inside the material is extremely small, which is in accordance with the measured results shown in Figure 4.5 (a).

When a laser with an output power of 50 W laser (1070 nm wavelength, CW (continuous wave) single-mode ytterbium fiber laser manufactured by IPG photonics corp., Burbach, Germany) was used as a light source, the beam shape after passing through the $(Tb_{0.6}Y_{0.4})_2O_3$ sample was slightly deformed due to the thermal lens effect ($1/f = 0.40\ m^{-1}$: change in beam waist of passed laser beam). When the same measurement method was used, the value for TGG crystal was $1/f = 0.35\ m^{-1}$, which is slightly better than that for the $(Tb_{0.6}Y_{0.4})_2O_3$ ceramics. However, in the case of Y_2O_3 ceramics which have similar optical loss, the value of thermal lens effect was $1/f = 0.34\ m^{-1}$. As seen in the external views of the samples shown in Figures 1(c) and 4(a), it is considered that a trace amount of Tb^{4+} ions remained in the $(Tb_{0.6}Y_{0.4})_2O_3$ ceramics, and optical absorption by these Tb^{4+} ions caused the thermal lens effect during laser irradiation. In addition, it was also confirmed that the material was not damaged by a power handling test which is generally used for commercial isolators developed for fiber lasers. In this test, a pulsed laser (pulse width 50 ps, peak power 0.3 MW, beam spot Φ 0.7 mm, power density 78 MW cm^{-2}) was irradiated at 2 MHz for 7000 h. In addition, when a laser damage test using an Nd:YAG laser with a wavelength of 1064 nm, a pulse width of 4 ms, and a laser focusing diameter of Φ 50 μm was performed, TYO ($(Tb_{0.6}Y_{0.4})_2O_3$) and TGG single crystal were damaged at an average power of 18 and 10 J cm^{-2}, respectively. From this result, it was also confirmed that the damage threshold of TYO ceramics is excellent, and the only technical issue is to reduce the thermal lens effect faintly generated during laser irradiation.

The wavelength dependencies of the Verdet constant for the TGG single crystal and the $(Tb_{0.6}Y_{0.4})_2O_3$ and Tb_2O_3 ceramics measured at wavelengths 633, 800, 980, 1030, and 1064 nm are shown in Figure 4.6 (a). At any wavelengths, the Verdet constants of $(Tb_{0.6}Y_{0.4})_2O_3$ and Tb_2O_3 ceramics were about two times higher than that of the TGG single crystal. In particular, in the case of the Tb_2O_3 ceramics, the Faraday rotation angle was found to be about 3.8 times (as a maximum) higher than that of the TGG single crystal. The relationship between the concentration of Tb ions (i.e., the occupancy of Tb^{3+} ions in the total number of cations) in TYO ceramics with a bixbyite structure and the Verdet constant for 1 μm wavelength is shown in Figure 4.6 (b). The Verdet constants of Faraday rotator materials with other crystal structures are also plotted in the same figure as a reference. The Verdet constant simply increased with increasing Tb ion concentration and reached 154 rad $T^{-1}\ m^{-1}$ as the highest value. As the Verdet constant increases, the required length of the Faraday rotator can be reduced.

In the case of paramagnetic materials, the required length of the Faraday elements such as TGG single crystal and TYO ceramics to provide a 45 ° Faraday rotation angle depends on the strength of applied magnetic field. In the case of TGG single crystal, a length of 20 mm is required to obtain a 45 ° Faraday rotation angle when 1 T of magnetic field is applied. By using the ceramics with the highest Verdet constant, the length can be shortened to 5.1 mm to obtain a 45 ° Faraday rotation angle under the given magnetic field, suggesting that the Faraday rotator device can be manufactured with a very compact size, whereas a commercial TGG crystal requires a length of about 20 mm. As seen in Figure 4.6 (b), TYO ceramics with a bixbyite structure showed very high Verdet constants against Tb concentration (i.e., Tb ion number per total cation number) compared to other Faraday rotator materials such as TGG [12], TSAG [13], TAG [14], NTF ($Na_{0.37}Tb_{0.63}F_{2.26}$) [15,16], KTF ($KTb_3F_{10}$) [17], and TTO ($Tb_2Ti_2O_7$) [18].

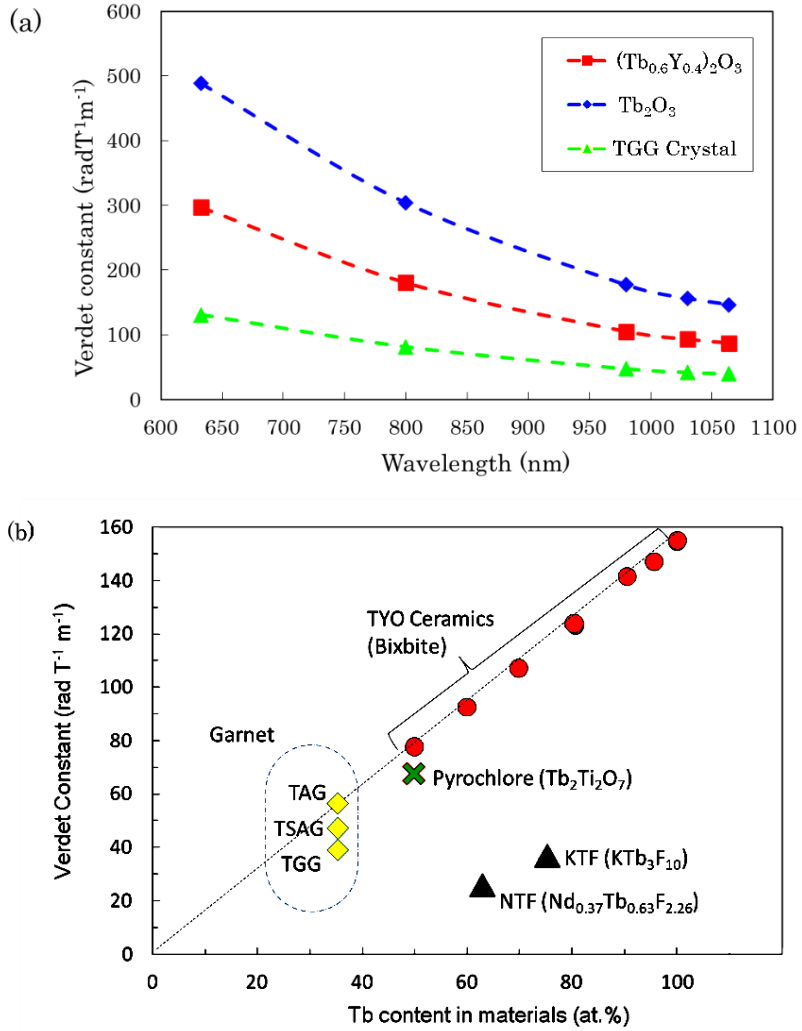

Figure 4.6 (a) Wavelength dependency of the Verdet constant for the TGG single crystal and the $(Tb_{0.6}Y_{0.4})_2O_3$ and Tb_2O_3 ceramics. (b) Relationship between the concentration of Tb ions in $(Tb_xY_{1-x})_2O_3$ ceramics and Verdet constant for 1 μm wavelength.

The measured results for transmitted laser power against the rotation angle of the polarizer under a 1 T magnetic field are shown in Figure 4.7. The Faraday rotation characteristics of the $(Tb_{0.6}Y_{0.4})_2O_3$ ceramics with very high Verdet constant were analogous to those of the commercial TGG single crystal, and their transmitted laser power values at a 45 ° rotation angle of the polarizer were comparable to each other (insertion loss: 0.04 dB). Compared with the maximum extinction ratio (E.R.) of the TGG single crystal (E.R.: 35 dB) where the rotation angle of polarizer was at −45 °, the extinction ratio for the $(Tb_{0.6}Y_{0.4})_2O_3$ ceramics was as high as 42 dB. These materials with a very high Verdet constant can provide an equivalent Faraday rotation angle and a high extinction ratio even from a half-length (8.0 mm) of the conventional TGG single crystal (length: 20 mm). In other words, an advantage to replacing existing Faraday rotators with a high-Verdet-constant Faraday rotator is that if the length is kept the same size as the conventional single crystal, the required magnetic field can be reduced by more than half. In the case of Tb_2O_3 ceramics, principally it can be reduced to about one-fourth to obtain the same Faraday rotation performance as $(Tb_{0.6}Y_{0.4})_2O_3$ ceramics. The Tb_2O_3 ceramic (t = 5.1 mm), which had the highest Verdet constant, also showed similar behavior to TGG crystal, its insertion loss (I.L.) was 0.19 dB at a 45 ° rotation angle of the polarizer, and its extinction ratio was 47 dB at a – 45 ° or 135 ° rotation angle of the polarizer.

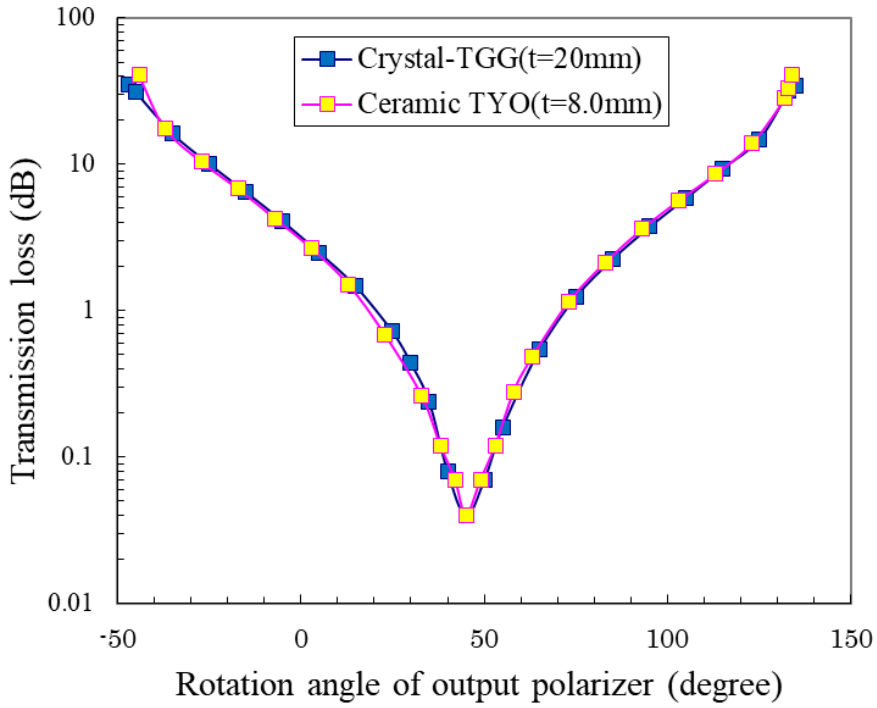

Figure 4.7 Faraday rotation characteristics of the TYO ceramics in comparison with those of the commercial TGG single crystal.

4-4. Discussion

The magneto-optical performance represented by the Verdet constant of Faraday rotator materials for the visible to 1.2 μm wavelength regions is not high enough since they do not include the magnetic element Fe in the composition of the materials. Although TAG [19–21] or TGG [12] single crystal has been commonly used there, their Verdet constants are limited, and there is practically no other material which possesses a higher Verdet constant. It is very difficult to grow TAG single crystals by the CZ (Czochralski) method with acceptable aperture size because of their incongruent melting nature and unstable TAG phase in the Tb_2O_3-Al_2O_3 system [20]. The FZ (floating zone) method has often been used to grow TAG crystal, but its application is limited to research purposes only. Recently, there has been several reports on the TGG and TAG polycrystalline ceramics [22-26], but these do not exceed the conventional single-crystal Faraday rotator in terms of fundamental performance. The authors have demonstrated high-quality $(Tb_{1-x}Y_x)_3Al_5O_{12}$ (TAG) ceramics showing superior optical properties than the TAG single crystals prepared by the FZ method. It is the only example that has solved the problems relating to TAG single crystals and the performance of the conventional TGG single crystal.

In order to obtain a 45 ° Faraday rotation angle using a conventional single crystal under 1 T magnetic field, the rotator material needs to be as long as 20 mm; hence, a larger magnet is needed to supply a large enough magnetic field. Basically, the value of the Faraday rotation angle of the Faraday rotator is defined by the value of the Verdet constant, and the Verdet constant is determined dominantly by the occupancy of Tb ions which contributes to the magneto-optical effect, i.e., the Ga ions in TGG do not contribute to the Faraday rotation. TAG and TGG both have a garnet structure; hence, the occupancy of Tb^{3+} ions (Tb/(Tb+Al)) in the total number of cations is limited to 37.5 %. Accordingly, garnet materials are not sufficient to achieve large Faraday rotation from the viewpoint of Tb^{3+} ion occupancy.

Based on the above viewpoint, Tb_2O_3 material may result in the highest occupancy of Tb^{3+} ions. However, since the melting point of Tb_2O_3 in its phase diagram is above 2300 °C and it has a phase transition from an orthorhombic ⇔ cubic crystal system near 1400 °C to an orthorhombic ⇔ hexagonal crystal system near 2100 °C [10,11], it is theoretically impossible to grow Tb_2O_3 single crystals by the conventional melt growth process. It was verified that the polycrystalline TYO (including Tb_2O_3) ceramics have appropriate properties as an efficient optical isolator. Moreover, the fabrication process is economically efficient. Hence, we filed a patent on the TYO ceramics in 2011 [27]. In 2015, light-yellow-colored Tb_2O_3 single crystals grown by using a $Li_6Tb(B_2O_3)_3$ system were reported with a low melting point flux around 1235–1160 °C, which is lower than the phase transition points [28]. However, the resulting crystal size was about 5 mm × 5 mm × 1 mm, which is too small for practical applications. Furthermore, optical quality was discussed there only by means of transmission curves, which are not enough to evaluate the opacity of thin film. The scattering loss of this material has been roughly estimated to be as large as around 10 % per pass which requires a rotator length of 5.1 mm from the Verdet constant. In addition to this, it is not possible to control the crystal orientation, i.e., axis of easy

magnetization, during crystal growth. Snetkov et al. synthesized Tb^{3+}:Y_2O_3 ceramics [29] but the transparency of their material is extremely poor, and it cannot be used for optical applications. Although the basic characteristics of the TYO ceramics were reported in our previous paper [30], it is important to demonstrate the total performance parameters which are required as a practical Faraday rotator material.

On the other hand, optical-grade YAG ($Y_3Al_5O_{12}$) and sesquioxide ceramics denoted by Re_2O_3 (Re: lanthanide rare-earths) have been reported recently. Basically, a small amount of laser active elements is doped into the Re_2O_3 host materials (Re: Sc, Y, Lu) which do not have phase transition points up to 2000 °C. Then they are sintered at high temperature (over 1700 °C) to produce transparent ceramic materials. It has been confirmed that those materials are suited to laser gain media or scintillators, etc. [31,32]. It has been found that the Tb-containing materials with composition TYO can solve the technical difficulties of the conventional isolators. Here, it is necessary to increase the content of Tb ions in the solid solution as high as possible. However, a technical issue there is that the fabrication temperature needs to be decreased with increasing Tb ion content in the solid solution. In particular, the ultimate material, Tb_2O_3, has very low phase transition temperature; hence, it is necessary to fabricate even Tb_2O_3 polycrystalline ceramics at temperatures lower than 1400 ºC. In this chapter, it was demonstrated that densifying the materials is very important to be improved to high transparency, and the possibility of their applications to optical isolators were discussed.

The question arises as to why single crystals have only been used as Faraday rotators so far. The reason for this is that optical scattering loss is small in single crystals and a uniform Faraday rotation angle can be achieved when a magnetic field is applied to a unidirectionally oriented crystal (<111> in general). It is well known that even a cubic crystal system has magneto-crystalline anisotropy. For example, in the case of TSAG (Terbium-Scandium-Aluminum Garnet) crystal, the Verdet constant of the <111> orientation, which has the smallest surface energy, is about 5–7 % larger than that of the <110> or <100> orientation [33]. It is anticipated that the Verdet constants of other crystal orientations in a cubic system, which have higher surface energy, will be smaller than that of the <111> orientation. Consequently, it is likely that the Verdet constant of polycrystalline ceramics composed of numerous microcrystallites with random crystal orientations might be different from one grain to another, and the Faraday rotation behavior of polycrystalline ceramics might be different from that of single-crystal Faraday rotator materials. However, this difference did not cause any disadvantages upon utilization. When they were compared to the TGG single crystalline materials, it was confirmed that the TYO ceramics have equivalent values of the Faraday rotation angle and higher extinction ratios. In addition, this study has revealed the discovery of a novel Faraday rotator material which possesses a Verdet constant approximately 4 times higher than that of the commercial TGG single crystal.

4-5. Summary

Since the Faraday effect was discovered in 1845, a wide variety of Faraday rotator materials, such as glass or single crystal, have been developed and have progressed into the practical phase with developments in the field of telecommunication and machining. Only single-crystal materials have been put into practical use until now, but this does not necessarily mean that Faraday rotator materials are only limited to single crystals. As this work demonstrated, it is also possible to create new materials with excellent performance by other inorganic material processes such as ceramic fabrication processes. Optical-grade TYO ceramics were successfully produced in this work, and their total performances as a Faraday rotator are summarized as follows;

1. Optical-grade polycrystalline TYO ceramics with extremely low scattering were successfully produced for the first time.
2. The Verdet constants of the TYO ceramics increased with increasing Tb concentration in the bixbyite structure, and Tb_2O_3 showed the highest value: 3.8 times higher than that of the commercially available TGG single crystal.
3. The Faraday rotation characteristics of the polycrystalline TYO ceramics were basically comparable to those of single-crystal isolator materials. In addition, there were some advantages such as a large extinction ratio and a large Verdet constant, which can improve the performance of the isolator and downsize the device.
4. The laser damage threshold of the TYO ceramics was as high as 18 J cm^{-2} and they were resistant to pulsed laser damage (power density 78 MW cm^{-2} and no damage during a 7000-hour durability test at 2 MHz).
5. The value of thermal lens effect, $1/f = 0.40\ m^{-1}$, of the TYO ceramics was slightly larger than that of TGG, probably due to a remaining trace amount of Tb^{4+} ions in the material. One of the remaining issues is to be able to use it for high-power and continuous-wave laser applications.

References

1. A. Ikesue, T. Kinoshita, K. Kamata, K. Yoshida, “Fabrication and Optical Properties of High-Performance Polycrystalline Nd:YAG Ceramics for Solid-State Lasers”, J. Am. Ceram. Soc.,**78**, 1033-1040 (1995).

2. J. Sanghera, W. Kim, G. Villalobos, B. Shaw, C. Backer, J. Frantz, B. Sadowski, I. Aggarwal, “Ceramic Laser Materials”, Mater., **5**, 258-277 (2012).

3. R. M. Yamamoto, B. S. Bhachu, K. P. Cutter, S. N. Fochs, S. A. Letts, C. W. Parks, M. D. Rotter, T. F. Soules, “The Use of Large Transparent Ceramics in a High Powered, Diode Pumped Solid State Laser”, Proceed. of Adv. Solid-State Phot., pp. WC5 (2008).

4. M. Tokurakawa, K. Takaichi, A. Shirakawa, K. Ueda, H. Yagi, S. Hosokawa, T. Yanagitani, A. A. Kaminskii, “Diode-pumped mode-locked Yb^{3+}:Lu_2O_3 Ceramic Laser”, Opt. Express **14**, 12832-12838 (2006).

5. A. T. Young, “Rayleigh scattering”, Appl. Opt., **20** [4], 533-535 (1981).

6. J. Strutt, “On the scattering of light by small particles”, Philos. Mag., **41**, 447-454, (1871).

7. A. Ikesue, Y. L. Aung, T. Taira, T. Kamimura, K. Yoshida, G. L. Messing, “Progress in Ceramics Lasers”, Annu. Rev. Mater. Res., 36, 397–429 (2006).

8. L. B. Kong, Y. Huang, W. Que, T. Zhang, S. Li, J. Zhang, Z. Dong, D. Tang, “Transparent Ceramics”, In Mining, Metallurgy and Material Engineering; Bergmann, C.P., Ed.; Springer: Berlin/Heidelberg, Germany, (2015).

9. A. Ikesue, Y. L. Aung, “Ceramic Laser Materials”, Nat. Photonics, **21**, 721-726 (2008).

10. G. Adachi, “Physics and Chemistry of Yttrium Compounds”, Bull. Ceram. Soc. Jpn., **23**, 430-437 (1988).

11. J. P. Coutures, R. Vegers, M. Foex, “Comparison of solidification temperatures of different rare earth sesquioxides; effect of atmosphere”, Rev. Int. Hautes Temp. Refract., **12**, 181-185 (1975).

12. N. P. Barnes, L. B. Petway, “Variation of the Verdet Constant with Temperature of Terbium Gallium Garnet”, J. Opt. Soc. Am. B, **9**, 1912–1915 (1992).

13. R. Yasuhara, I. Snetkov, A. Starobor, E. Mironov, O. Palashov, “Faraday rotator based on TSAG crystal with <001> orientation”, Opt. Express, **24**, 15486-15493 (2016).

14. Y. L. Aung and A. Ikesue, “Development of Optical Grade $(Tb_xY_{1-x})_3Al_5O_{12}$ Ceramics as Faraday Rotator Material”, J. Am. Ceram. Soc. **100** [9], 4081-4087 (2017).

15. E. A. Mironov, O. V. Palashov, A. V. Voitovich, D. N. Karimov, and I. A. Ivanov, “Investigation of Thermo-Optical Characteristics of Magneto-Active Crystal $Na_{0.37}Tb_{0.63}F_{2.26}$”, Opt. Lett., 40, 4919-4922 (2015).

16. D. N. Karimov, B. P. Sobolev, I. A. Ivanov, S. I. Kanorsky, A. V. Masalov, “Growth and Magneto-Optical Properties of $Na_{0.37}Tb_{0.63}F_{2.26}$ Cubic Single Crystal”, Crystallogr. Rep., 59, 718-723 (2014).

17. K. T. Stevens, W. Schlichting, G. Foundos, A. Payne, E. Rogers, “Promising Materials for High Power Laser Isolators”, Laser Tech. J., **3**, 18-21 (2016).

18. F. Guo, Y. Sun, X. Yang, X. Chen, B. Zhao, N. Zhuang, J. Chen, “Growth, Faraday and inverse Faraday characteristics of $Tb_2Ti_2O_7$ crystal”, Opt. Express, **24**, 5734-5743 (2016).

19. A. Yoshikawa, Y. Kagamitani, D.A. Pawlak, H. Sato, H. Machida, T. Fukuda, “Czochralski Growth of $Tb_3Sc_2Al_3O_{12}$ Single Crystal for Faraday Rotator”, Mater. Res. Bull., **37**, 1-10 (2002).

20. M. Geho, T. Takagi, S. Chiku, T. Fujii, “Development of Optical Isolators for visible light using Terbium Aluminum Garnet ($Tb_3Al_5O_{12}$) Single Crystals”, Jpn. J. Appl. Phys., **44**, 4967-4970 (2005).

21. S. Ganschow, D. Klimm, P. Reiche, R. Uecker, “On the Crystallization of Terbium Aluminum Garnet”, Cryst. Technol., 34, 615–619 (1999).

22. H. Yoshida, K. Tsubakimoto, Y. Fujimoto, K. Mikami, H. Fujita, N. Miyanaga, H. Nozawa, H. Yagi, T. Yanagitani, Y. Nagata, H. Kinoshita, “Optical Properties and Faraday Effect of Ceramic Terbium Gallium Garnet for a Room Temperature Faraday Rotator”, Opt. Express, **19** [16] 15181-15187 (2011).

23. R. Yasuhara, S. Tokita, J. Kawanaka, T. Kawashima, H. Kan, H. Yagi, H. Nozawa, T. Yanagitani, Y. Fujimoto, H. Yoshida, M. Nakatsuka, “Cryogenic temperature characteristics of Verdet constant on terbium gallium garnet

ceramics", Opt. Express, **15**, 11255-11261 (2007).

24. R. Yasuhara, I. Snetkov, A. Starobor, D. Zheleznov, O. Palashov, E. Khazanov, H. Nozawa, T. Yanagitani, "Terbium gallium garnet ceramic Faraday rotator for high-power laser application", Opt. Lett., **39**, 1145-1148 (2014)

25. D. Zheleznov, A. Atarobor, O. Palashov, C. Chen, S. Zhou, "High Power Faraday Isolators based on TAG Ceramics", Opt. Express, **22**, 2578–2583 (2014).

26. D. Zheleznov, A. Atarobor, O. Palashov, H. Lin, S. Zhou, "Improving Characteristics of Faraday Isolator based on TAG Ceramics by Cerium Doping", Opt. Lett., **39**, 2183–2186 (2014).

27. S. Makikawa, A. Yahagi, A. Ikesue, "Transparent Ceramic, Method for Manufacturing Same, and Magneto-Optical Device", U.S. Patent 9,470,915, 10 October (2016).

28. P. Veber, M. Velazquez, G. Gardet, D. Rytz, M. Peltz, R. Decourt, "Fluxgrowth at 1230 °C of Cubic Tb_2O_3 Single Crystals and Characterization of their Optical and Magnetic Properties", Cryst. Eng. Commun., **17**, 492–497 (2015).

29. I. L. Snetkov, D.A. Permin, S.S. Balabanov, O. V. Palashov, "Wavelength Dependence of Verdet constant of Tb^{3+}:Y_2O_3 Ceramics", J. Appl. Phys. Lett., 108, 161905 (2016).

30. A. Ikesue, Y. L. Aung, S. Makikawa, A. Yahagi, "Polycrystalline $(Tb_xY_{1-x})_2O_3$ Faraday Rotator", Opt. Lett., **42**, 4399–4401 (2017).

31. L. Wang, H. Huang, D. Shen, J. Zhang, H. Chen, Y. Wang, X. Liu, D. Tang, "Room Temperature continuous-wave Laser Performance of LD pumped Er:Lu_2O_3 and Er:Y_2O_3 Ceramics at 2.7 μm", Opt. Express, **22**, 19495–19503 (2014).

32. G. A. Newburgh, A. Word-Daniels, A. Michael, L. D. Merkle, A. I. M. Dubinskii, "Resonantly Diode-Pumped Ho^{3+}:Y_2O_3 Ceramic 2.1μm Laser", Opt. Express, **19**, 3604 (2011).

33. Y. Kagamitani, D. A. Pawlak, H. Sato, A. Yoshikawa, J. Martinek, H. Machida, T. Fukuda, "Dependence of Faraday Effect on the Orientation of Terbium- Scandium- Aluminum Garnet Single Crystal", J. Mater. Res., , 19, 579–583 (2004).

Chapter 5 Development of High Performance Magneto-optical Dy_2O_3 Ceramics with Optical Grade

5-1. Introduction

From the results discussed in Chapters 2 to 4, in order to enhance the magneto-optical performance of the non-magnetic Faraday rotating element (especially the improvement of Verdet constant), it is necessary to explore novel materials other than garnet composition, and further to maximize the concentration of magnetic active Tb^{3+} ion. It was also proved that bixbyite structure is the most promising crystal structure, and Tb_2O_3 showed the highest Verdet constant. In lanthanide series in periodic table, the atomic number of Dy (Dysprosium) is 66 and considering the electronic structure (configuration of f-electron spin), Dy_2O_3 can be a promising Faraday rotator material with the second highest Verdet constant next to the Tb_2O_3. However, the Dy_2O_3 ceramics developed up to now have extremely low optical performance [1-3] and cannot be practically applied to the optical isolator. Therefore, the purpose of this study was to develop high performance magneto-optical Dy_2O_3 ceramics with optical grade by sintering process.

5-2. Experimental Procedure

Dy_2O_3 powder (purity 99.99%, particle size 0.5 μm, commercially available) was used as starting materials, and 0.1% high-purity ZrO_2 (purity 99.9%, particle size 30 nm, commercially available) was added as a sintering aid to suppress grain growth during sintering. Then, PVA (polyvinyl alcohol) was added as a binder, and ball milling was done for 10 hours using ZrO_2 balls as a grinding medium in an ethanol solvent. The obtained slurry was dried on a hot-plate magnetic stirrer, and the obtained powder was molded into green powder compacts with different lengths (< 45 mm) using a metal mold (Φ8 mm), and additionally pressed in CIP (cold isostatic pressing) machine at 98 MPa. These samples were calcined at 800 °C, and pre-sintered at 1550 °C for 2 hours under a vacuum of 1×10^{-3} Pa to reach relative density approximately 98%. Then, these pre-sintered samples were subjected to HIP (hot isostatic pressing) treatment under the condition of 1500 °C for 3 hours (Ar gas pressure at 176 MPa) and transparent sintered bodies were obtained.

Microstructural observations of the ceramic materials were performed using a reflection, transmission, and polarization optical microscope (BX-50, Olympus Co., Tokyo, Japan). Polarizer (SVP-200, Toshiba Co., Tokyo, Japan) was used for birefringence measurement of the whole material, and a photo-spectrometer (V670, JASCO Co., Tokyo, Japan) was used for transmittance measurement. In order to measure the optical quality of the material, TEM_{00} mode (Traverse Electro-Magnetic Wave, Single Mode) laser with a wavelength of 633 nm was irradiated into the polished Dy_2O_3 ceramics, and the beam shape before and after irradiation was observed with a beam profiler (SP620U, Ophir-Spiricon, LLC, Logan, USA). The Verdet constant and extinction ratio of the material at a wavelength of 633 nm were measured with a measuring device similar to that described in Chapter 2.

5-3. Results and discussion

Figure 5.1 (a) is a photograph of the appearance of the obtained 4 x 4 x 15 mm size Dy_2O_3 ceramics. As seen in this photo, it has a yellowish green color and very high transparency. Figure 5.1 (b) shows a distant landscape seen through the Dy_2O_3 ceramics of Φ6 x L30 mm, and a building several kilometers far away can be clearly observed. Original laser beam pattern of the TEM_{00} mode He-Ne laser having a wavelength of 633 nm and the laser beam pattern having passed through a 15 mm thick sample shown in Figure 5.1 (a) with AR (anti-reflection) coated are compared in Figure 5.1 (c). There is no significant difference in the two beam patterns, which is also an evidence that the optical homogeneity inside the material is excellent.

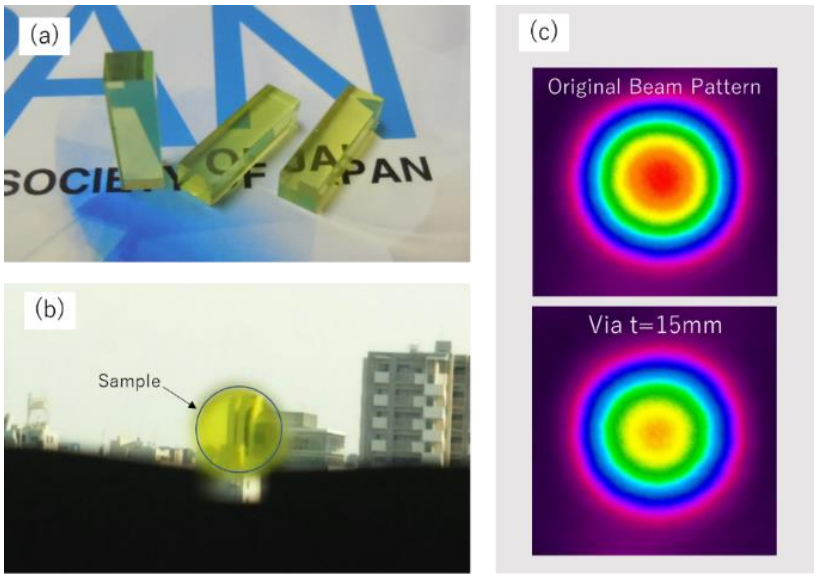

Figure 5.1 (a) Appearance of the produced Dy_2O_3 ceramics, (b) outside view via the Dy_2O_3 ceramics with 15mm thick, and (c) laser beam pattern passed through a specimen with 15mm thickness, and original beam as a reference by beam profiler.

Samples with different thickness (Φ6 x t1 mm and t7 mm) were observed under a polarizer with two polarizing plates crossed over these samples, and the results are shown in Figure 5.2. Only a dark field was confirmed, and birefringence was not recognized qualitatively inside the materials.

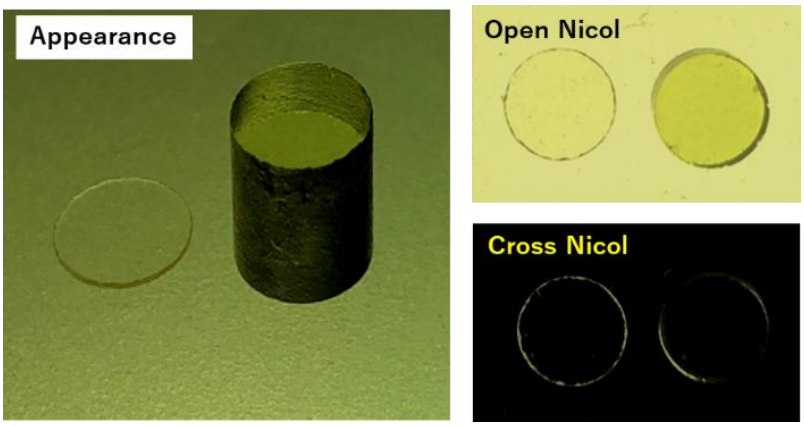

Figure 5.2 Observation under polarizer for the produced Dy_2O_3 ceramics.

Figure 5.3 (a) is a reflection micrograph of a polished Dy_2O_3 ceramic sample that was thermally etched, and it was observed that the transparent Dy_2O_3 ceramics consisted of uniform grains of 2~3 μm, and there were no pores on the surface. Figures 5.3 (b) and 5.3 (c) are transmission and transmission polarizing optical microscopic photographs, respectively. In a transmission microscope observation on the 4 x 4 x 15 mm sample, there are no scattering sources such as a single pore or inclusions that may cause Mie scattering. In addition, since it is a dark field in polarized light observation, there is no cause of optical anisotropy such as a grain boundary phase even on a microscale. Therefore, the Dy_2O_3 ceramics obtained are optically isotropic, and there is no segregation of ZrO_2 which was added as a sintering aid.

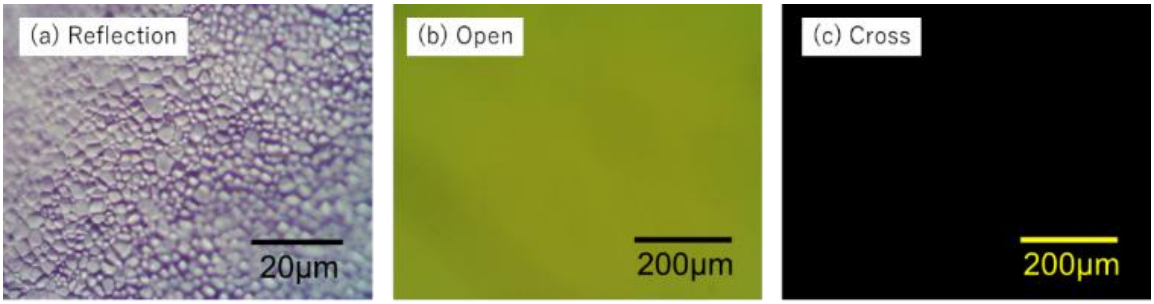

Figure 5.3 (a) Reflection, (b) transmission (open nicol) and (c) transmission (crossed nicol) polarizing optical micrographs of Dy_2O_3 ceramics.

Figure 5.4 shows the transmission spectra of Dy_2O_3 ceramics with thicknesses of 7 and 15 mm in the wavelength region between 300 and 2400 nm. Although the window of Dy_2O_3 (transmission region without absorption) is around 600 and 2000 nm, it is difficult to determine the baseline of the transmission spectrum for thick samples because of the large absorption coefficient by Dy ions.

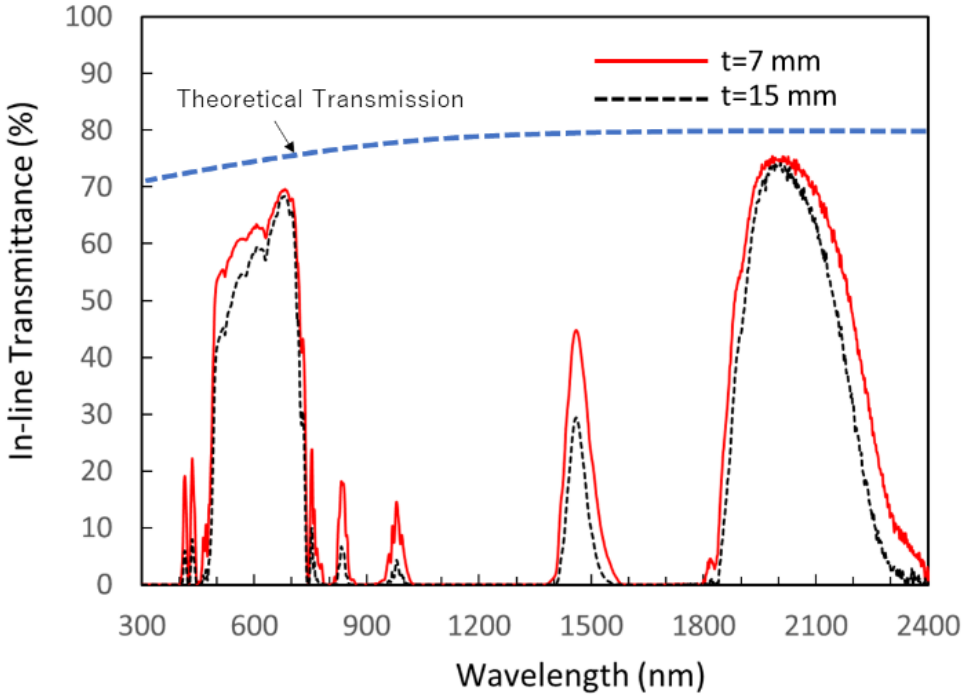

Figure 5.4 Transmission spectra of Dy_2O_3 with different thickness. t=7mm (solid line) and t=15mm (dash line).

However, in the window regions at 680 and 2000 nm, the difference in the transmittance of these long samples with a thickness difference of 8 mm is only 0.05 %, thus it is considered that the optical loss is smaller than 0.1 % cm^{-1}. Accordingly, this Dy_2O_3 ceramic has far superior transmission characteristics to those reported to date.

Figure 5.5 (a) shows the polarization characteristics of a 7 mm thick Dy_2O_3 ceramic sample without applying magnetic field and with a magnetic flux intensity of 1.16 T. As seen in the figure without magnetic field, the output polarizing plate repeats maximum transmission and minimum transmission (extinction) at 0 deg. and 90 deg., alternatively at a cycle of 90 deg. From the measurement data, it was confirmed that the phase difference between without magnetic field and with a magnetic field of 1.16 T is 16.6 deg., and the minimum of the signal totally shifted 196.6 deg. (i.e., 180 + 16.6 deg.). Accordingly, the Verdet constant that can be directly calculated by using the equation (1.1) shown in Chapter 1 is 422 rad T^{-1} m^{-1}.

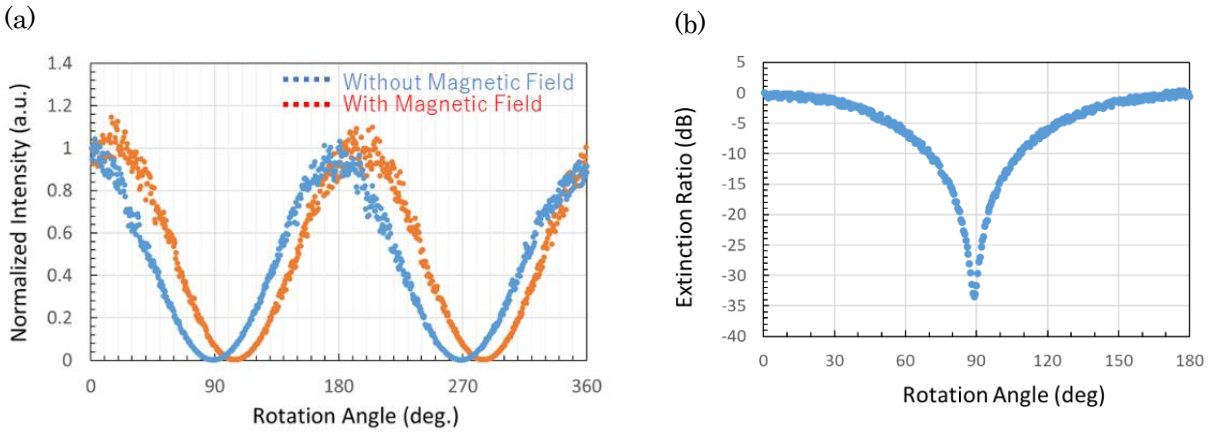

Figure 5.5 (a) Polarization characteristics of Dy_2O_3 ceramics with 7 mm thickness measured under a magnetic flux intensity of 1.16 T and without magnetic field. (b) Extinction characteristics of the same Dy_2O_3 ceramics without magnetic field.

According to a report by Morales et al. [1], the Verdet constant of Dy_2O_3 at 633 nm is 300 rad T^{-1} m^{-1}, and that of $(Dy_{0.90}Y_{0.05}La_{0.05})_2O_3$ ceramics by Snetkov et al. [2] is 297 rad T^{-1} m^{-1} (as it is for 90 %-Dy_2O_3, 330 rad T^{-1} m^{-1} is estimated for pure Dy_2O_3), and Slezak et al. [3] reported 347 rad T^{-1} m^{-1}. Since the optical quality of Dy_2O_3 ceramics reported in the past was extremely low, the Verdet constant was measured with a sample length of around 0.5 mm, and it is likely that an accurate rotation angle could not be measured due to poor transmission characteristics. From the viewpoint of electron spin configuration, the material with the highest Verdet constant is Tb_2O_3, and the authors have obtained 495 rad T^{-1} m^{-1} at 633 nm [4]. In this study, the optical loss of the Dy_2O_3 ceramics was extremely small and the Verdet constant showed the maximum value when measured using a sample with a sufficient thickness. Therefore, using this ceramic material it is possible to construct a compact isolator device with an element length of only 1.6 mm under a magnetic flux density of 1.16 T, for a 633 nm laser wavelength.

Extinction characteristics of this material with 7 mm thickness measured without magnetic field is shown in Figure 5.5 (b). Similar to the Figure 5.5 (a), the rotation angle of the polarizing plate and the transmittance thereof are shown. The rotation angles at 0 and 180 deg in the figure show the maximum transmission and the position at 90 deg shows the extinction position. Although the scattering loss of this material is small, the absorption by Dy ions at 633 nm is large, hence the insertion loss was not measured in this work, but an extinction ratio of 34 dB was obtained for the Dy_2O_3 sample with a thickness of 7 mm. The extinction ratio at 1064 nm is reported to be 35 dB for commercial high quality TGG single crystals [5]. Although there is a difference in the measuring wavelength, the extinction ratio of the Dy_2O_3 ceramics of this study showed a value comparable to that of the commercial single crystal. As shown in above Figures 5.2 and 5.3, when observing polarized light

without applying a magnetic field on the ceramic sample, only the dark field on the macro to micro scale was observed, which is the explanation for the large extinction ratio of this ceramic material.

5-4. Summary

The results of this study are summarized below.

1) By adding a small amount of ZrO_2 to high-purity Dy_2O_3 powder and successive HIP-treatment, a highly transparent Dy_2O_3 ceramic was obtained.

2) It was confirmed that there were no residual pores or optically heterogeneous phases in the sintered ceramics, the scattering loss was extremely small, and the optical quality was excellent from the polarization observation and transmitted laser beam quality.

3) The Verdet constant of the obtained Dy_2O_3 ceramics at a wavelength of 633 nm was 422 rad T^{-1} m^{-1}, and the extinction ratio was 34 dB, which was the most excellent property reported to date.

Therefore, it is possible to construct a compact isolator device using this ceramic material with an element length of only 1.6 mm under a magnetic flux density of 1.16 T, for a 633 nm laser wavelength.

References

1. J. R. Morales, N. Amos, S. Khizroev, J. E. Garay, “Magneto-Optical Faraday Effect in Nanocrystalline Oxides”, J. Apply. Phys., **109**, 093110 (2011).

2. I. L. Snetkov, A. I. Yakonviev, D. A. Permin, S. S. Balabanov, O. V. Palashov, “Magneto- Optical Faraday Effect in Dysprosium Oxide (Dy_2O_3) Based Ceramics Obtained by Vacuum Sintering”, Opt. Lett., **43** [16], 4041-4044 (2018).

3. O. Slezak, R. Yasuhara, D. Vojna, H. Furuse, A. Lucianetti, T. Mocek, “Temperature - Wavelength Dependence of Verdet Constant of Dy_2O_3 Ceramics”, Opt. Mater. Expr., **9** [7], 2971-2981 (2019).

4. A. Ikesue, Y. L. Aung, S. Makikawa, A. Yahagi, “Total Performance of Magneto-Optical Ceramics with a Bixbyite Structure”, Mater., **12** [3], 421 (2019).

5. A. Ikesue, Y. L. Aung, S. Makikawa, A. Yahagi, “Polycrystalline $(Tb_xY_{1-x})_2O_3$ Faraday Rotator”, Opt. Lett., **42** [21], 4399-4401 (2017).

Chapter 6 Development of Optical Grade Polycrystalline YIG Ceramics for Faraday Rotator

6-1. Introduction

Faraday rotator materials are classified into iron-free paramagnetic materials and iron-containing ferrimagnetic materials. Development of novel polycrystalline Faraday rotator materials composed of paramagnetic materials were described in Chapter 2 to Chapter 5. In this chapter, development of polycrystalline ferrimagnetic materials for optical isolators mostly applied in telecommunication field for infra-red wavelength regions longer than 1.2 μm is described. The ferrimagnetic iron garnet is generally expressed by a chemical formula, $Re_3Fe_5O_{12}$ (Re: Y and lanthanide rare earth elements), which is being used as a microwave material and in magnetic recording [1-3] and as a magneto-optical material in Faraday device [3]. Most of the materials [4-6] to which Bi is added to the above materials are produced by FZ (Floating Zone Method) or LPE (Liquid Phase Epitaxial) method. But, until now, there is no report on transparency of such materials in polycrystalline ceramic form. It is general to produce magneto-optical materials by melt-growth method. However, in the synthesis of YIG single crystal, since crystals are grown via peritectic reaction [7], synthesis method is restricted to FZ method and so the feasible crystal size is limited. Although the Bi-added iron garnet has an advantage that the Faraday rotation angle can be greatly increased, its production method is limited to LPE, and epitaxial growth can be performed only on the GGG ($Gd_3Ga_5O_{12}$) based substrate material, and further the growth rate is "0.1~0.3 mm per day" which is extremely slow [8]. In recent years, many attempts have also been made to synthesize a transparent iron garnet thin film using a gas phase synthesis method such as a sputtering method, but it is extremely difficult to obtain a film thickness required for practical Faraday rotation angle [9-11]. Technical and economic merits will be extremely great if a sintering process can be used for the synthesis of iron garnet materials, but there are still no reports on the transparency of this material up to now [12-16]. Therefore, in this work Y_2O_3 and α-Fe_2O_3 powder were used as starting materials in order to develop infra-red transparent polycrystalline YIG ceramics by sintering process without additives. Its magneto- optical properties were compared with the YIG single crystal grown by the conventional FZ method.

6-2. Experimental procedure

As for the starting materials, Y_2O_3 (particle size 60 nm, commercially available) and α-Fe_2O_3 (particle size 1 μm, commercially available) having a purity of 99.99 % reported so far have been used. Each powder was weighed so as to have a garnet composition and mixed in a ball mill for 15 hours. The resulting slurry was dried with a spray drier to prepare granules of about 20 to 30 μm. This powder was molded into a disc shape having a diameter of 12 to 70 mm and then subjected to CIP (Cold Isostatic Press) at 147 MPa. The sintering behavior of the powder compacts was measured by a thermo-mechanical analyzer (TMA8140, Rigaku, Tokyo, Japan) in an oxygen atmosphere from room temperature to 1540 °C, and the relative density at the time of each sintering (heating rate: 5 °C min^{-1}, cooling rate: 20 °C min^{-1}) was also measured. Transmittance at wavelength range from

850 nm to 2500 nm was measured by a photo-spectrometer (V670, JASCO Co., Tokyo, Japan). SEM (Scanning Electron Microscope, SU8000, Hitachi Co., Tokyo, Japan)) was used to observe the microstructures during sintering steps, and XRD (X-ray diffraction, RINT-2000, Rigaku Co.,) method was used to analyze the generated phase at each sintering step.

A similar experimental setup described in the previous Chapter 2, was applied to evaluate the Faraday rotation performance of YIG ceramics developed in this work. Wavelength of laser diode used was 1550 nm and the maximum output power was 5 mW. A polarization plane of laser light was rotated by the Faraday effect because of the magnetic field (magnetic field intensity applied at measurement: 0.3 T). Produced YIG ($Y_3Fe_5O_{12}$) ceramics (processed from Φ35 x t5 mm to Φ9 x t 2 mm samples) and $Y_3Fe_5O_{12}$ single crystal (Φ5 x t 2 mm, Deltronic Crystal Industries Inc., New Jersey, USA) with <111> orientation were used as sample Faraday materials.

6-3. Results and discussion

Shrinkage behavior and relative density change of Y_2O_3-Fe_2O_3 powder compacts against various heating temperatures with 5 °C min^{-1} heating rate are shown in Figure 6.1. Significant shrinkage started around 1000 °C, and it was occurred in 2 steps. Increasing rate of density change became slower around 1300 °C because of the formation of intermediate phase to form YIG phase as shown in Figure 6.2.

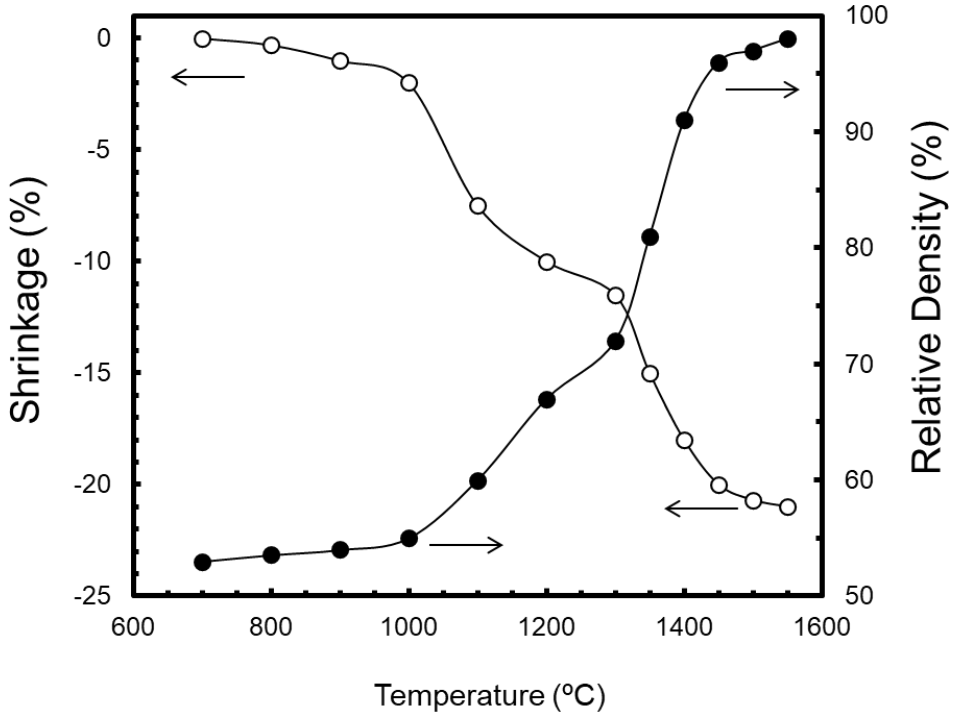

Figure 6.1 Sintering shrinkage and relative density of Y_2O_3-Fe_2O_3 sintered bodies against heating temperature.

Figure 6.2 shows the XRD pattern at each heating temperature. YIP ($YFeO_3$) was formed as an intermediate layer by the reaction of Y_2O_3 and Fe_2O_3, and finally the reaction of $YFeO_3$ (5.70 g cm^{-3}) + Fe_2O_3 → YIG ($Y_3Fe_5O_{12}$, 5.17 g cm^{-3}) progressed. This behavior is a solid-phase reaction behavior similar to YAG ($Y_3Al_5O_{12}$) reported before [18, 19], the shrinkage and the density rise became slow at around 1300 °C is due to the formation of the garnet phase via ortho-ferrite.

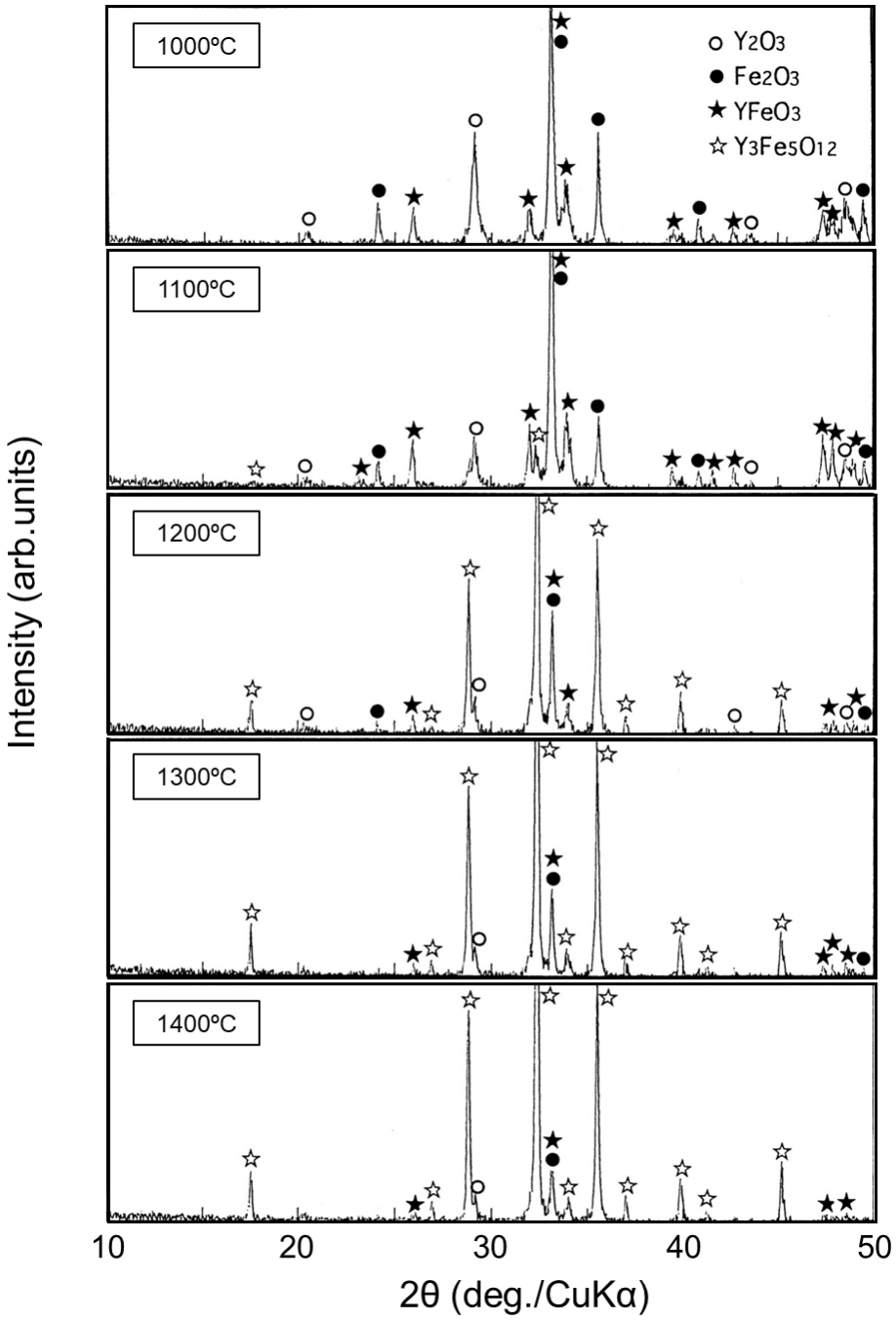

Figure 6.2 XRD patterns of the samples heated at 5 °C min^{-1} and cooled down at 20 °C min^{-1} from each heating temperature.

Figure 6.3 shows the microstructure of the powder compacted body (polished surface) heated from 1000 to 1500 °C. Densification and grain growth progressed as the temperature raised, but grain growth became noticeable when the temperature raised to 1500 °C, and the existence of residual pores inside some grains were observed. Although the melting point of YIG is 1580 °C, it is preferable to sinter at less than 1500 °C because voids (residual pores) are likely to be formed in the material when sintering above 1500 °C from the result of microstructure observation.

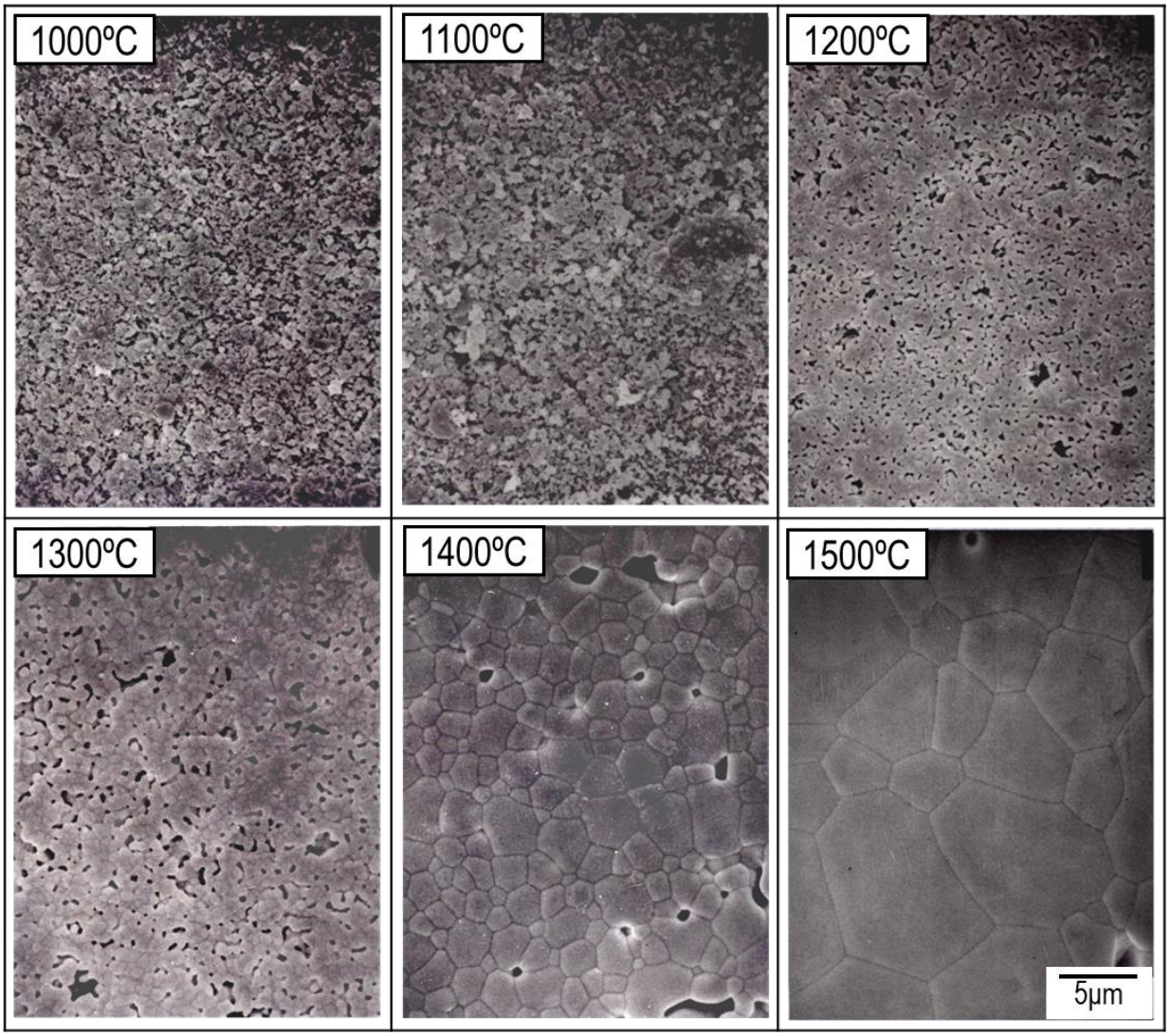

Figure 6.3 SEM microstructure of YIG ceramic samples at middle step of sintering.

Figure 6.4 (a) shows the appearance photo of the YIG ceramics prepared (after O_2 – HIP treatment at 1300°C for 1 h under 147 MPa) in this work. In the FZ method, the size of YIG single crystal is normally limited to a diameter of 5 to 6 mm and a length of several tens of mm, but in the case of sintering process there will be no limitation on the size of material that can be synthesized. In this work, large-scaled media with up to Φ2

inches x 20-40 mm in thicknesses were demonstrated. Figure 6.4 (b) is a SEM image of YIG ceramic sample prepared by pressureless sintering. Figures 6.4 (c) and 6.4 (d) show the microstructures of YIG ceramic sample prepared by HIP treatment, observed by reflection polarizing microscope and SEM. Secondary phases such as YIP or Fe_2O_3 were not observed in both pressureless sintering and HIP-treated samples, which was a pore-free structure composed of random and several μm of YIG micro grains.

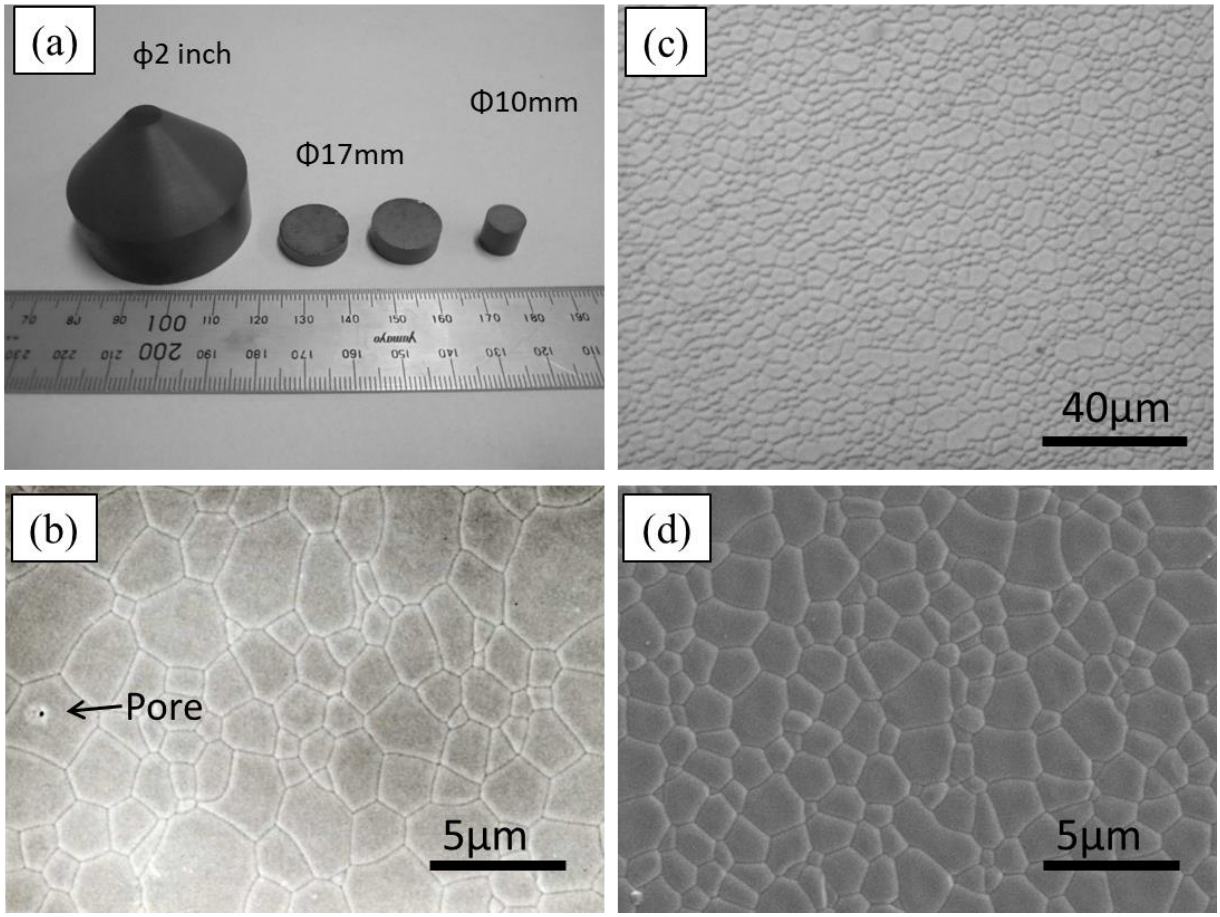

Figure 6.4 (a) Appearance of YIG ceramics after HIP. (b) SEM image of YIG ceramics after pressureless sintering at 1400°C for 10 h. (c) Reflection polarizing microscopy and (d) SEM image of YIG ceramics after O_2-HIP treatment at 1300°C for 1 h under 147 MPa.

Figures 6.5 (a) and 6.5 (b) are photographs of transmitted and transmitted polarized light (polarized light is taken by orthogonally crossing two polarizing plates) obtained by observing the produced YIG ceramics at wavelength longer than 800 nm. Residual pores can hardly be observed on the surface and the number of pores was very few. Polarized light observation of the material is completely dark field, hence it is composed of optically garnet single phase (cubic structure) and free from impurity phases such as Fe_2O_3, $YFeO_3$ and so on. Figures 6.5 (c) and 6.5 (d) compare the magnetic domain structure of YIG ceramics of this work and Bi-doped GIG single crystal with <111> orientation prepared by LPE (Liquid Phase Epitaxial) method. Observation was

with a single polarizing plate with a transmission microscope using wavelength longer than 800 nm as described above. YIG single crystal with a single orientation and polycrystalline YIG ceramics composed of 2-3 μm crystal grains with random orientations before applying a strong magnetic field, have different magnetic domain structures even though they have the same garnet structure.

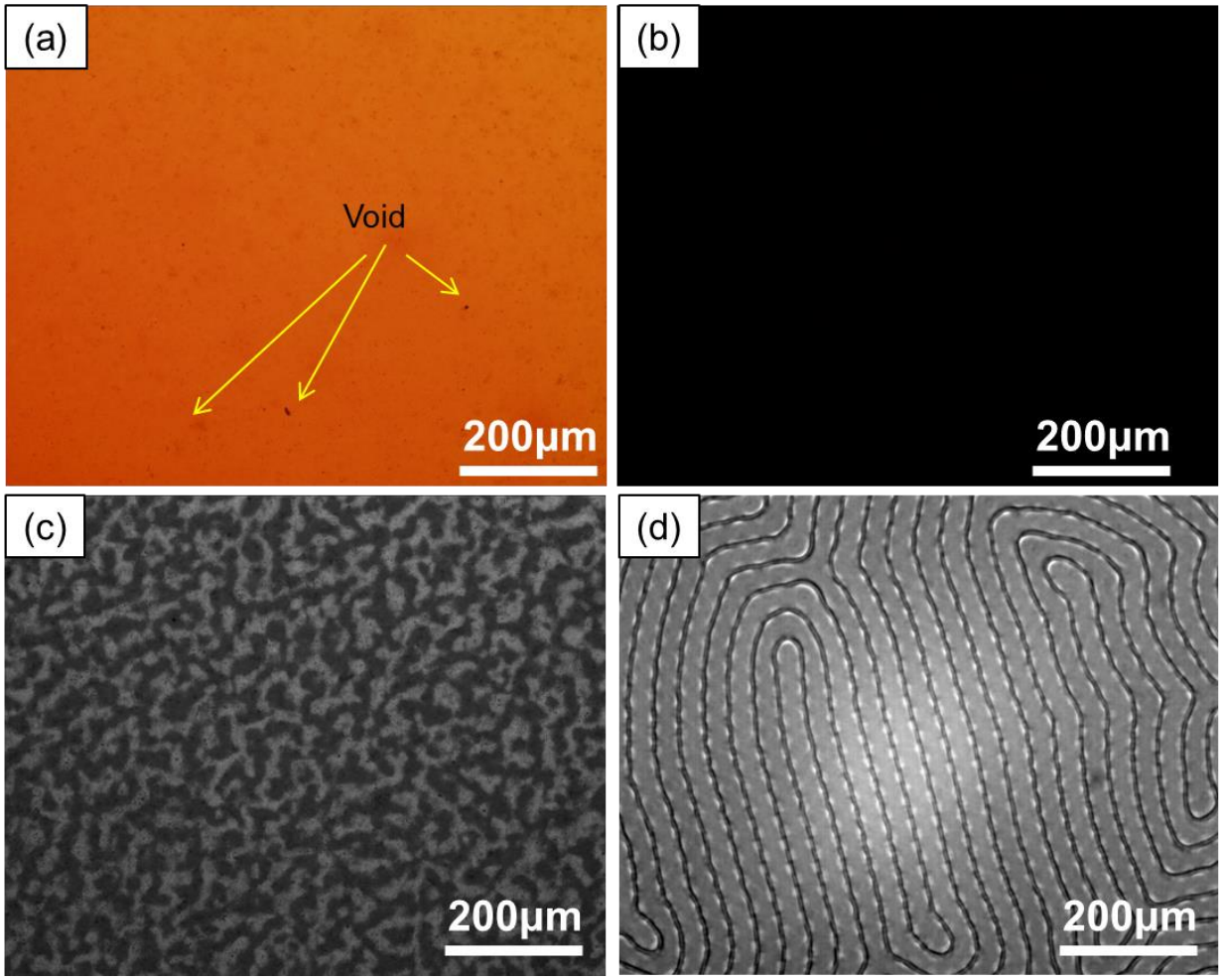

Figure 6.5 (a) Open nicol and (b) crossed nicol (double polarizer) of YIG ceramics measured by transmission optical microscopy. Magnetic domain structure of (c) polycrystalline YIG ceramics (single polarizer) and (d) Bi-doped GIG single crystal from liquid phase epitaxial method by transmission/polarizing microscopy.

Figure 6.6 is a Schlieren image observed at wavelength longer than 1200 nm at which YIG can transmit. The refractive index distribution in the plane is almost uniform. LD light with a wavelength of 1550 nm was arbitrarily irradiated at 10 different points and the transmitted light intensities were measured. Since these errors were less than ±1%, the materials have uniform optical characteristics.

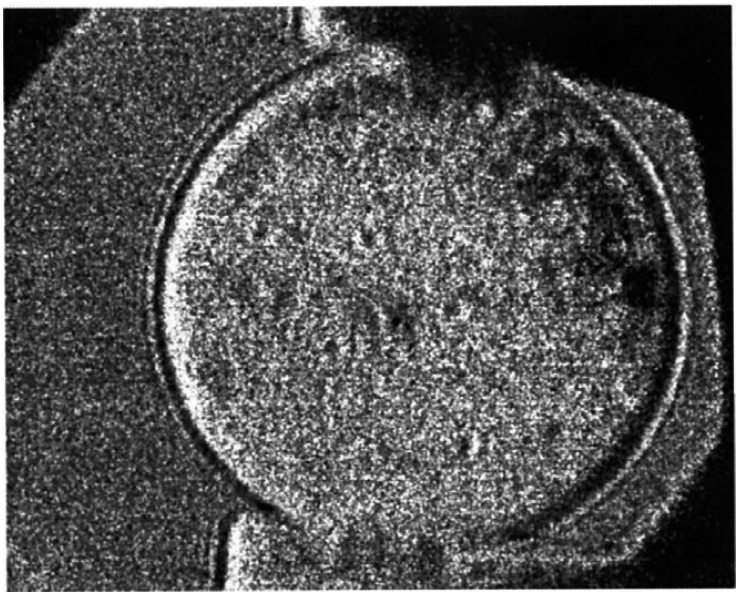

Figure 6.6 Infrared Schlieren image of YIG ceramics (t = 2mm) after O_2-HIP treatment at 1300°C for 1 hour under 147 MPa.

Figure 6. 7 shows in-line transmittance spectra of three types of YIG samples; a commercially available YIG single crystal with 1.0 mm thickness as a reference, a ceramic YIG sample produced by O_2-HIP treatment (here, sample thickness is set to 2.0 mm, which can give a Faraday rotation angle of 45 ° for 1300 nm wavelength) and a normal ceramic YIG sample produced by only pressureless sintering (1.0 mm thickness). The transmittance of the pressureless sintered sample was as low as 2%-3%, but the transmission characteristics of the HIP treated sample and the reference YIG single crystal were almost the same from 1700 to 2500 nm wavelength regions. A step difference of 2%-3% around 1.6 μm was observed for the transmittance of the sample produced by HIP treatment.

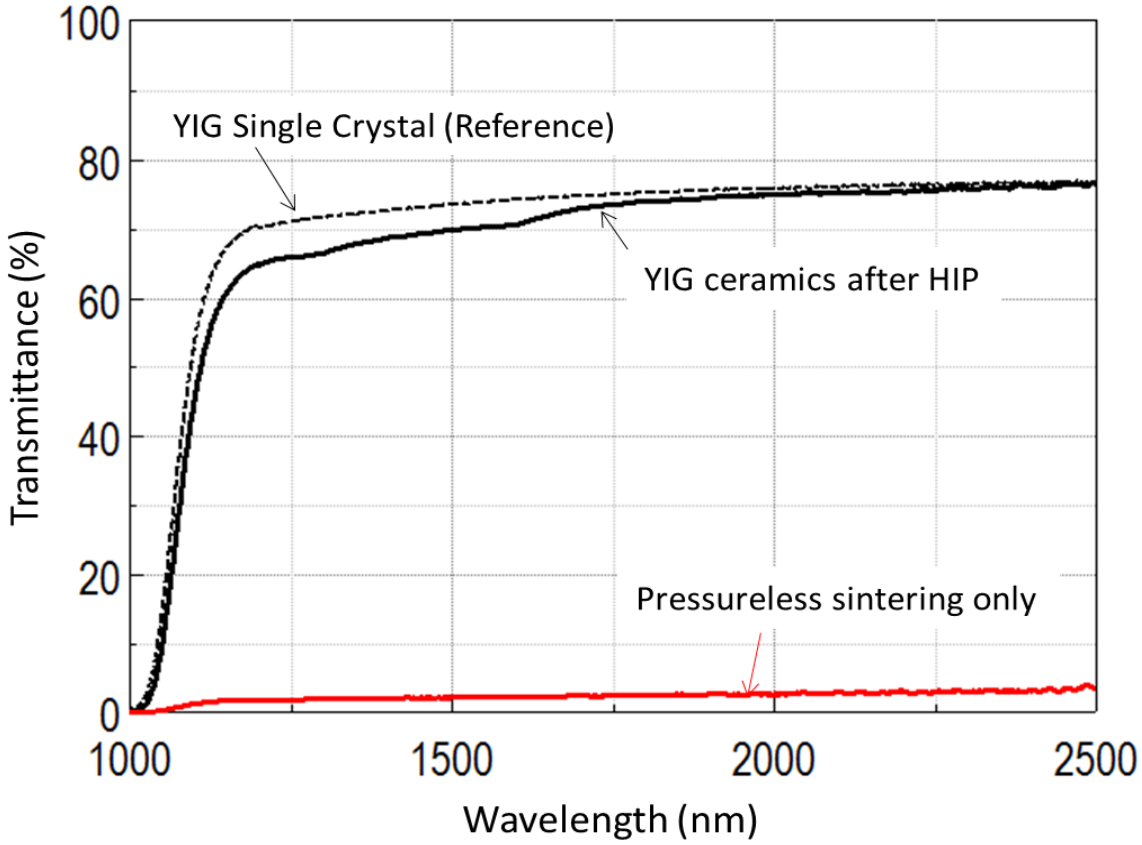

Figure 6.7 In-line transmittance spectra of YIG ceramics after pressureless sintering (t = 1mm) and O_2-HIP treatment (t = 2 mm). Thickness of reference YIG crystal = 1 mm.

When significant Rayleigh scattering occurs in the materials, theoretically such a step does not occur. Typically, when Rayleigh scattering occurs, as the measurement wavelength becomes shorter, the transmittance becomes lower. As shown in the above Figures 6.5 (a) and 6.5 (b), there were no impurity phases other than garnet phase in the material, and only the residual pores of several micrometers were confirmed in the optical microscope observation, so the cause of the absorption step in the transmission curve is considered to be Mie scattering due to residual pores. However, the difference in transmission loss between the single crystal and the polycrystalline sample in the region shorter than 1600 nm got bigger as the wavelength became shorter. The fact that the transmission loss depends on the measuring wavelength cannot deny the influence of Rayleigh scattering in this case. Therefore, it is necessary to clarify in detail the grain-boundary structure of HIP sintered sample by HRTEM analysis etc. and to clarify why produced YIG ceramics caused such decrease in transmittance at short wavelength regions. Reducing or eliminating the scattering source in the measurement wavelength region is very important for improving the optical performance as the Faraday element of this material, in particular, low insertion loss (I.L.). The difference in optical characteristics between the single crystal and the ceramic sample subjected to HIP treatment was very small, but when a semiconductor laser of 1550 nm is used as a light source

in telecommunication, further reduction of transmission loss at this wavelength is still necessary.

Table 6.1 compares the magneto-optical properties of the YIG single crystal, and the sample subjected to HIP treatment. YIG single crystal and ceramics showed similar performance but the insertion loss of YIG ceramics was 0.3 dB which is fairly large. Although it was a disadvantage of this ceramic material, there is also an advantage that the extinction ratio was large. If the insertion loss of ceramics can be reduced more, ceramics will have various advantages such as extinction ratio, large size, mass productivity and so on.

Table 6.1 Magneto-optical properties of YIG single crystal and polycrystalline ceramics

Sample	FZ Method	This work
Saturated magnetic field (mT)	178	180
Faraday rotation angle (deg./cm)	174[a] 224[b]	175[a] 224[b]
Extinction Ratio (dB)[a]	30	35
Insertion loss (dB) [a]	0.1	0.3
[a] and [b] measured at 1550 and 1300 nm, respectively.		

Takeuchi et al. reported on Faraday rotation angle and basic properties of polycrystalline Bi-substituted iron garnet ceramics produced by hot-press method [5]. However, the absorption coefficient of their ceramics was as large as 10^3~ 10^4 level, and there were no descriptions on I.L. and E.R. values in their report. Therefore, YIG crystal which is synthesized only by the FZ method has been applied to an isolator for optical communication etc. in the wavelength region of 1.3 μm or more, but currently, Bi added iron garnet having a larger Verdet constant is mainly used. However, Bi iron garnet can be produced only by the LPE method in which the growth rate is extremely slow, and it is necessary to use a GGG single crystal substrate with lattice constant matched with this material. Imaeda et al. tried to synthesize YIG single crystal by sintering method [20, 21], but many internal defects (voids etc.) were found in the material, and the insertion loss of the sample with 1 mm thickness even after AR (Anti-Reflection) coating was as large as 2 dB, which is greater than 20 times (more than 200 times larger in terms of transmission loss) as compared with the high quality commercial YIG single crystal in terms of dB value [21]. This value is 10 times larger than the polycrystalline YIG of this work in terms of the dB value. Also, to give an accurate Faraday rotation angle, it is considered that a single crystal is more preferable than a polycrystalline body composed of random and numerous crystallites having magneto-optical anisotropy. Especially <111> YIG crystal with easy axis of magnetization has been used.

From this data, it can be said that the basic performance as Faraday rotation element of polycrystalline ceramics and <111> YIG single crystal is similar. Moreover, the reason why the YIG ceramics which was dense and transparent so far could not be made is still unknown. However, in this work it was demonstrated that not only to achieve high transparency of this ceramic material for the first time by solid phase reaction of Y_2O_3 and Fe_2O_3, but also to obtain magneto-optical performance comparable to single crystal even in polycrystalline state of this material.

Technical and economic problems as described above are still unsolved in both YIG and Bi-added iron garnet single crystals produced by the melt-growth method which have been put into practical use. Therefore, polycrystalline materials produced by the sintering method can be expected as a great advantage to use as Faraday rotators.

6-4. Summary

The results of this work are summarized below.

1. Solid phase reaction of Y_2O_3 and Fe_2O_3 powders enabled to synthesize dense and translucent YIG ceramics.
2. When the above sintered body was subjected to O_2 - HIP treatment, the transmittance was significantly improved, and equaled to that of commercially available YIG single crystal (low optical loss grade) in 1700~2500 nm wavelength region.
3. Faraday rotation angle of polycrystalline YIG ceramics at 1300 and 1550 nm was 224 and 175 deg cm^{-1}, respectively, which was almost the same as that of the corresponding YIG single crystal reported to date.
4. Insertion loss at a polarization angle of 45 degrees at 1550 nm of polycrystalline YIG (2 mm thickness) ceramics was 0.3 dB, which is rather inferior to the corresponding single crystal, but 35 dB of extinction ratio is advantageous.

Although only the <111> YIG single crystal having an easy axis of magnetization has been used as Faraday rotator element, it was proved in this work that polycrystalline YIG ceramics with random orientations possesses almost the same Faraday rotation characteristics as in the corresponding single crystal. If a small number of residual pores in the produced YIG ceramics can be completely removed, the insertion loss of ceramics will reach the level of single crystal. Ceramics Faraday rotators have many advantages in performance, productivity, and economy because they possess large extinction ratio and can be produced in large scale.

References

1. A. C. Blankenship, R. L. Huntt, “Microwave Characteristics of Fine-Grain High Power Garnets and Spinel”, J. Appl. Phys., **37** [3] 1066-1068 (1966).

2. M. Hasegawa, T. Miura, “Present Status of Magnetic Material Developments in Radio Frequency”, Bull. Ceram. Soc. Jpn., **34** [8] 609-614 (1999).

3. A. E. Paladino, E. A. Magurie, “Microstructure Development in Yttrium Iron Garnet”, J. Am. Ceram. Soc., **53** [2] 98-102 (1970).

4. T. Tokumatsu, “Optical Isolator”, Bull. Ceram. Soc. Jpn., **31** [1] 15-18 (1996).

5. H. Takeuchi, “The Faraday Effect of Bismuth Substituted Rare-Earth Iron Garnet”, Jpn. J. Apply. Phys., **14** [12] 1903-19 (1975).

6. T. Okada, “Magnetic Material”, Bull. Ceram. Soc. Jpn., **23** [5] 468-470 (1988).

7. H. J. Van Hook, “Phase Relation in the System Fe_2O_3 – Fe_3O_4 – $YFeO_3$ in Air”, J. Am. Ceram. Soc., **44** [5] 208-214 (1961).

8. I. Nomi, K. Nakashima, K. Machida, H. Ishikawa, “Magneto-optoelement materials”, JPN Patent: H2-51494 (1988).

9. D. C. Bullock, “Negative Resistance, Conductive Switching, and Memory Effecting Silicon-Doped Yttrium-Iron Garnet Crystal”, Appl. Phys. Lett., **17**, 199-201 (1970).

10. Y. Sun, Y.Y. Song, M. Wu, “Growth and Ferromagnetic Resonance of Yttrium Iron Garnet Thin Films on Metals”, Appl. Phys. Lett., **101**, 0824051-3 (2012).

11. Q. Fu, Q. Xu, Z. Zhao, X. Liu, Y. Huang, X. Hu, N. Zhuang, J. Chen, “New Magneto-Optical Film of Ce, Ga:GIG with High Performance”, J. Am. Ceram. Soc., **99** [1] 234-240 (2016).

12. K. Sato, “Magneto-Optics and Ceramics”, Bull. Ceram. Soc., **28** [2] 124-129(1993).

13. H. Haneda, T. Yanagitani, A. Watanabe, S. Shirasaki, “Preparation of Ytterbium Iron Garnet Powder by Homogeneous Preparation Method and its Sintering”, J. Ceram. Soc. of Jpn., **98** [3] 285-291(1990).

14. R. J. Young, T. B. Wu, “Preparation of Yttrium Iron Garnet by Reaction Sintering”, Mat. Res. Bull. **22** [11] 1475-1482 (1987).

15. P. Grosseau, A. Bachiorrini, B. Guilhot, “Preparation of polycrystalline yttrium iron garnet ceramics”, Powder Technol., **93** [3] 247-251 (1997).

16. H. Yu, L. Zeng, C. Lu, W. Zhang, G. Xu, “Synthesis of Nanocrystalline Yttrium Iron Garnet by Low Temperature Solid State Reaction”, Mater. Charact., **62** [4] 378-381 (2011).

17. Y. L. Aung A. Ikesue, “Development of optical grade $(Tb_xY_{1-x})_3Al_5O_{12}$ ceramics as Faraday rotator material”, J. Am. Ceram. Soc., **100**, 4081-4087 (2017).

18. A. Ikesue, T. Kinoshita, K. Kamata, K. Yoshida, “Fabrication and Optical Properties of High-Performance Polycrystalline Nd:YAG Ceramics for Solid State Lasers”, J. Am. Ceram. Soc., **78** [4] 1033-1040 (1995).

19. A. Ikesue, Y. L. Aung, “Ceramic Laser Materials”, Nat. Photonics, **21**, 721-728 (2008).

20. S. Matsuzawa, K. Kozuka, “Method for producing Ferrite Single Crystal by Solid- Solid Reaction”, Adv. Ceram., **15**, 527-532 (1985).

21. M. Imaeda, S. Matsuzawa, “Growth of Yttrium Iron Garnet Single Crystal by Solid- Solid Reaction”, Proc. 1st Jpn. International SAMPE Symposium, Nov. 28 – Dec. 1st, 419-434 (1989).

Chapter 7 Transparent $Tb_3Fe_5O_{12}$ Ceramics as Mid-IR Isolator

7-1. Introduction

In Chapter 6, it was verified that the transmission characteristics and magneto-optical characteristics of the dense and transparent polycrystalline iron garnet ceramics are similar to those of the single crystal counterpart material having the same composition. In the case of paramagnetic materials, the research results described in Chapters 2 to 5 confirmed that the Faraday rotation characteristics significantly improved as the occupancy of the magnetically active ion Tb^{3+} increased. Regarding the fabrication of iron garnet ceramics, reports on powder synthesis [1] and some reports on synthesis of sintered bodies [2,3] can be found in the literatures. However, there were no reports on polycrystalline $Re_3Fe_5O_{12}$, as well as polycrystalline transparent $Tb_3Fe_5O_{12}$ (TIG) ceramics due to the theoretical problems mentioned previously and also the requirement of advanced synthesis techniques. Therefore, in this work, the synthesis of transparent polycrystalline TIG ceramics was attempted to investigate their optical characteristics and Faraday rotation performance. Because TIG has the best magnetic characteristics among other $Re_3Fe_5O_{12}$ materials and also has an excellent temperature coefficient that the change in Faraday rotation angle is extremely small even when the device temperature changes in the applied temperature range (0 to 60 °C).

7-2. Experimental procedure

For synthesis of TIG ceramics, Tb_4O_7 (agglomerated particle size: 3 μm, commercially available) and Fe_2O_3 (particle size: 1 μm, commercially available) with high purity of 99.99 wt.% were used. Both of the raw materials were weighed to have a stoichiometric composition, a small amount of dispersant and binders were added, and then ball milled with steel balls in ethanol for 10 hours. Here, the amount of wear of the steel ball during milling was measured, and an extra amount of Tb_4O_7 was added in advance to compensate the trace amount of Fe_2O_3 increased during ball milling. The ethanol solvent was removed by drying the obtained slurry at 90 °C. Powder compacts with sizes of Φ12 × 5 mm, Φ42 × 6 mm and 10 × 100 × 30 mm were prepared by a uniaxial press, followed by CIP (Cold Isostatic Press) at 98 MPa, and then calcined at 900 °C for 3 hours to remove the residual organic binders. After that, they were pre-sintered in oxygen gas at 1320 °C for 3 hours and then treated with HIP (Hot Isostatic Press) furnace at 1300 °C for 1.5 hours under a pressure of 176 MPa using 10 % O_2-Ar (oxygen-argon) gas medium. After adjusting the thickness of the obtained ceramic samples, both surfaces were mirror polished and their magneto-optical properties were measured by the similar method described in the previous chapters. Microstructure characterization using microscopies including SEM, SEM-EDS and TEM was also performed as described in the previous chapters.

7-3. Results and discussion

TIG ceramic sample having a thickness of 100 μm (both surfaces mirror-polished) was observed by a

transmission near-infrared microscope with a wavelength of 900 nm light under non-polarized (open nicol) and polarized (cross nicol) conditions. Results are shown in Figures 7.1 (a) and 7.1 (b). Birefringence were not detected inside the material. Non-cubic phase, grain boundary phase and optical stress were not observed in the materials. In the transmission image, residual pores of approximately 1μm are observed in the depth direction of the material, which are the only scattering sources in transmission optical microscope observation. Figure 7.1 (c) shows a reflection microscope photograph of the same sample after thermal etching at 1300 °C. The material was composed of uniform grains of approximately 5 to 10 μm, and scattering sources such as pores and inhomogeneous phases cannot be detected in the surface observation. In addition, fracture surface of the same sample observed by SEM is shown in Figure 7.1 (d). It was a highly dense microstructure with pore free condition as the surface. The fracture surface of the material was almost trans-granular fracture.

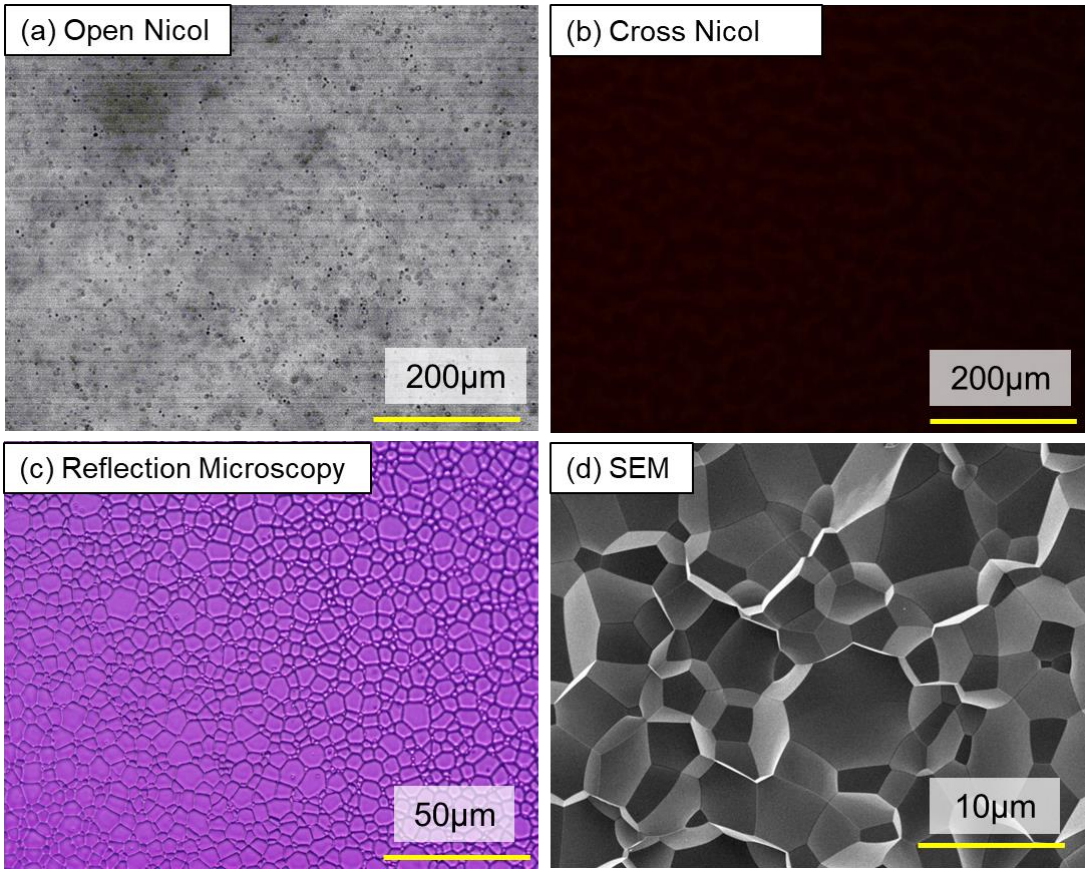

Figure 7.1 (a) Open and (b) cross nicol images by polarizing transmission microscopy, (c) reflection microscopy image after polished and thermal etching, and (d) fracture surface of TIG ceramics by SEM.

Figure 7.2 shows the observation at the triple point of the material by HR-TEM. The existence of amorphous and heterogenous phases at the grain boundary and the triple points cannot be recognized. EDS analysis was performed at three different positions; inside grain (Point (a)), at grain boundary (Point (b)) and the

triple point (Point (c)) of TIG ceramics, but there was no compositional difference between them, and clean grain boundary structure was observed. Figure 7.3 shows the transmission spectrum from 950 to 2500 nm of TIG ceramics with 0.9 mm, which is required thickness for 45 ° Faraday rotation at 1300 nm. Characteristic absorption of Tb was observed in the wavelength region longer than 1.6 μm, but the transmittance of the baseline was 51 %. Compared to the transmittance (70 %) of the TIG single crystal, the transmission loss of this TIG ceramics can be estimated as large as 21 % mm^{-1}. However, since there was no wavelength dependency of the transmittance, it can be considered that the optical loss was mainly caused by residual pores observed in Figure 7.1 (a) and not because of very small scatterer (e.g., grain boundary phase) at the grain boundary. It is assured that optical quality can be significantly improved by removal of these residual pores in this TIG ceramics. Besides, there was almost no difference in the transmission characteristics of the TIG ceramic samples obtained by sintering powder compacts of Φ12 × 5 mm, Φ42 × 6 mm, and 10 × 100 × 30 mm.

Insertion loss was not measured because the transmittance of the TIG ceramics is not sufficient, but the Faraday rotation angle of the TIG single crystal and the polycrystalline TIG ceramics were measured to be the same (350 deg cm^{-1} at 1300 nm). In the previous reports of TAG ($Tb_3Al_5O_{12}$) and TYO (Tb_2O_3-Y_2O_3) ceramic isolator materials [4,5] which are used in visible to near infrared wavelength regions, the extinction ratio of the polycrystalline material was superior to that of the single crystal.

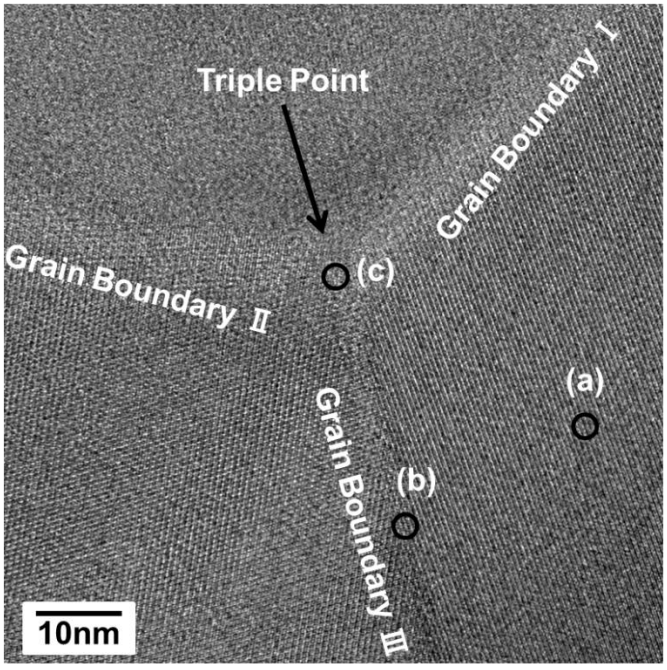

	Fe / at%	Tb /at%
Point (a)	62.46	37.54
Point (b)	62.56	37.44
Point (c)	62.36	37.65

Figure 7.2 High –resolution TEM image around triple point of produced TIG ceramics and EDS analysis of inner grain, grain boundary and triple point of TIG ceramics.

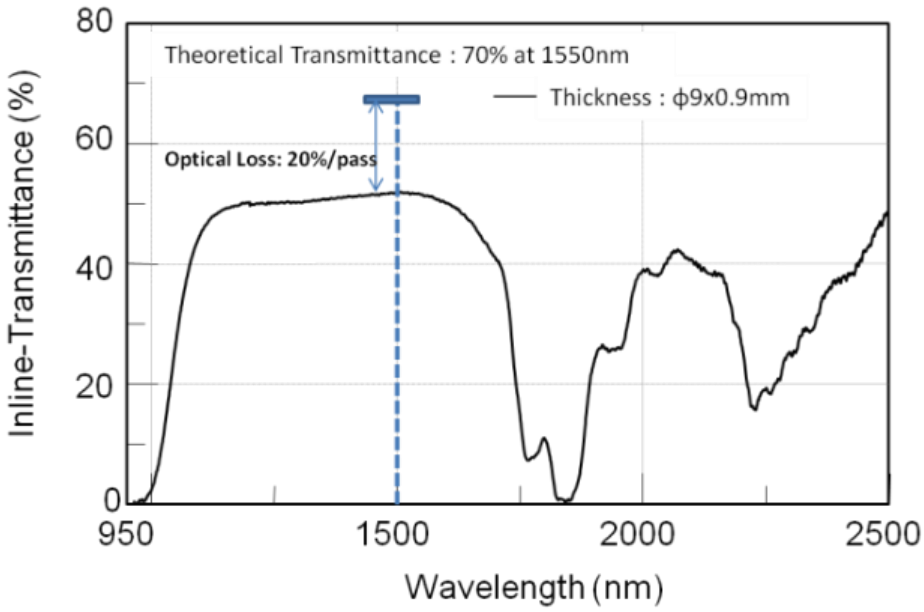

Figure 7.3 In-line transmittance between 950 and 2500 nm of TIG ceramics with 0.9 mm thick.

Figure 7.4 (a) shows external view of TIG ceramic samples having sizes of Φ10 x 2 mm, Φ32 x 4 mm, and 16 x 72 x 6 mm produced in this work. By HIP process, it is also possible to produce a large size which is difficult to produce by the FZ method, and there was no decline in optical performance due to the increase in the size of the sample. A Schlieren image of the TIG ceramics (t = 1 mm) taken by an infrared camera is shown in Figure 7.4 (b), an infrared light source with a wavelength longer than 1200 nm (wavelengths of Xenon lamp shorter than 1200 nm was cut with a filter) was used. Although a portion with a slightly high transmission was observed in a part of the outer periphery of the material, it was recognized that the material has good homogeneity in the infrared region. Magnetic domain structures of the polycrystalline TIG ceramics and Bi:GIG single crystal (prepared by LPE method, crystal orientation <111>) are shown in Figure 7.4 (c) and (d), respectively. Although TIG ceramics is a bulk material composed of numerous grains of 5~10 μm (polycrystals) with random crystal orientations, while Bi:GIG is composed of a single crystal of <111> orientation, their magnetic domain structure are found to be different to each other without applying a strong magnetic field.

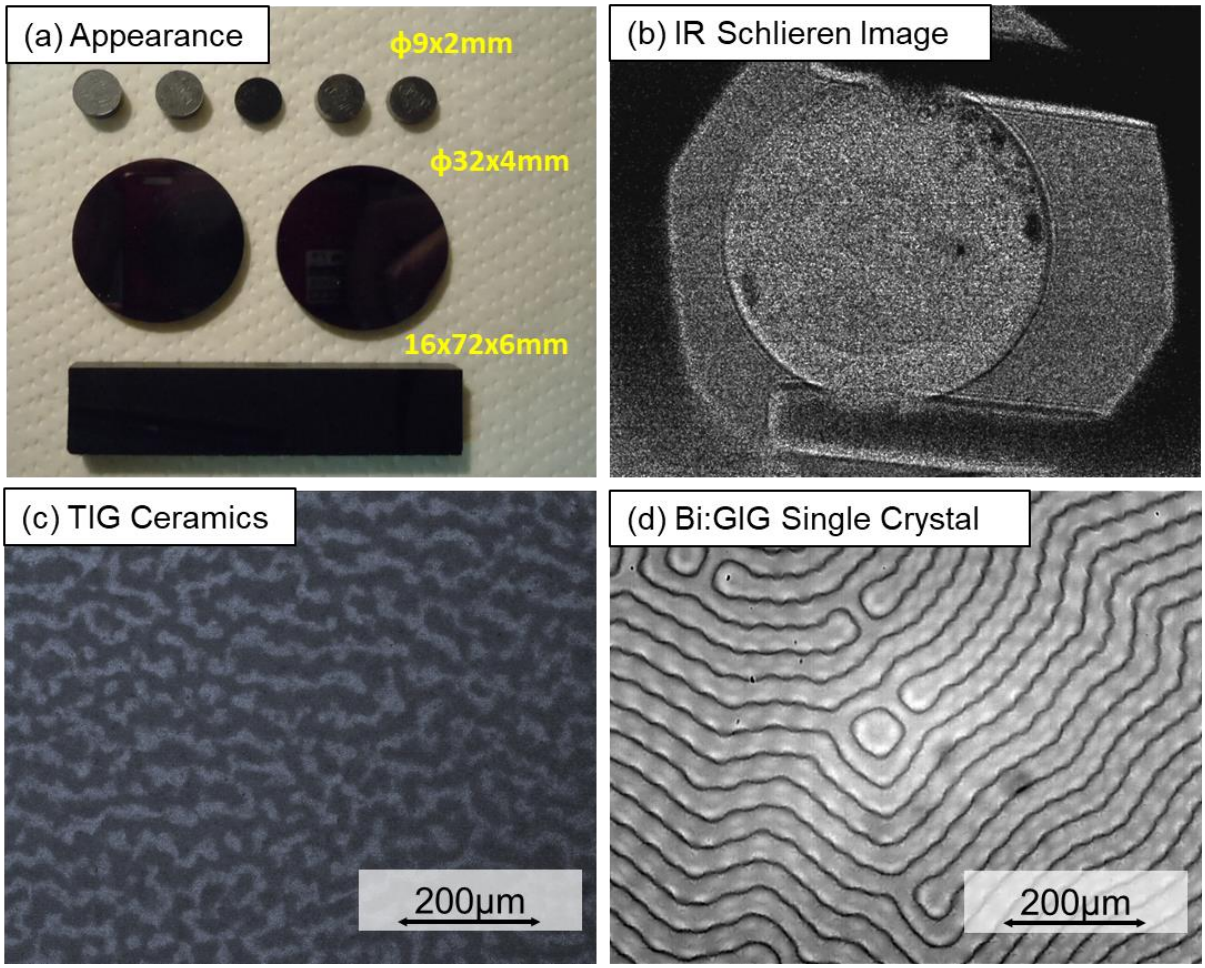

Figure 7.4 (a) Appearance of TIG ceramics, (b) IR Schlieren image, magnetic domain structure of (c) polycrystalline TIG ceramics and (d) Bi:GIG single crystal by liquid phase epitaxial method.

In recent years, various types of transparent ceramics have been developed not only for lasers and window materials but also for magneto-optical materials. Some typical examples of non-magnetic optical isolator ceramic materials for visible to 1 μm wavelength region are: TGG ($Tb_3Ga_5O_{12}$) having the same Faraday performance [6,7] as its single crystal counterpart, TAG ($Tb_3Al_5O_{12}$) exceeding the optical performance of its single crystal counterpart [4], and TYO ($(Tb_xY_{1-x})_2O_3$) having an extremely high Verdet constant [5], which is almost impossible to be produced by the conventional melt-growth method. In this work, we succeeded for the first time in synthesizing transparent magnetic (ferrimagnetic) TIG ceramics which is difficult to be produced by sintering technology and there is no report about such transparent TIG up to now.

7-4. Summary

Although it is still necessary to improve the optical properties of this ceramic material, especially the transmittance, the following facts can be concluded in this study.

1. A transparent TIG ceramics was obtained for the first time by solid phase reaction of Tb_4O_7 and Fe_2O_3, which

is the simplest process. It was optically homogeneous in an infrared Schlieren image or a transmission infrared microscope. In principle, it is possible to produce large sample which is difficult to produce with the FZ method.

2. There were no scattering sources such as inclusions, birefringence, and grain boundary phases in the obtained TIG ceramics, but it was confirmed that the only scattering sources were residual pores of approximately 1 μm.
3. There was no wavelength dependency of the transmittance, and only the residual pores were main cause of scatterings. Therefore, it is considered that only Mie scattering occurred in this material.
4. The magnetic domain structure of TIG ceramics composed of fine grains of random crystal orientation was obviously different from that of the commercial Bi:GIG system single crystal consisting of single orientation.
5. Faraday rotation angle of single crystal TIG and polycrystalline TIG ceramics was the same (350deg cm^{-1} at 1300 nm).

Further, it is still necessary to investigate the difference in magneto-optical characteristics of the single crystal having magnetic anisotropy and ceramics material having the magnetic isotropy.

References

1. H. Haneda, T. Yanagitani, A. Watanabe, S. Shirasaki, "Preparation of Ytterbium Iron Garnet Powder by Homogeneous Preparation Method and its Sintering", J. Ceram. Soc. of Jpn., **98** [3] 285-291(1990).

2. R. J. Young, T.B. Wu, "Preparation of Yttrium Iron Garnet by Reaction Sintering", Mat. Res. Bull. **22** [11] 1475-1482 (1987).

3. P. Grosseau, A. Bachiorrini, B. Guilhot, "Preparation of polycrystalline yttrium iron garnet ceramics", Powder Technology, **93** [3] 247-251 (1997).

4. Y. L. Aung and A. Ikesue, "Development of Optical Grade $(Tb_xY_{1-x})_3Al_5O_{12}$ Ceramics as Faraday Rotator Material", J. Am. Ceram. Soc., **100** [9] 4081-4087 (2017).

5. A. Ikesue, Y. L. Aung, S. Makikawa, A. Yahagi, "Polycrystalline $(Tb_XY_{1-X})_2O_3$ Faraday Rotator", Opt. Lett., **42** [21] 4399-4401 (2017).

6. R. Yasuhara, S. Tokita, J. Kawanaka, T. Kawashima, H. Kan, H. Yagi, H. Nozawa, T. Yanagitani, Y. Fujimoto, H. Yoshida, M. Nakatsuka, "Measurement of Magneto-Optical Properties and Thermal Conductivity on TGG Ceramic for Faraday Material of High-Peak and High Average Power Laser", Rev. Laser Eng., 35, 806-810 (2007).

7. H. Yoshida, K. Tsubakimoto, Y. Fujimoto, K. Mikami, H. Fujita, N. Miyanaga, H. Nozawa, H. Yagi, T. Yanagitani, Y. Nagata, H. Kinoshita, "Optical Properties and Faraday Effect of Ceramic Terbium Gallium Garnet for a Room temperature Faraday Rotator", Opt. Express, **19** [16], 15181-15187 (2011).

Chapter 8 Bi Substituted YIG Ceramics Isolator for Optical Communication

8-1. Introduction

As described in Chapter 6, iron garnets represented by YIG ($Y_3Fe_5O_{12}$) [1-3] can transmit wavelengths longer than 1.2 μm and exhibit ferrimagnetic properties, and thus they possess much larger Faraday rotation angle than the paramagnetic TGG ($Tb_3Ga_5O_{12}$) [4-7] or TAG ($Tb_3Al_5O_{12}$) [8-10] Faraday rotator materials. Therefore, they are the majority of optical isolators for the mid-infrared region longer than 1.3 μm. In addition, since a huge Faraday rotation angle can be obtained by adding Bi to an iron garnet material, it is generally used in an optical isolator for communication of 1.5 μm band which can be downsized.

YIG single crystal that does not contain Bi can be synthesized by the FZ (Floating Zone) method [1,3], but the size of the single crystal obtained is limited. Since YIG single crystals produced by the melt growth method are obtained with <111> orientation of the magnetic easy axis, Imaeda et al. tried to synthesize <111> YIG single crystals by sintering method [11]. However, the magneto-optical performance of their grown single crystal was not suitable for practical use because the insertion loss was very large. The possibility of synthesis of polycrystalline YIG ceramics with enhanced magneto-optical performance comparable to single crystal has been demonstrated in Chapter 6 [12]. The fact noted is that the magneto-optical properties of polycrystalline ceramics are same as single crystals. This means that there is no advantage of single crystalline materials in terms of magneto-optical performance although single crystal has a certain crystal orientation.

Since Bi-substituted iron garnet is a material having a huge Faraday rotation performance, it is used in an isolator device for optical communication and is indispensable as a communication tool. In addition, when applying automatic driving and telemedicine (e.g., da Vinci surgical system) etc., it is expected that 5G mobile communication of ultra-high speed and large capacity information transmission will be put to practical use in the near future. However, the demand for high-capacity optical fiber and optical isolator, which is a protection device for signal transmission laser, is considered to be rapidly expanding. In this sense, there is a special need for a manufacturing process that can realize mass productivity with high speed that can replace the conventional LPE method and material development with equivalent or better performance that has been created from a new viewpoint. In the case of synthesizing Bi-doped iron garnet, it is not easy to dissolve Bi having a large ion radius in iron garnet. In general, it is essential to make the temperature gradient near the growth interface steep by using LPE (Liquid Phase Epitaxy) technology and to form an iron garnet thick film on a GGG ($Gd_3Ga_5O_{12}$)-based substrate with extremely small lattice constant mismatch [13-19]. A thick film of approximately sub mm ~ 1 mm is formed on a GGG-based substrate while controlling evaporation of Bi, which has a high vapor pressure, but since the growth rate is extremely slow (0.3~0.4 μm min^{-1}), it takes about one week to grow a thickness that is required for use as Faraday rotator materials [20]. In addition to the LPE method, there are some papers which describe the synthesis of the same thin film by the vapor phase method [21, 22]. However, productivity is still an issue even nowadays. Therefore, the purpose of this study was to synthesize Bi-substituted YIG polycrystalline ceramics by the reactive sintering method, which can replace the single crystal material by the LPE method, which has many technical problems.

8-2. Experimental Procedure

Commercially available Y_2O_3, Fe_2O_3 and Bi_2O_3 powders having 99.99 % purity were used as starting materials and their primary particle sizes were 60 nm, 1 μm and 1 μm, respectively. These raw materials were weighed with a stoichiometric composition of $(Bi_xY_{3-x})Fe_5O_{12}$ [x=0~1.1], and ball-milled with steel balls for 10 hours in ethanol solvent. Then the slurry was dried and crashed into powders. Powder compacts with diameter of 12~20 mm with a few millimeters thickness were formed by a uniaxial press, and then subjected to CIP (Cold Isostatic Press) at 98 MPa. The powder compacts were calcined at 600 °C and then pre-sintered at 900-1350 °C in O_2. Pre-sintered samples with relative density higher than 95 % were treated with HIP (Hot Isostatic Press) in a temperature range of 1000~1400 °C using 5 % O_2-Ar (oxygen-argon) gas. (HIP temperature was adjusted depending on the amount of added Bi.) The pressure at the highest temperature during HIP treatment was 147 MPa. The melting point of each material changes depending on the amount of Bi added. Accordingly, the pre-sintering temperature and the HIP processing temperature need to be optimized. The obtained sintered body was mirror-polished on both sides, then microstructure of the material was observed with a reflection microscope, an element mapping and spot analysis were carried out by SEM (Scanning Electron Microscopy)- EDS (Energy Dispersive Spectroscopy) and HR-TEM (High Resolution Transmission Electron Microscopy)-EDS under the same manner described in the previous chapters. Identification of crystal structure was done by XRD (X-ray Diffraction, RINT-2000, Rigaku Co., Tokyo, Japan) method. Magnetic domain structure was observed by using transmission polarization microscope, transmission spectrum was measured by a Spectrophotometer, and Faraday rotation angle of the material was measured in a magnetic field of 0.3 T as described in the previous chapters.

8-3. Results and discussion

Figure 8.1(a) shows transmission spectra at 1000 to 2500 nm of $(Bi_{0.4}Y_{2.6})Fe_5O_{12}$ ceramics and $(Bi_{1.1}Gd_{1.9})Fe_5O_{12}$ single crystals prepared by the LPE method. There is almost no difference between the two transmittance curves. Figure 8.1(b) shows transmission spectra of $(Bi_{0.4}Y_{2.6})Fe_5O_{12}$ ceramics with the stoichiometric composition and ceramics with (Y_2O_3 + Bi_2O_3) rich composition and Fe_2O_3 rich composition deviated by 0.03 mol% from the stoichiometric composition. When the composition of the ceramic deviated from the stoichiometric composition, the transmittance decreases in both cases, but in particular, the ceramic with (Y_2O_3 + Bi_2O_3) rich composition has an extreme decrease in optical properties. The reasons are (1) excess Bi_2O_3 promotes rapid grain growth (> 200 μm), leaving residual pores inside the material; (2) Bi_2O_3 segregates at grain boundaries, which significantly increases optical scattering.

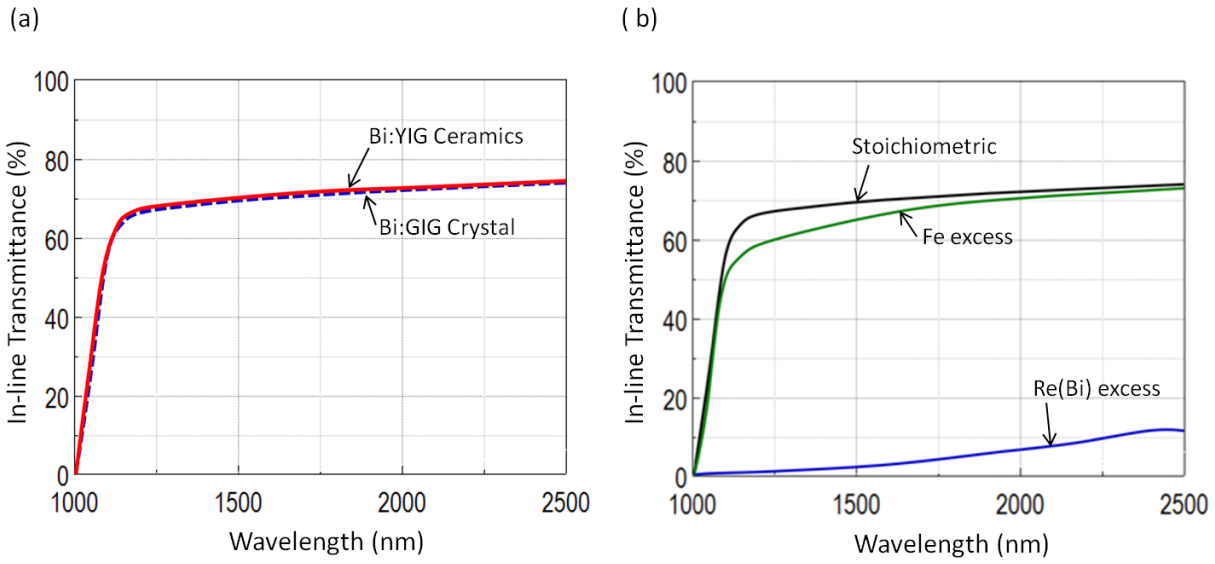

Figure 8.1 (a) Transmittance spectra of Bi doped GIG single crystal by LPE method and Bi doped YIG ceramics by reactive sintering, and (b) transmittance spectra of Bi doped YIG ceramics with just stoichiometric, Re(Bi) excess, and Fe excess compositions. (Thickness of all samples is 0.35 mm)

Figure 8.2 is a reflection micrograph of $(Bi_xY_{3-x})Fe_5O_{12}$ ceramic with Bi substitution amount x = 0, 0.4, 0.8 and 1.1. Although the grain size decreases depending on the amount of Bi substituted, no residual pores or secondary phases can be detected in any of the materials. Sample with the YIG composition (x = 0) was presintered at 1350 °C and HIP treated at 1400 °C. As for the Bi:GIG (x = 1.1) composition, the presintering temperature and HIP temperature were 900 °C and 1000 °C, respectively. As the x value is larger, the sintering temperature is lower, so the average grain size was smaller, and in the case of x = 1.1, it becomes fine grains of less than 1 μm.

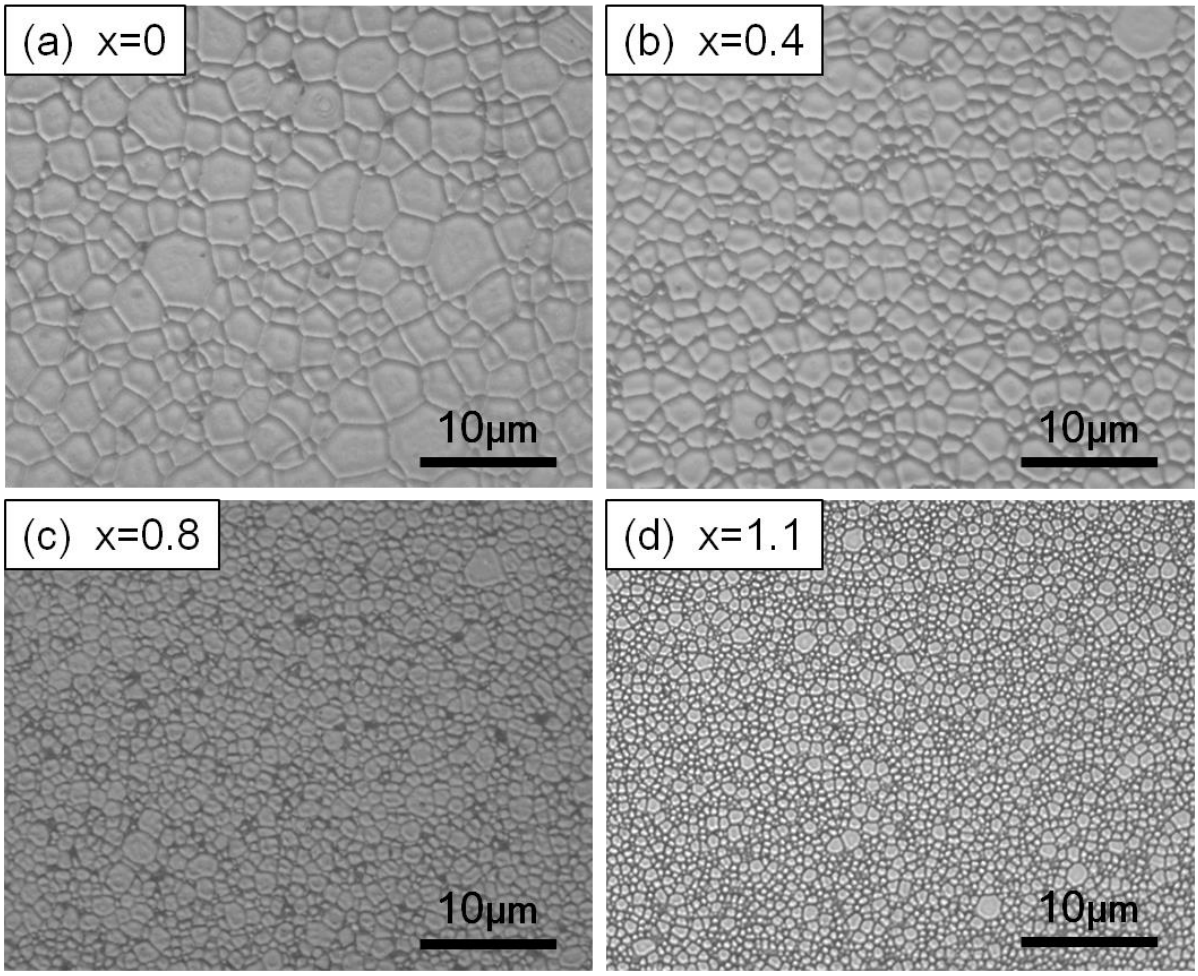

Figure 8.2 Microstructure of (a) YIG ceramics and (b)~(d) Bi doped YIG ceramics ($(Bi_xY_{3-x})Fe_5O_{12}$ with x=0.4 ~ 1.1) observed by reflection microscopy.

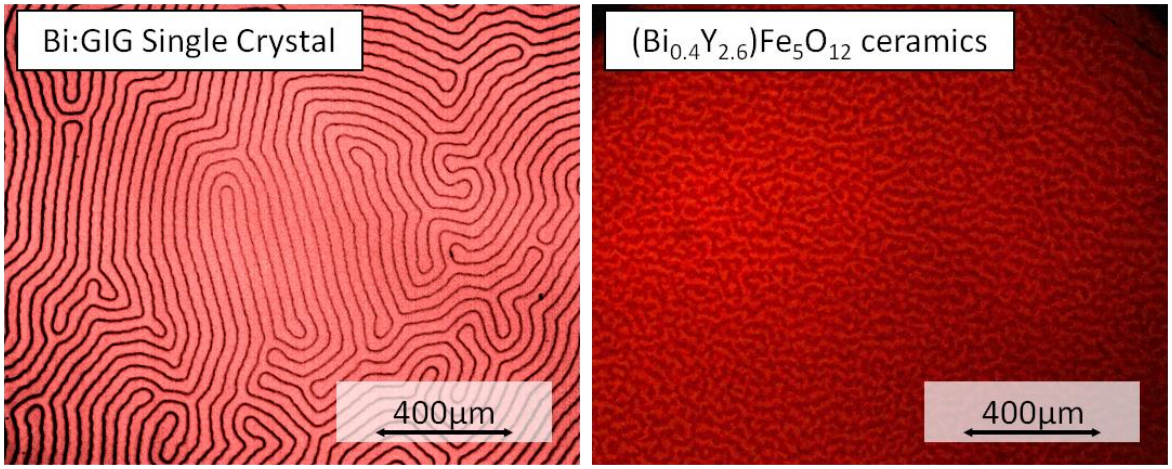

Figure 8.3 Magnetic domain structure of Bi doped GIG single crystal and Bi doped YIG ceramics by polarizing-transmission microscopy.

Figure 8.3 shows the magnetic domain structure of $(Bi_{0.4}Y_{2.6})Fe_5O_{12}$ ceramic and $(Bi_{1.1}Gd_{1.9})Fe_5O_{12}$ single crystal. Bi substituted YIG ceramics also show unique magnetic domain structure similar to the polycrystalline YIG ceramics that we have already reported [19], and they are clearly different from single crystal materials. As shown in Figure 8.2, the produced ceramic has almost no pore on the surface, but some internal pores are observed in the magnetic domain structure by polarizing and transmission microscopy.

Figure 8.4 shows a composition image (BEI, back scattered electron image) of the polished surface of $(Bi_{0.4}Y_{2.6})Fe_5O_{12}$ ceramic and an elemental mapping of Bi, Y, Fe and O. As seen in the above reflection micrograph (Figure 8.2), pores and heterogeneous portions due to different compositions were not observed, and Bi was uniformly distributed.

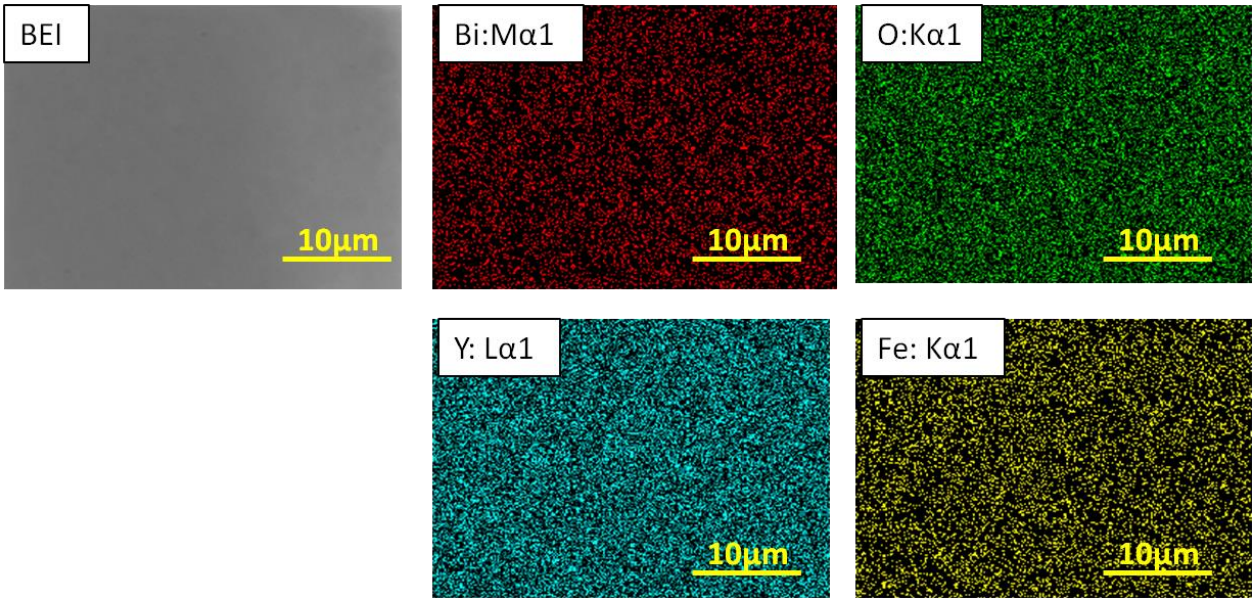

Figure 8.4 BEI image and elements distribution of $(Bi_{0.4}Y_{2.6})Fe_5O_{12}$ ceramics by SEM-EDS system.

Figure 8.5 (a) shows microstructure by conventional TEM observation and Figure 8.5 (b) shows lattice structure of $(Bi_{0.8}Y_{2.2})Fe_5O_{12}$ ceramics observed by HR-TEM and spot analysis result of inner grain and grain boundary by EDS. In observation at low magnification, the grain size of the ceramic material was about 1 to 2 μm, and there was no grain boundary phase between each grain even when observed macroscopically. When the observation was performed at high magnification, the grain boundary has an unclear region (about 1 nm wide) in which two grains slightly overlap, but the existence of the grain boundary phase cannot be confirmed. The results of spot analysis revealed that the composition of Bi is slightly different inside of the grains and grain boundaries. Since no grain boundary phase is detected at grain boundaries, it is considered that the occupancy ratio of Bi in the basic structure of garnet $Re_3Fe_5O_{12}$ (Re: Y, Bi) is increased.

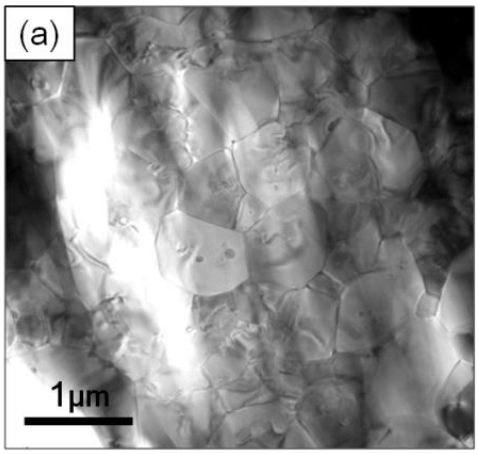

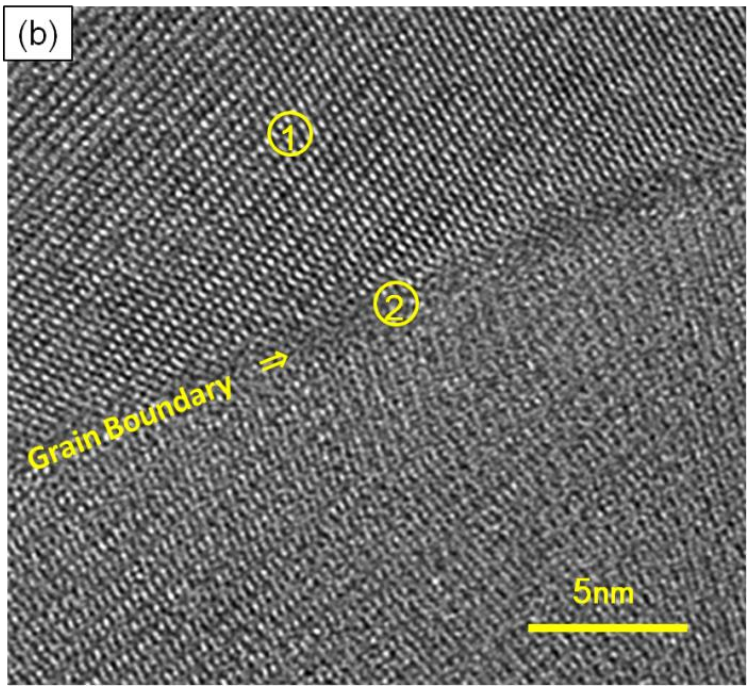

(Atomic %)	Fe	Y	Bi
(1) Inner Grain	62.5	25.6	9.9
(2) Grain Boundary	62.8	22.8	12.4

Figure 8.5 (a) Microstructure by conventional TEM and (b) lattice structure of $(Bi_{0.8}Y_{2.2})Fe_5O_{12}$ ceramics observed by HR-TEM and spot analysis of inner grain and grain boundary by EDS system.

Even if there is segregation of Bi at grain boundaries, the thickness can be estimated to be less than 1 nm, and the required thickness for practical application is sub-mm level, so the effect of Rayleigh scattering due to the grain boundary layer should be minor in this case. In addition, when there is a region where the amount of Bi in YIG increases, the variation of the refractive index of that portion is not large either, so the scattering should be very small also in this case.

Figure 8.6 shows the XRD (X-ray diffraction) patterns of $(Bi_{1.1}Gd_{1.9})Fe_5O_{12}$ single crystal produced by LPE method, and $(Bi_xY_{3-x})Fe_5O_{12}$ ceramics with Bi substitution amount x = 0.4 and 0.8, together with the JCPDS card for yttrium iron bismuth oxide as a reference. $(Bi_{1.1}Gd_{1.9})Fe_5O_{12}$ single crystal has a diffraction pattern with only <111> orientation, the ceramic has a pattern similar to that shown in the JCPDS card, and secondary phases were not detected.

Figure 8.7 shows measured values of the Faraday rotation angle at 1550 nm for $(Bi_{0.4}Y_{2.6})Fe_5O_{12}$ ceramic in which Bi is substituted with x = 0 ~ 1.1. The Faraday rotation angle of YIG is +174 deg cm^{-1}, but it is noted that the rotation direction is negative for Bi substituted samples. The rotation angle increased linearly with the substituted amount of Bi, and the Faraday rotation angle at x = 1.1 was -970 deg cm^{-1}. By calculation in this plot, the rotation angle per unit amount of Bi was -31.2 deg cm^{-1} in terms of 1 atomic % of Bi. GIG shows +40 deg cm^{-1} Faraday rotation angle when Bi: x = 0, and it rotates to the negative direction similar to in Bi substituted YIG and rotation angle increased with an increase of Bi addition amount. The rotation angle per Bi unit amount of the Bi-substituted GIG single crystal was -30.0 deg cm^{-1} when calculated by 1 atomic % of Bi. The fact that

all the Bi-substituted YIG ceramics show translucency, and the contribution of the substituted Bi to the Faraday rotation angle suggests that Bi has been replaced with Y at the dodecahedron site of the garnet structure. When the substituted Bi is solid-dissolved in iron garnet host, the Faraday rotation angle per atomic percent of Bi is about 30~31 deg cm^{-1} for both polycrystal and single crystal.

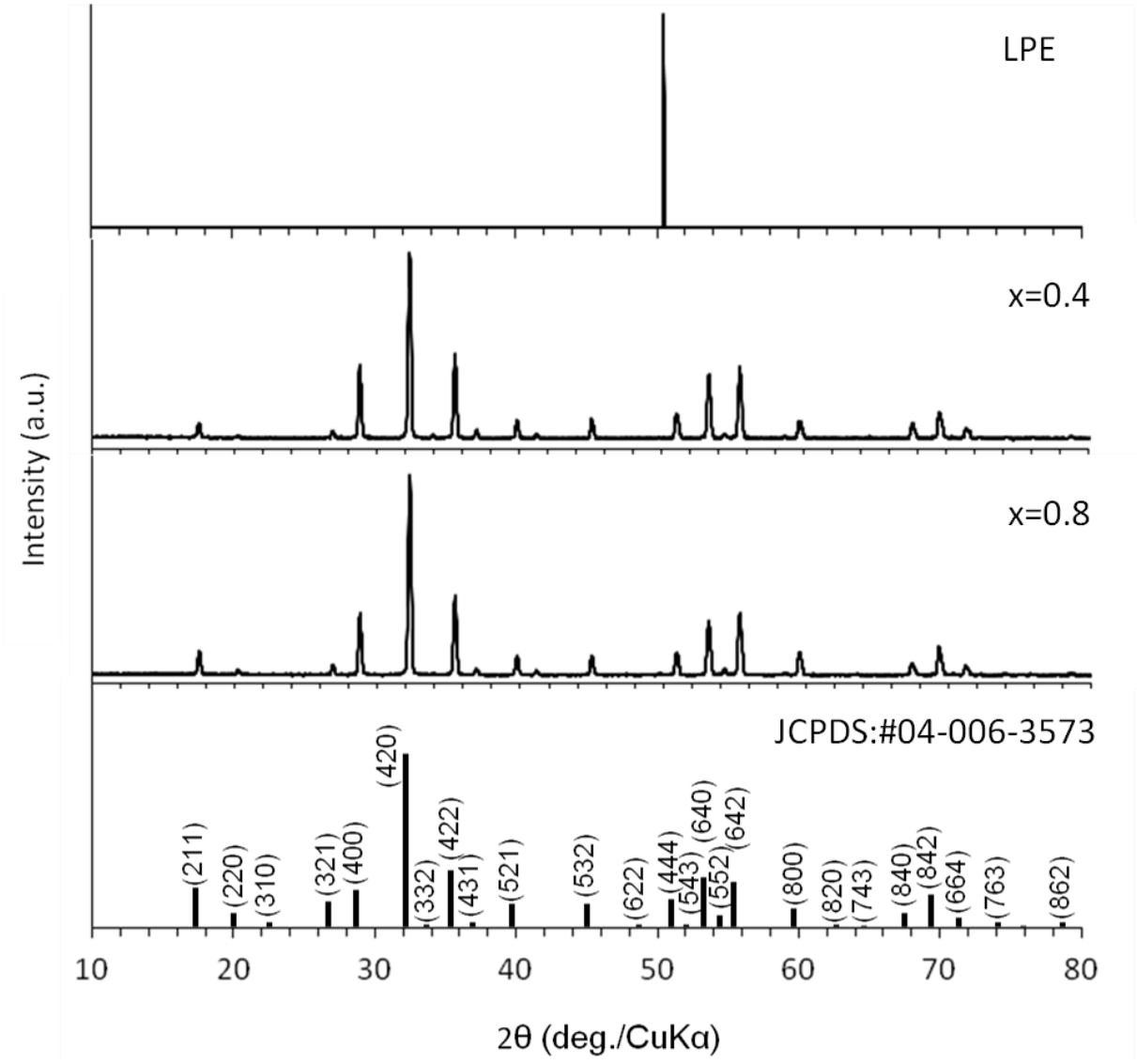

Figure 8.6 XRD patterns of $(Bi_{1.1}Gd_{1.9})Fe_5O_{12}$ single crystal by LPE method and $(Bi_xY_{3-x})Fe_5O_{12}$ ceramics with x=0.4 and 0.8, and JCPDS card for yttrium iron bismuth oxide.

Bi substituted iron garnets are known to exhibit huge magneto-optical effects, but conventionally only LPE method is available for industrial production. In addition, a single crystal wafer substrate with a lattice constant that matches the Bi-substituted iron garnet to be manufactured is required (a single crystal substrate in which a specific element is added to GGG in order to minimize the lattice constant mismatch). It takes three to

seven days to grow. However, in the sintering method, the growth of single crystal substrate is unnecessary, and the production time is extremely short, and it is possible to produce a large amount of ceramics at one time. In single crystal growth from the melt, since the segregation coefficient of Bi to iron garnet is small, an LPE method capable of providing a steep temperature gradient is essential. Since a solid-liquid interface does not exist in the sintering method, it is not necessary to consider the segregation coefficient of Bi, and it can be solid-dissolved up to the limit of the lattice constant that can maintain garnet crystal structure. Therefore, synthesis of Bi substituted iron garnet by reactive sintering becomes possible. In this work, when x = 1.1 or larger, significant segregation of Bi and a decrease in Faraday rotation angle were confirmed, and it is necessary to determine the solid solution limit of Bi in the case of reactive sintering.

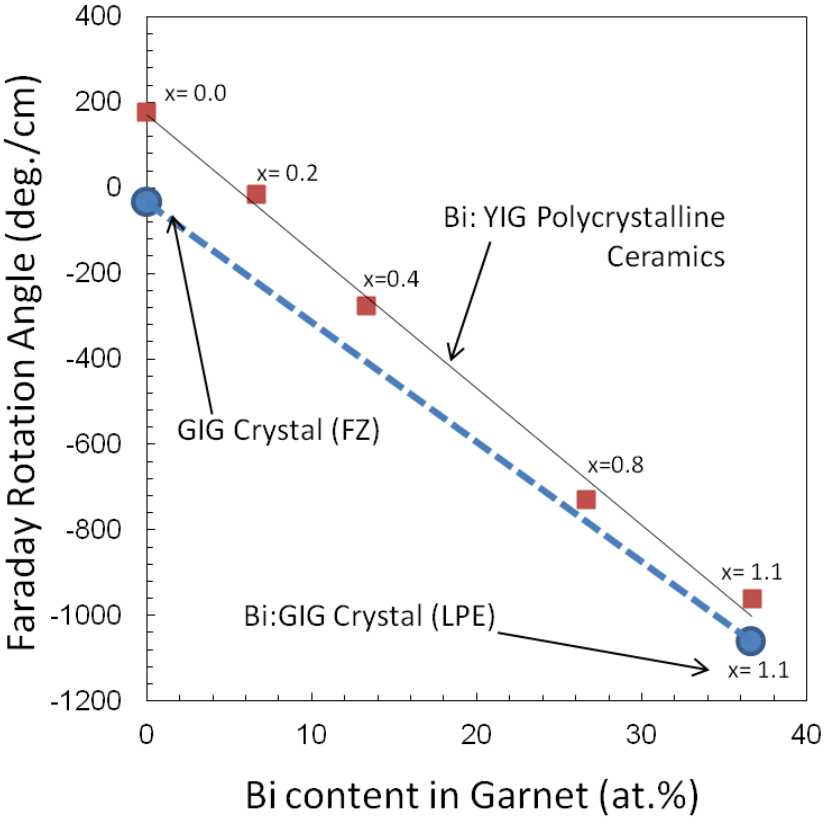

Figure 8.7 Faraday rotation angle of produced $(Bi_xY_{3-x})Fe_5O_{12}$ ceramics and Bi doped GIG single crystal against Bi content at 1550 nm.

8-4. Summary

Fabrication of Bi substituted iron garnet ceramics was successful for the first time which was only able to synthesize by LPE method conventionally and confirmed promising characteristics as Faraday isolator for optical communication. The results obtained are summarized below.

1. We have succeeded in synthesizing polycrystalline $(Bi_xY_{3-x})Fe_5O_{12}$ [x=0~1.1] ceramics by the reactive sintering method of Y_2O_3, Fe_2O_3, and Bi_2O_3.
2. Segregation of Bi was not detected in the obtained $(Bi_xY_{3-x})Fe_5O_{12}$ ceramics by XRD and SEM analysis. However Bi segregation (or YIG lattice with high Bi concentration) at near grain boundary area less than 1 nm was confirmed by HR-TEM-EDS analysis.
3. The transmission characteristics are very sensitive to the stoichiometric composition.
4. The transmission characteristics of the obtained ceramics are very close to that of the Bi:GIG single crystal produced by LPE method.
5. The Faraday rotation angle per atomic percent of Bi of the polycrystalline ceramics and the single crystal exhibits the similar value around -30~31 deg cm^{-1} at 1550 nm.

Until now, Bi-substituted iron garnets which are transparent in a wavelength band longer than 1.2 μm were able to produce only by the LPE method. But in this work, it was demonstrated that polycrystalline ceramics by the sintering method can also provide similar characteristics. It is no doubt that a new technology that can replace the LPE method was finally discovered. In addition, even a randomly oriented microcrystalline body having many grain boundaries can have magneto-optical properties equivalent to those of a single crystal. This invention opens the door to new material science.

References

1. T. Tokumatsu, “Optical Isolator”, Bull. Ceram. Soc. Jpn., **31** [1] 15-18 (1996).

2. T. Nakano, H. Yuri, U. Kihara, “Magneto-Optical Properties of YIG Single Crystal by TSFZ Method”, IEEE Trans. Magn., **20** [5] 986-988 (1984).

3. S. Kimura, K. Kitamura, I. Shido, “Growth of Rare Earth Garnet Crystals by the Floating Zone Method”, J. Cryst. Growth, **65** [1/3] 543-548 (1983).

4. E. Khazanov, N. Andreev, O. Palashov, A. Poteomkin, A. Sergeev, O. Mehl, H. David, “Effect of Terbium Gallium garnet Crystal Orientation on the Isolation Ratio of a Faraday Isolator at High Average Power”, Appl-Opt., **41** [3], 483-492 (2002).

5. N. P. Barnes, “Variation of the Verdet Constant with Temperature of Terbium Gallium Garnet”, J. Opt. Soc. Am. B, 9 [10], (1992).

6. T. Tamaki, H. Kaneda, N. Kawamura, “Magneto-Optical Properties of Terbium Bismuth Iron Oxide ($(TbBi)_3Fe_5O_{12}$) and Its Application to a 1.5μm Wideband Optical Isolator”, J. Appl. Phys., **70** [8], 4581-4583 (1991).

7. R. Yasuhara, S. Tokita, J. Kawanaka, T. Kawashima, H. Kan, H. Yagi, H. Nozawa, T. Yanagitani, Y. Fujimoto, H. Yoshida, M. Nakatsuka, “Measurement of Magneto-Optical Properties and Thermal Conductivity on TGG Ceramic for Faraday Material of High-Peak and High Average Power Laser”, Rev. Laser Eng., **35**, 806-810

(2007).

8. M. Geho, T. Sekijima, T. Fujii, “Growth of Terbium Aluminum Garnet ($Tb_3Al_5O_{12}$: TAG) Single Crystals by the Hybrid Laser Floating Zone Machine”, J. Cryst. Growth, **267**, 188-793 (2004).

9. S. Ganschow, D. Klimm, P. Reiche and R. Uecker, “On the Crystallization of Terbium Aluminum Garnet”, Cryst. Technol. 34 [5-6] 615-19 (1999).

10. Y. L. Aung, A. Ikesue, “Development of Optical Grade $(Tb_xY_{1-x})_3Al_5O_{12}$ Ceramics as Faraday Rotator Material”, J. Am. Ceram. Soc., **100** [9] 4081-4087 (2017).

11. M. Imaeda, S. Matsuzawa, “Growth of Yttrium Iron Garnet Single Crystal by Solid-Solid Reaction”, Proc. 1st Jpn. International SAMPE Symposium, Nov. 28 – Dec. 1st, 419-434 (1989).

12. A. Ikesue, Y. L. Aung, “Development of Optical Grade Polycrystalline YIG Ceramics for Faraday Rotator”, J. Am. Ceram. Soc., **101** [11], 5120-5126 (2018).

13. K. Tsushima, N. Koshizuka, “Research activities on Magneto-optical devices in Japan”, IEEE Trans. Magn., **23** [5], 3473-3478 (1987).

14. H. Takeuchi, “The Faraday Effect of Bismuth Substituted Rare-Earth Iron Garnet”, Jpn. J. Appl. Phys., **14** [12] 1903-1919 (1975).

15. T. Hibiya, “Liquid Phase Epitaxial Growth of Thick Garnet Films – “Perfectness” of Crystal Quality”, J. Magn. Soc. Jpn., **11** [S1] 167-172 (1987).

16. V. Tolksdori, “Growth and Properties of Garnet Films for Storage Application”, IEEE Trans. Magn., 11 [5] 1074-1077 (1975).

17. Y. Yokoyama, H. Umezawa, T. Takahashi, T. Okumura, N. Koshizuka, “Hydrogen Annealing Effects on The Optical Absorption of Bi-Substituted Iron Garnet Films”, J. Magn. Soc. Jpn., **11** [S1] 203-206 (1987).

18. P. Hansen, B. Hill, W. Tolksdorf, “Optical Switching with Bismuth-Substituted Iron Garnet”, Philips Tech. Rev., **41** [2] 33-45 (1983/84).

19. H. Takeuchi, “The Faraday Effect of Bismuth Substituted Rare-Earth Iron Garnet”, Jpn. J. Appl. Phys., **14** [12] 1903-1919 (1975).

20. Japanese Unexamined Patent Application Publication No. 2-51494 (1990).

21. H. Hayashi, S. Iwasa, N. J. Vasa, T. Yoshitake, K. Ueda, S. Yokoyama, S. Higuchi, “Characteristics of Bi:YIG Magneto-Optic Thin Films Fabricated by Pulsed Laser Deposition Method for an Optical Current Transformer”, Jpn. J. Appl. Phys., **41** 410 (2002).

22. M. C. Onbasli, L. Beran, M. Zahradník, M. Kučera, R. Antoš, J. Mistrík, G. F. Dionne, M. Veis, C. A. Ross, “Optical and magneto-optical behavior of Cerium Yttrium Iron Garnet thin films at wavelengths of 200–1770 nm”, Sci. Rep. **6**, 23640 (2016).

Chapter 9 Giant Faraday Rotation in Heavily Ce-doped YIG Bulk Ceramics

9-1. Introduction

Paramagnetic materials such as TGG ($Tb_3Ga_5O_{12}$) and TAG ($Tb_3Al_5O_{12}$) described in Chapters 2 to 5, are being used as Faraday rotator in optical isolators for 1 μm band fiber laser because they have excellent Faraday characteristics in the visible to near infrared wavelength regions [1-4]. However, since they have small Verdet constants, a longer length of Faraday rotator element and also stronger magnetic field are required for applications longer than 1 μm wavelengths, which causes problems for practical application. As described in Chapter 6, the iron garnet represented by YIG ($Y_3Fe_5O_{12}$) can transmit light in a wavelength region longer than 1.2 μm and it exhibits ferrimagnetic properties, enabling the technical problem of paramagnetic materials to be solved. Faraday rotators with higher Faraday rotation angle are required for optical communication applications. In Chapter 8, it was demonstrated that a huge Faraday rotation angle can be obtained by adding Bi to the iron garnet materials, so that the optical isolator device can be downsized. Thus, Bi-substituted iron garnet (Bi:YIG) can be generally used for a 1.5 μm band optical communication [5, 6]. Currently, Bi:YIG single crystals can only be produced by the LPE (Liquid phase Epitaxial) method. In this method, it is necessary to grow the Bi:YIG crystals on an expensive GGG ($Gd_3Ga_5O_{12}$) single crystal substrate although their lattice constants mismatch, and it requires from 3 to 7 days to grow a thick film of approximately 1 mm [7]. For new applications such as automatic driving and telemedicine (tele-operative surgery using Da Vinci system, etc.), an ultra-high-speed and high-capacity 5G telecommunication system is expected to be put into practical use in the near future. Even in this current case, the systems using optical fibers are unchanged and optical isolators essential for fiber transmission are also positioned as important fundamental technologies, and their demand is expected to increase rapidly. Thus, in this sense, there is a background for manufacturing processes that can realize high-speed and mass-productivity which are different from the conventional LPE method, and new material development that exceeds the conventional performance is essential.

Ce has been reported as an effective additive element exhibiting a Faraday rotation angle equal to or greater than Bi. Ce-substituted iron garnet single crystals have been synthesized using the FZ (Floating Zone) method or the flux method [8-10], but the segregation coefficient of Ce against iron garnet is extremely small, and it is difficult to form a solid solution inside the single crystal. Even if a Ce-substituted iron garnet single crystal can be produced by the FZ method, the basic optical property of the material is low, and the Ce concentration in the crystal growth direction is not constant. Hence, the Faraday rotation angle of the processed specimens varies from one to another. Therefore, it is difficult to use it for industrial applications.

In Chapter 6, the synthesis of transparent polycrystalline YIG ceramics [11,12] which was considered as quite difficult to synthesize, was succeeded for the first time in the world by our research work. Moreover, it was shown in Chapter 8 that the magneto-optical performance of Bi-substituted transparent polycrystalline YIG ceramics [13], which exhibits a huge Faraday rotation, is comparable to that of the same crystal by the LPE

method. Therefore, based on these findings, the purpose of this work is to synthesize by the sintering method the Ce-substituted transparent YIG polycrystalline ceramics, which are difficult to synthesize even by the single crystal growth method.

9-2. Experimental procedure

Starting materials were Y_2O_3 (60 nm), Fe_2O_3 (1 μm) and CeO_2 (1 μm) having >4N (99.99 %) purity. These starting materials were weighed so as to have a stoichiometric composition of $(Ce_xY_{3-x})Fe_5O_{12}$ [x=0~0.24], and ball milled with high purity alumina balls in ethanol for 15 hours. Tablets of Φ8 and 12 mm size were formed by uniaxial press, and then treated in CIP (Cold Isostatic Press, Model CIP-133, Kobe Steel, Ltd., Tokyo, Japan) at 98 MPa. The preformed body was calcined at 600 °C and then sintered at 1250 to 1450 °C for 2 hours in O_2. In order to obtain transparent Ce:YIG ceramics, a sintered body having a relative density of approximately 95 % was obtained by pre-sintering at 1350 °C. This sintered body was treated with HIP (Hot Isostatic Press, Model O_2-Dr. HIP, Kobe Steel, Ltd., Tokyo, Japan) using 10 % O_2-Ar gas under the conditions of 1300 °C for 1 hour (pressure at the maximum temperature was 98 MPa). After adjusting the thickness of the obtained ceramic samples, both surfaces were mirror polished and the Faraday rotation angle of the obtained material was measured in a magnetic field of 0.3 T under the same manner described in the previous chapters. Microstructure characterization using microscopies including SEM, SEM-EDS and TEM was also performed as described in the previous chapters.

9-3. Results and discussion

Figure 9.1 shows the microstructures of samples obtained by sintering a green powder compact having a $(Ce_{0.12}Y_{2.88})Fe_5O_{12}$ composition at 1250 to 1400 ºC for 2 hours at each sintering temperature and then mirror polishing and thermal etching. As seen in these pictures, densification is insufficient at 1250 ºC and the relative density is only 87 %. The density and grain size increase with increasing sintering temperature. In the sample sintered at 1250 °C, high brightness portions (secondary phase with high Ce concentration) are observed, but the number of these portions decreases as the sintering temperature increases. In the sample sintered at 1400 °C for 5 hours, the secondary phase almost completely disappeared.

Figure 9.2 shows reflection micrographs of $(Ce_xY_{3-x})Fe_5O_{12}$ [x = 0.06, 0.12 and 0.24 (Ce concentration 2, 4, 8 at.%)] ceramics HIP treated with 10 % O_2-Ar gas at 49 MPa pressure and 1300 °C for 1 hour. These ceramics have an average grain size of approximately 3~5 μm, independent of Ce concentration. Residual pores and secondary phases cannot be detected on the surface and only a garnet single phase was observed.

A conventional low magnification image (C-TEM) and high-resolution transmission electron microscopic (HR-TEM) image near the grain boundary of $(Ce_xY_{3-x})Fe_5O_{12}$ [x=0.12] ceramics are shown in Figure 9.3 (a) and (b), respectively. A garnet lattice structure is formed up to the vicinity of the grain boundary, and the grain

boundary phase cannot be detected. In addition, since the secondary phase and the grain boundary phase cannot be detected even by observation with a C-TEM, it can be believed that the synthesized Ce:YIG ceramics formed a clean grain boundary structure and is composed of a garnet single phase.

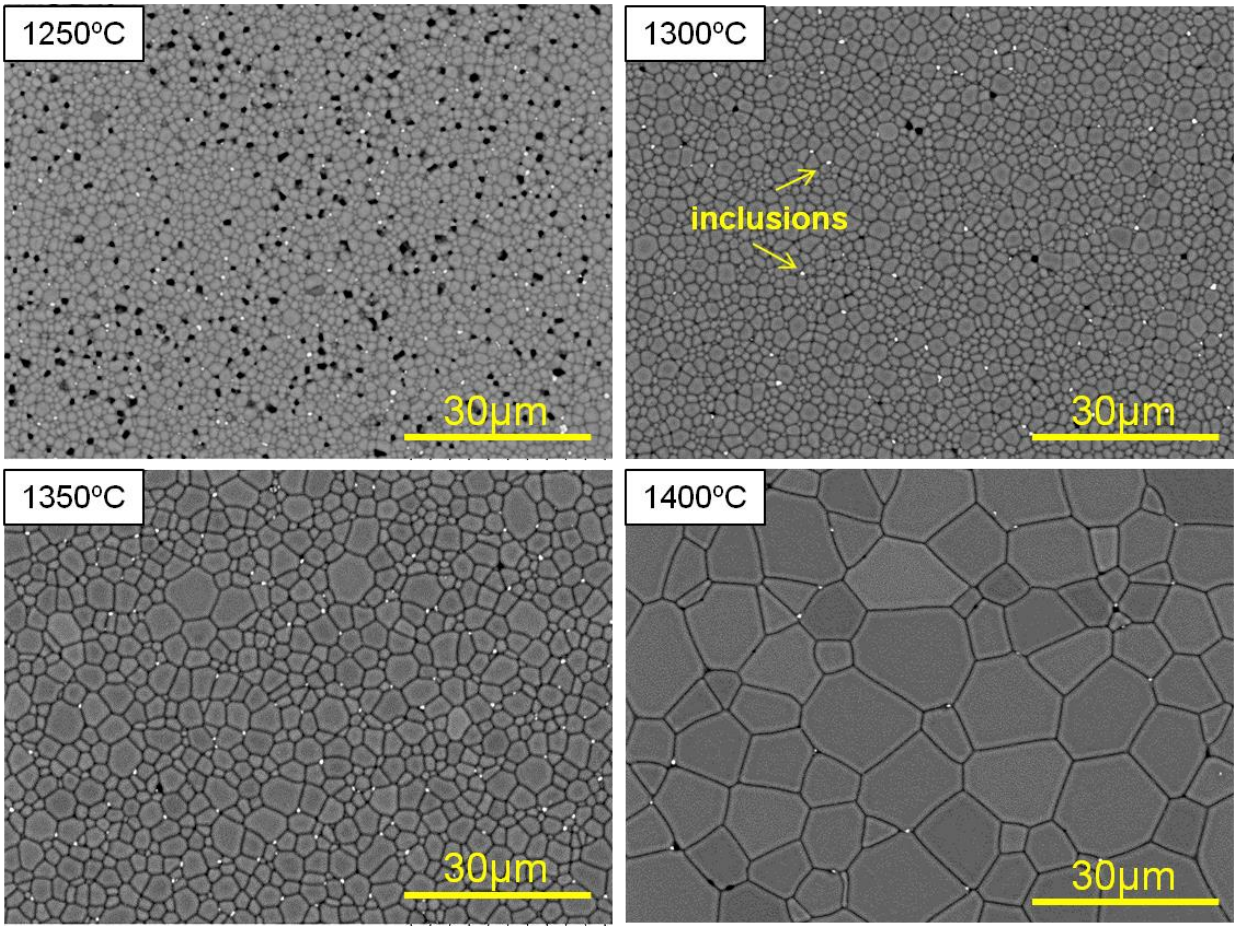

Figure 9.1 Microstructure of $(Ce_{0.12}Y_{2.88})FeO_{12}$ ceramics sintered at 1250 ~ 1400 ºC for 2 hours by BEI (back-scattered electron image).

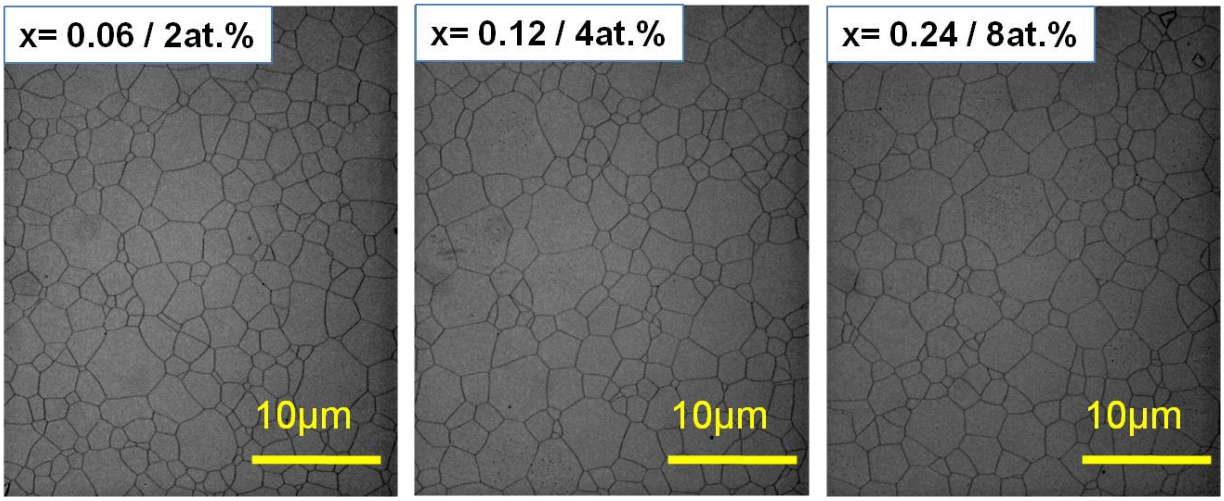

Figure 9.2 Reflection microscopic photograph of $(Ce_xY_{3-x})Fe_5O_{12}$ ceramics after HIP at 1300 ºC.

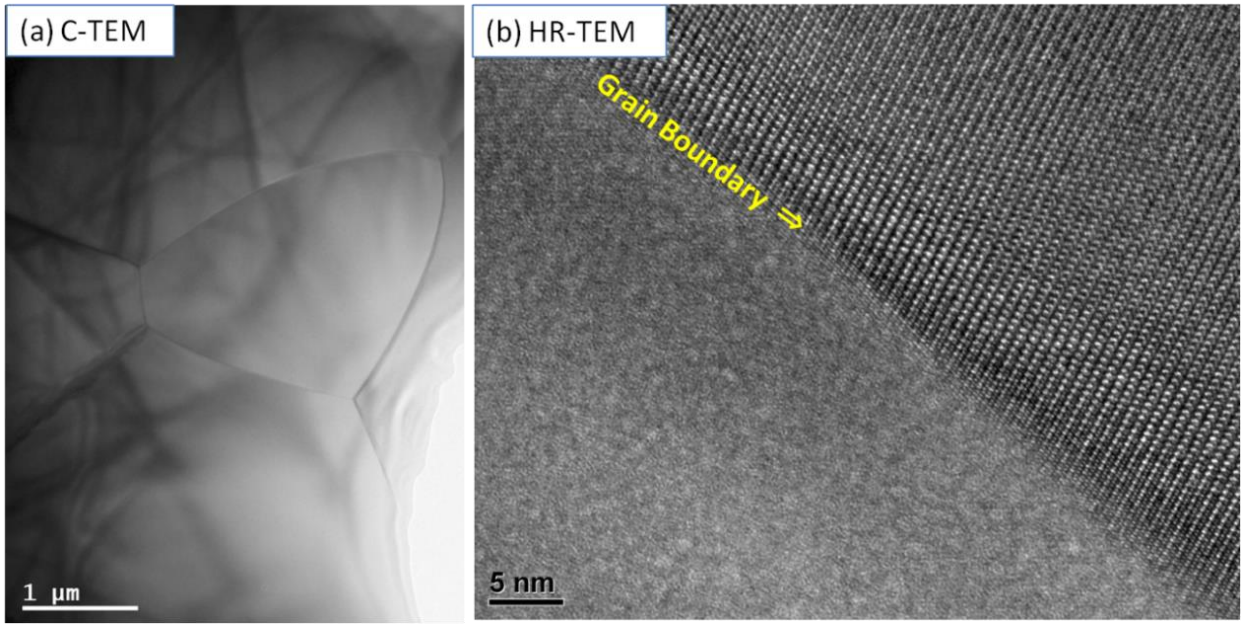

Figure 9.3 (a) Conventional TEM image and (b) lattice structure near the grain boundary of $Ce_{0.12}Y_{2.88}Fe_5O_{12}$ Ceramics after HIP by HR-TEM.

Figure 9.4 shows the XRD patterns of the prepared $(Ce_{0.12}Y_{2.88})Fe_5O_{12}$ ceramic shown in the above figures and the JCPDS (# 04-006-357) data of YIG as a reference. The material produced is similar to the diffraction pattern of reference YIG (the difference was only the change in lattice constant due to the addition of Ce). The impurity phases associated with the segregation of $YFeO_3$, Fe_2O_3, or Ce due to the compositional deviation from the stoichiometric composition could not be detected. This shows that the material is also garnet single phase as measured by the XRD diffraction.

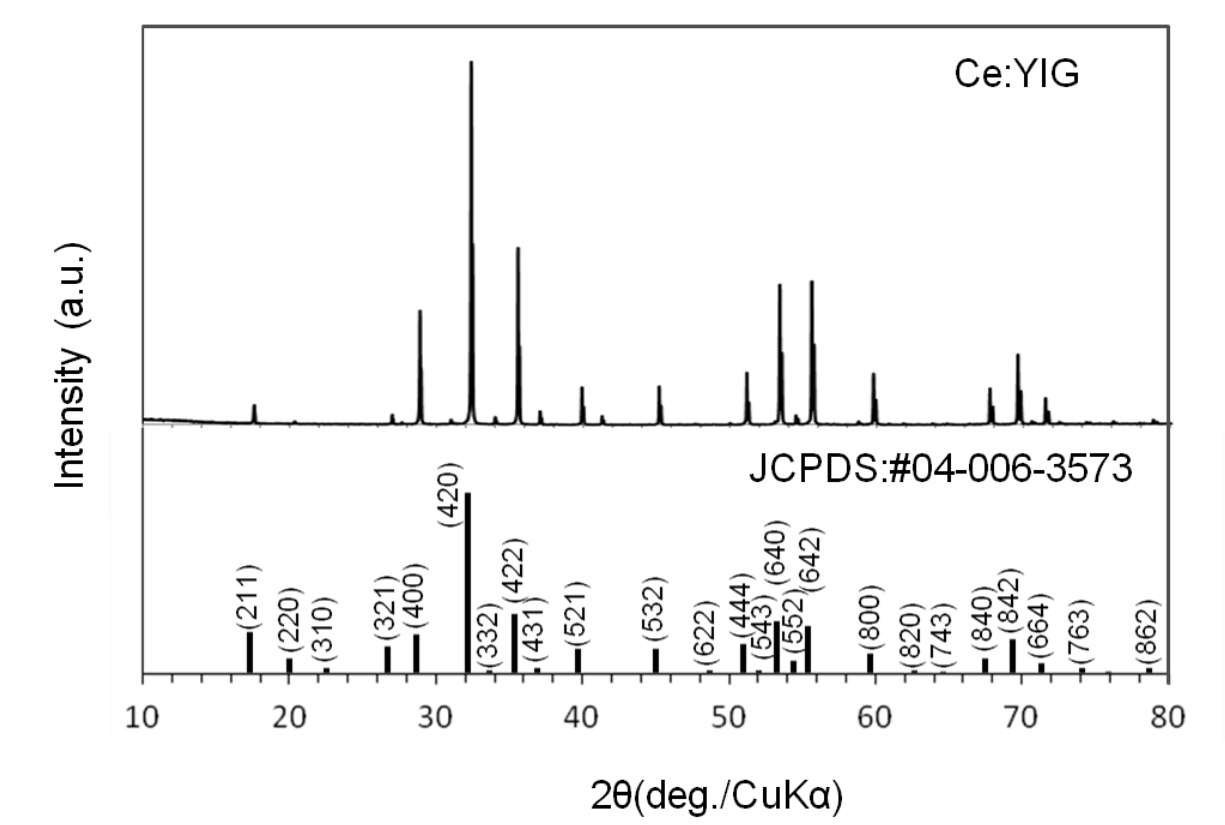

Figure 9.4 XRD pattern of Ce:YIG ceramics with reference JCPDS card.

Figure 9.5 shows a spot analysis result of the Ce concentration inside a $(Ce_{0.12}Y_{2.88})Fe_5O_{12}$ ceramic of Φ6 × L20 mm using SEM-EDS. It was confirmed that the Ce concentration in the radial direction and the length direction of the material was almost constant, and there was no segregation similar to the single crystal produced by the FZ method. In addition, Ce:YIG single crystals synthesized by the FZ method have a very low transmittance, thus there is a problem of Ce segregation (precipitation of Ce compound and optical transmission loss) simultaneously with the concentration gradient of Ce in the material.

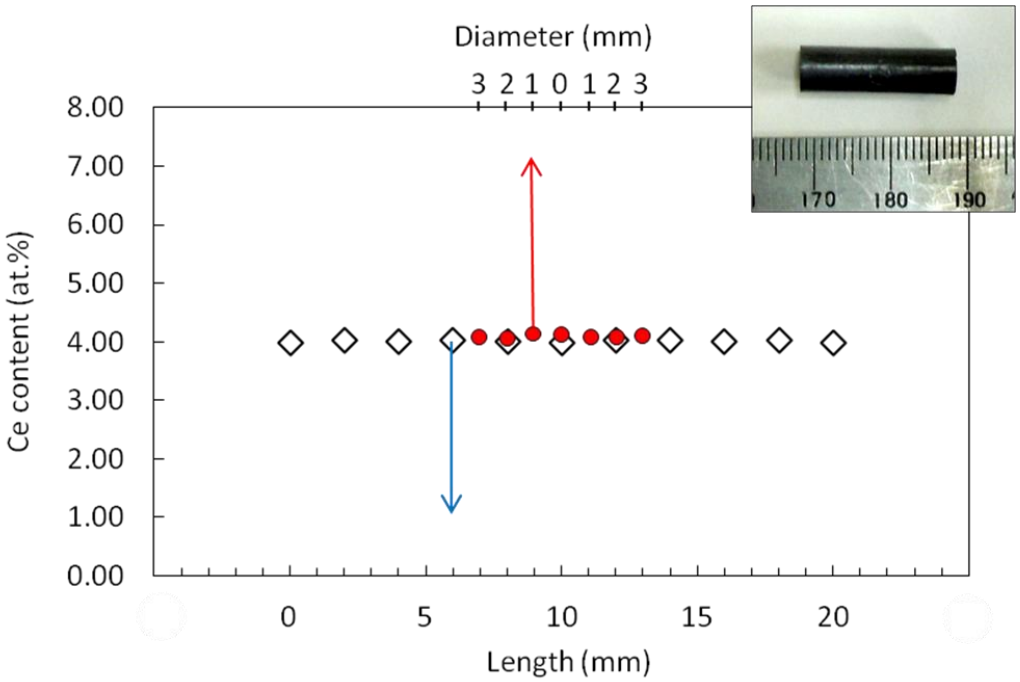

Figure 9.5 Appearance of Ce:YIG ceramics (inset) and distribution of Ce concentration in the radial direction and the length direction of the material by spot analysis.

Figure 9.6 shows the magnetic domain structure and cross Nicol image of $(Ce_{0.12}Y_{2.88})Fe_5O_{12}$ ceramics. This shows an intrinsic magnetic domain structure similar to previously reported polycrystalline YIG and TbIG ($Tb_3Fe_5O_{12}$) ceramics [11, 12], which is obviously different from that of single crystal materials. In addition, when the material is observed with polarized light, it shows a dark field (a black image without light transmission), thus birefringence does not exist in the produced Ce:YIG ceramics. The magnetic domain structure was also observed inside the material and a small number of residual pores with less than 1 μm were observed at higher magnification.

Figure 9.7 (a) shows the transmission spectrum of $(Ce_{0.12}Y_{2.88})Fe_5O_{12}$ ceramic with a thickness of 0.5 mm, and the transmission in the 1500~2000 nm region was 62~70 %. The Ce-doped YIG single crystal (thickness 0.2 mm) synthesized by the flux method has a transmittance of approximately 72 % (wavelength at 1550 nm). [8] Pure YIG without Ce doping has a theoretical transmittance of 75 % [8], but the doping of Ce increases the refractive index, which lowers the theoretical transmittance. Since the refractive index of this material developed in this work is unknown, it is not possible to calculate the Fresnel loss. However, it is a fact that the transmission characteristic of this material is superior to that of the single crystals synthesized by the flux or FZ methods [10]. However, the absorption coefficient of this material at a wavelength of 1550 nm is 0.3 cm^{-1} (refer Figure 9.7 (b)), and hence the presence of Mie and Rayleigh scattering inside the material cannot be denied due to the wavelength dependence of transmittance.

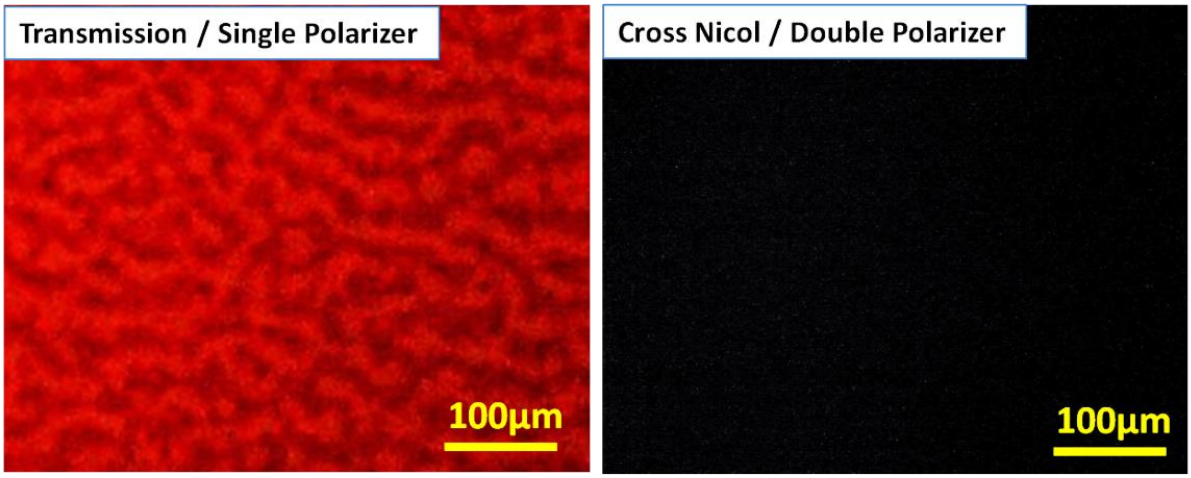

Figure 9.6 Magnetic domain structure and crossed polarizing of $(Ce_{0.12}Y_{2.88})FeO_{12}$ ceramics.

A sintered body of the same composition with a density of 99.9 % was prepared by atmospheric pressure (i.e., normal pressure) sintering in an O_2 atmosphere. However, even though this sample was polished to the same thickness as the above ceramics, it does not transmit light at all. By further observations, it was confirmed that there was no segregation of Ce (Ce compound) in the atmospheric pressure sintered sample, and no scattering sources other than a few residual pores. In addition, it was confirmed that light is transmitted (t = 0.5 mm, transmittance of about 40 % at a wavelength of 1500 nm) when this normal pressure sintered sample was treated by O_2-HIP. From this fact, it is considered that Fe^{2+} is formed in the sample without O_2-HIP treatment, and that significant absorption occurs in the measuring wavelength ranges.

Figure 9.7 (b) shows the absorption coefficients at a wavelength region of 1200~2400 nm for 8 at.% Ce:YIG single crystal prepared by FZ method and 4 at.% Ce:YIG ceramic prepared in this work by sintering method and Bi-substituted iron garnet single crystal prepared by LPE method as a reference [10]. Generally, the absorption coefficient indicates the transparency of the base material including absorption and scattering due to impurities, etc., however the ceramics obtained in this work are much more transparent than Bi-substituted iron garnet and Ce:YIG single crystal (absorption coefficient is less than 1/10 in all wavelength ranges). It has been reported that the synthesis of Ce:YIG single crystals is extremely difficult. By this study, it was found that even Bi:YIG crystals which are only producible by the FZ method cannot reach the performance of the polycrystalline Ce:YIG ceramics synthesized by the sintering method.

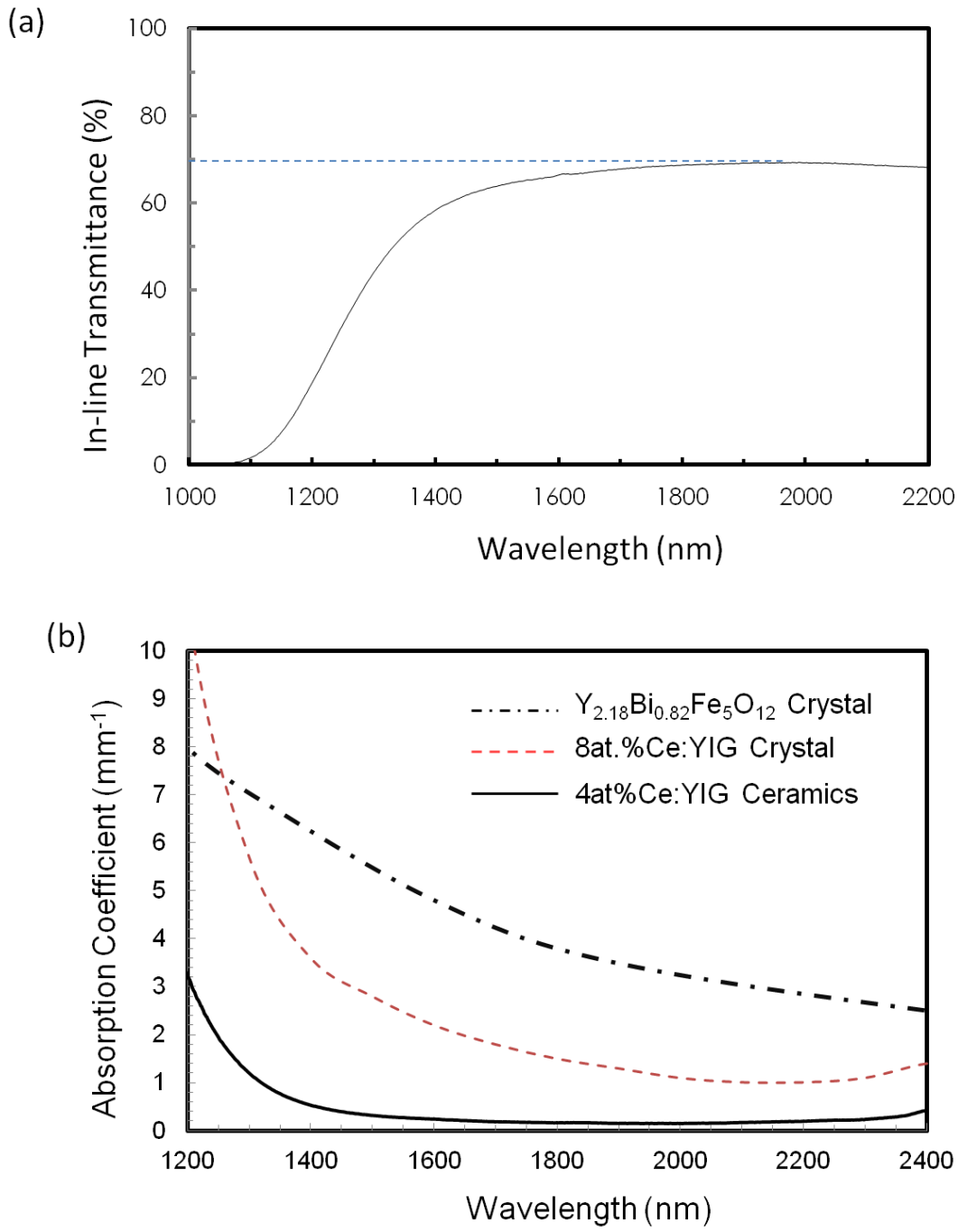

Figure 9.7 (a) In-line transmission spectrum of $(Ce_{0.12}Y_{2.88})FeO_{12}$ ceramics (t=0.5 mm) measuring between 1000 and 2500 nm. (b) Comparative data of absorption coefficient between Ce:YIG single crystal by FZ method and Ce:YIG ceramics produced in this work, and Bi:YIG ceramics as a reference ranging from 1200 to 2400 nm.

Figure 9.8 shows measured values of the Faraday rotation angle at a wavelength of 1550 nm of $(Ce_xY_{3-x})Fe_5O_{12}$ ceramics in which Ce is dissolved in YIG with 2, 4, and 8 at.%. YIG has a Faraday rotation angle of +175 deg cm^{-1}, however the rotation direction is reversed when Ce is doped. The rotation angle varied linearly with the Ce doping amount, and the Faraday rotation angle at Ce 4 at.% and 8 at.% was -352 and

-990 deg cm^{-1}, respectively. The amount of change in the rotation angle per 1 at.% Ce is -144 deg cm^{-1}. In the figure, the Faraday rotations of GIG ($Gd_3Fe_5O_{12}$) single crystal by the FZ method and $(Bi_{1.1}Gd_{1.9})Fe_5O_{12}$ (Bi = 37 at.% doped) synthesized by the LPE method are shown.

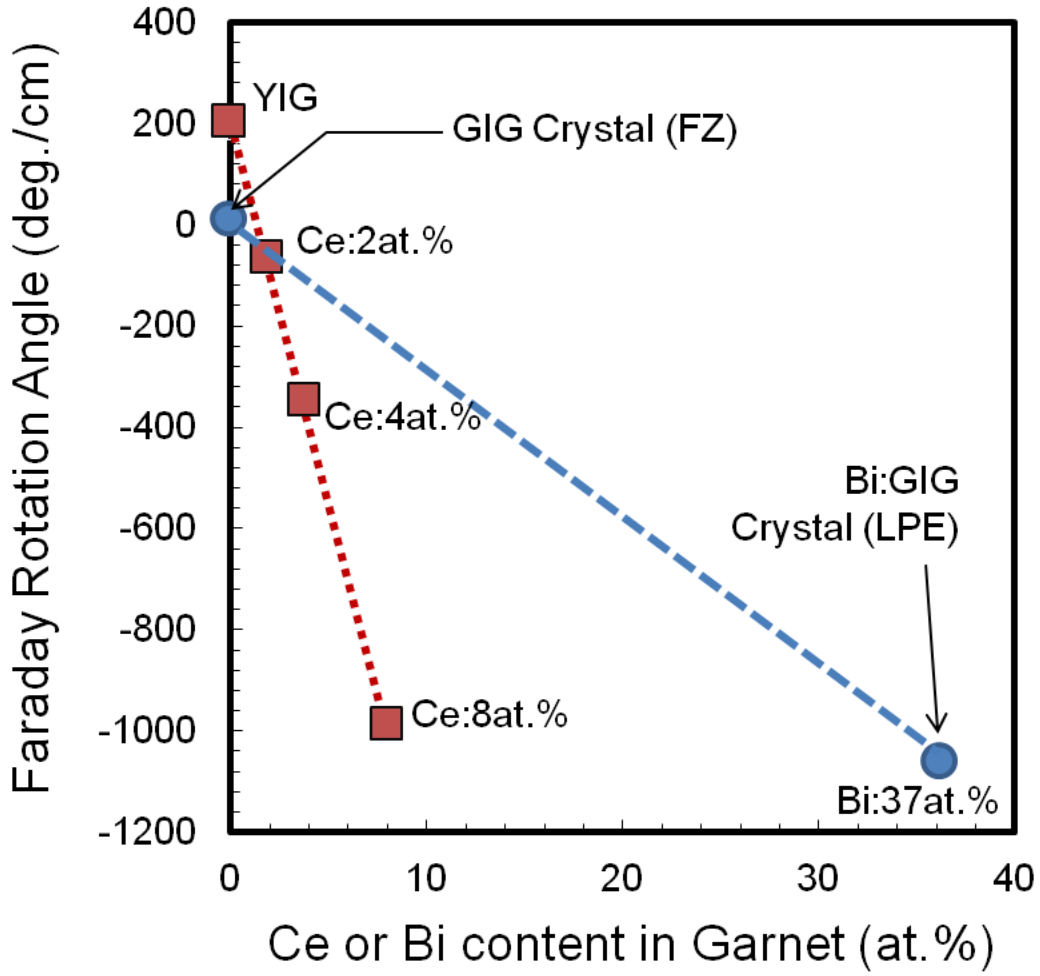

Figure 9.8 Faraday rotation angle of produced $(Ce_xY_{3-x})Fe_5O_{12}$ ceramics and Bi doped GIG single crystal against Ce or Bi content at 1550 nm.

In the case of Bi system, the Faraday rotation angle per 1 at.% Bi is -29 deg cm^{-1}. Thus, Ce system shows an excellent magneto-optical effect about 5 times higher than that of Bi system. The added Ce contributes to the Faraday rotation angle, suggesting that Ce was substituted for Y in the dodecahedron site of garnet structure. If the added Ce was totally dissolved in the host iron garnet, it was proved that the performances were far superior to the currently used Bi-substituted iron garnet crystal. It is well known that iron garnet material doped with Bi exhibits a huge magneto-optical effect and is applied in industry. However, problem is that Bi:YIG crystal can

only be produced by the LPE method. In addition, a single crystal wafer substrate having a lattice constant that matches the Bi-substituted iron garnet to be produced (a single crystal substrate obtained by adding a specific element to GGG in order to reduce mismatch of lattice constants) is indispensable, and it also requires from 3 to 7 days to form a thick film of approximately 1 mm. In single crystal growth from melt, the segregation coefficient of Bi to iron garnet is small, thus the LPE method that can provide a steep temperature gradient is indispensable. Bi-substituted iron garnet thick film single crystals are extremely low in productivity, thus there is an economic problem that requires numerous crystal growth equipment. On the other hand, Ce substitution is necessary to exceed the performance of Bi-substituted iron garnet, but its synthesis is difficult under the LPE method. Therefore, FZ method was applied to synthesize Ce:YIG crystal. S. Higuchi et al. reported that it is extremely difficult to form a solid solution of Ce doped iron garnet crystal [9,10]. Inhomogeneous and steep Ce concentration gradient is generated especially in the growth direction. Since the Ce concentration differs by 2 times or more at the beginning stage and at the end of crystal growth, the Faraday rotation angle cannot be controlled. (The analysis results in their paper show only changes in Ce concentration, and they did not confirm whether the added Ce was appropriately dissolved or not [10].) M. Huang et al. produced a Ce-substituted YIG single crystal using the flux method. The Faraday rotation angle at 1550 nm of the $Ce_{0.122}Y_{0.2878}Fe_5O_{12}$ single crystal is significantly lower than 50 deg cm^{-1} (the change amount of Faraday rotation angle per 1 at.% Ce is also less than 10 deg cm^{-1}), and transmission property is also very poor [8]. The reason why the Faraday rotation angle does not improve even when Ce is added to the YIG single crystal in their work is considered to be that only a part of the added Ce is replaced with Y. However, in this study, the synthesis of ceramics is based on a sintering method (reactive sintering) and there is no occurrence of solid-liquid interface, hence Ce is uniformly dissolved in YIG produced by this solid-state process without segregation. (However, there is a solid solution limit of Ce that forms an iron garnet lattice even in a ceramic process synthesized by solid-state reaction.) Therefore, as long as the Ce concentration of the whole ceramic material is uniform, and the problem of segregation inherent to the melt-growth single crystal does not principally occur in ceramics. A similar phenomenon is that a large amount of laser-active element (Nd) having a large ionic radius can be uniformly dissolved in YAG ($Y_3Al_5O_{12}$) ceramics, and it was proved that laser oscillation is possible by using the highly transparent Nd:YAG ceramics [14,15]. The author reported that a small amount of SiO_2 (derived by thermal decomposition of TEOS: Tetra-Ethyl Ortho Silicate), added as a sintering aid, was effective for solid solution of Nd in YAG grains. In this study, no sintering aid was added, but if a sintering aid effective for Ce solid solution in YIG material can be found, it would be possible to produce this material with more uniformity in large quantity.

M. C. Onbasli et al. [16] used a pulsed laser deposition (PLD) method to form a Ce:YIG thin film about 80 nm thick on a GGG single crystal substrate and measured the Faraday rotation angle at 1550 nm. The change amount of Faraday rotation angle per 1 at.% Ce is as good as -165 deg cm^{-1}, but the optical loss of the formed film is orders of magnitude larger than that of the Ce:YIG single crystal produced by FZ method [16]. The optical

loss of the Ce:YIG film obtained by vapor phase synthesis such as PLD method is very large, and there is also the fatal problem that a sample with practical thickness cannot be formed [17-19]. Shahrokhvand et al. [20] also used the PLD method to synthesize $Ce_{1.0}Y_{2.0}IG$ thin films on a GGG single crystal substrate to obtain 2.4×10^4 deg cm^{-1} at a wavelength of 635 nm, although there was no data for the 1.5 μm band. E. Lage et al. [21] also produced a $Ce_{0.59\pm0.18}Y_{2.86\pm0.18}Fe_{4.55\pm0.18}O_{12}$ thin film by the PLD method and confirmed that a Faraday rotation angle of about 4×10^3 deg cm^{-1} was generated in the 1.5 μm region. The thin film method was a method capable of synthesizing translucent Ce-substituted iron garnet. The PLD method is a synthesis from the gas phase and, as in the sintering method, the material is synthesized by a process in which very little (or no) Ce segregation occurred due to the presence of the solid-liquid interface. Therefore, it is considered that immense magneto-optic effect can be obtained by Ce substitution.

Although there are some reports on YIG, Bi and Ce substituted YIG ceramics [22-29], the facts related to the optical properties are not reported. Other than this author, there is only a report of YIG single crystal synthesized by sintering method by M. Imaeda [30]. The insertion loss (I.L.) of the fabricated <111> YIG single crystal ceramics is 2 dB even for a sample with a measurement wavelength of 1300 nm and a thickness of 1 mm (but a thickness of 2 mm is required to provide 45 ^{o} Faraday rotation for 1300 nm wavelength). Since the I.L. of lower than 0.1 dB is a recent requirement, it is not useful for practical applications. The development of paramagnetic TGG, TAG, and TYO ceramics has proved that Faraday elements can be used even in polycrystalline form if the optical quality is sufficiently high [31-33]. Magneto-optical ceramics have many technological and economic advantages such as no need of a single crystal wafer substrate, a short production time, uniform optical quality, and no size limitation. Therefore, ceramic optical isolators will be used in the mid-infrared optical communication field in the future.

9-4. Summary

The results obtained by this study are summarized below.

1. By the reactive sintering and HIP process using Y_2O_3, Fe_2O_3 and CeO_2 as starting materials, we could synthesize transparent Ce:YIG ceramics for the first time in the world.
2. The absorption coefficient of the obtained material is low, and the optical quality is far superior to that of the same single crystal or Bi-substituted single crystal synthesized by the FZ method.
3. The Faraday rotation performance of Ce:YIG ceramics is extremely high, -144 deg cm^{-1} per 1 at.% Ce, and 5 times larger than the rotation angle per 1 at.% Bi of a Bi:GIG single crystal prepared by LPE method.

Until now, there are many reports on Ce-substituted iron garnet ceramics, but they are not transparent materials and there is no information regarding their magneto-optical properties as well. The reason for this is unknown, but in the development of optical materials, Mie scattering (residual pores and heterogeneous phases)

and Rayleigh scattering issues (formation of clean grain boundaries) must be completely solved, and Fe^{2+} formation must be minimized. It seems that these key technologies have not been systematically controlled so far. From the above results, the polycrystalline Ce:YIG ceramics that can be fabricated by the sintering method surpassed the performance of Bi-substituted iron garnet, which is the main material of existing optical isolators applied in optical communication. In addition, this sintering method does not require a single crystal substrate, which is normally necessary in crystal growth process. This suggests that production by sintering method may give extremely excellent productivity. Thus, it is highly expected that this new material and method will form a promising Faraday rotator material and isolator device for optical communications moving to new 5G networks. Now magneto-optical materials are approaching a generational change from single crystal materials to polycrystalline ceramic materials.

References

1. N. P. Barnes, L. B. Petway, "Variation of the Verdet Constant with Temperature of Terbium Gallium Garnet", J. Opt. Soc. Am. B, **9** [10] 1912-1915 (1992).

2. E. Khazanov, N. Andreev, O. Palashov, A. Poteomkin, A. Sergeev, O. Mehl, D. H. Reitze, "Effect of Terbium Gallium Garnet Crystal Orientation on the Isolation Ratio of a Faraday Isolator at High Average Power", Appl. Opt., **41** [3] 483-492 (2002).

3. M. Geho, T. Takagi, S. Chiku, T. Fujii, "Development of Optical Isolators for Visible Light using Terbium Aluminum Garnet ($Tb_3Al_5O_{12}$) single crystals," Jpn. J. Appl. Phys., **44** [7A] 4967-4970 (2005).

4. M. Geho, T. Sekijima, T. Fujii, "Growth of Terbium Aluminum Garnet ($Tb_3Al_5O_{12}$: TAG) Single Crystals by the Hybrid Laser Floating Zone Machine", J. Cryst. Growth, 267, 188-793 (2004).

5. H. Takeuchi, "The Faraday Effect of Bismuth Substituted Rare-Earth Iron Garnet", Jpn. J. Appl. Phys., **14** [12] 1903-1919 (1975).

6. T. Tokumatsu, "Optical Isolator", Bull. Ceram. Soc. Jpn., **31** [1] 15-18 (1996).

7. I. Nomi, K. Nakashima, K. Machida, H. Ishikawa, "Magneto-Opto Element Materials" JPN Patent Opening No. H2-51494 (1988).

8. M. Huang, S. Y. Zhang, "Growth and Characterization of Cerium-Substituted Yttrium Iron Garnet Single Crystals for Magneto-Optical application", Appl. Phys. A, **74**, 177-180 (2002).

9. S. Higuchi, Y. Furukawa, S. Takekawa, O. Kamada, K. Kitamura, K. Ueda, "Magneto-optical Properties of Cerium-Substituted Yttrium Iron Garnet Single Crystals for Magnetic-Field Sensor", Sen. Actuators A Phys., **105**, 293-296 (2003).

10. S. Higuchi, K. Ueda, H. Hayashi, H. Kurobayashi, "Magneto-Optical Properties of Cerium- Substituted Yttrium Iron Garnet for Magnetic Field Sensor", T. IEE Japan, **121-**A [6], 541-546 (2001).

11. A. Ikesue, Y. L. Aung, "Development of Optical Grade Polycrystalline YIG Ceramics for Faraday Rotator".

J. Am. Ceram. Soc., **101** [11] 5120-5126 (2018).

12. Y. L. Aung, A. Ikesue, "Transparent $Tb_3Fe_5O_{12}$ Ceramics as MID-IR Isolator", J. Alloy Compd., **773**, 739-742 (2018).

13. Y. L. Aung, A. Ikesue, T. Watanabe, S. Makikawa, Y. Iwamoto, "Bi substituted YIG Ceramics Isolator for Optical Communication", J. Alloy Compd., **811**, 152059 (2019).

14. A. Ikesue, K. Kamata, "Role of Si on Nd Solid-Solution of YAG Ceramics", J. Jpn. Ceram. Soc., **103** [5] 489-493 (1995).

15. A. Ikesue, Y. L. Aung, T. Taira, T. Kamimura, K. Yoshida, G. L. Messing. "Progress in Ceramic Lasers", Mat. Res. Annual Rev., **36**, 397-429 (2006).

16. M. C. Onbasli, L. Beran, M. Zahardnik, M. Kucera, R. Antos, J. Mistrik, G. F. Dionne, M. Veis, C. A. Ross, "Optical and Magneto-Optical Behavior of Cerium Yttrium Iron Garnet Thin Films at Wavelengths of 200 – 1770nm", Sci. Rep. **6**, 23640 (2016).

17. T. Shintaku, A. Take, S. Mino, "Ce-substituted Yttrium Iron Garnet Films Prepared on $Gd_3Sc_2Ga_3O_{12}$ Garnet Substrates by Sputter Epitaxy", Appl. Phys. Lett., **71**, 1640-1642 (1997).

18. L. Bi, J. Hu, G. F. Dionne, L. Kimerling, C. A. Ross, "Monolithic Integration of Chalcogenide Glass / Iron Garnet Waveguides and Resonators for On-Chip Nonreciprocal Photonic Devices", Proc. SPIE 7941, 794105 (2011).

19. T. Goto, M. C. Onbasli, C. A. Ross, "Magneto-Optical Properties of Cerium Substituted Yttrium Iron Garnet Films with Reduced Thermal Budget for Monolithic Photonic Integrated Circuits", Opt. Express, **20**, 28507-28517 (2012).

20. S. M. Shahrokhvand, A. S. H. Rozatian, M. Mozaffari, S. M. Hamidi, M. M. Tehranchi, "Preparation and investigation of Ce:YIG thin films with a high magneto-optical figure of merit", J. Phys. D: Appl. Phys., **45** [23] 235001 (2012).

21. E. Lage, L. Beran, A. U. Quindeau, L. Ohnoutek, M. Kucera, R. Antos, C. A. Ross, "Temperature-dependent Faraday rotation and magnetization reorientation in cerium-substituted yttrium iron garnet thin films", APL Mater., **5** [3], 036104 (2017).

22. Tze-Chern Mao, Jyh-Chen Chen, "Influence of tea Addition of CeO_2 on Microstructure and the Magnetic Properties of Yttrium Iron Garnet Ceramics", J. Magnet. Magnet. Mat., **302**, 74-81 (2006).

23. Q. Fu, Q. Xu, Z. Zhao, X. Liu, Y. Huang, X. Hu, N. Zhuang, J. Chen, "New Magneto-Optical Film of Ce, Ga:GIG with High Performance", J. Am. Ceram. Soc., **99** [1] 234-240 (2016).

24. R. J. Young, T. B. Wu, "Preparation of Yttrium Iron Garnet by Reaction Sintering", Mat. Res. Bull., **22** [11] 1475-1482 (1987).

25. P. Grosseau, A. Bachiorrini, B. Guilhot, "Preparation of Polycrystalline Yttrium Iron Garnet Ceramics", Powder Technol., **93** [15] 247-251 (1997).

26. H. Yu, L. Zeng, C. Lu, W. Zhang, G. Xu, “Synthesis of Nanocrystalline Yttrium Iron Garnet by Low Temperature Solid State Reaction”, Mater. Charat., **62** [4] 378-381 (2011).

27. H. Haneda, T. Yanagitani, A. Watanabe, S. Shirasaki, “Preparation of Ytterbium Iron Garnet Powder by Homogeneous Preparation Method and its Sintering”, J. Ceram. Soc. of Jpn., **98** [3] 285-291 (1990).

28. A. E. Paladino, E. A. Magurie, “Microstructure Development in Yttrium Iron Garnet”, J. Am. Ceram. Soc., **53** [2] 98-102 (1970).

29. R.J. Young, T.B. Wu, “Preparation of Yttrium Iron Garnet by Reaction Sintering”, Mat. Res. Bull., **22** [11] 1475-82 (1987).

30. M. Imaeda, S. Matsuzawa, “Growth of Yttrium Iron Garnet Single Crystal by Solid- Solid Reaction”, Proc. 1st Japan Int. SAMPE Symp, 419-424 (1989).

31. H. Yoshida, K. Tsubakimoto, Y. Fujimoto, K. Mikami, H. Fujita, N. Miyanaga, H. Nozawa, H. Yagi, T. Yanagitani, Y. Nagata, H. Kinoshita, “Optical Properties and Faraday Effect of Ceramic Terbium Gallium Garnet for Room Temperature Faraday Rotator”, Opt. Express, **19** [16] 15181-15187 (2011).

32. Y. L. Aung, A. Ikesue, “Development of Optical Grade $(Tb_xY_{1-x})_3Al_5O_{12}$ Ceramics as Faraday Rotator Material”, J. Am. Ceram. Soc., **100** [9] 4081-4087 (2017).

33. A. Ikesue, Y. L. Aung, S. Makikawa, A. Yahagi, “Polycrystalline $(Tb_xY_{1-x})_2O_3$ Faraday Rotator”, Opt. Lett., **42** [21] 4399-4401 (2017).

Chapter 10 Conclusions

In this study, an explorative synthesis of new materials regarding the paramagnetic materials and ferrimagnetic materials was executed by an advanced ceramic synthesis process as well as the evaluation and analysis of their performances. Novel polycrystalline magneto-optical ceramic elements composed of fine grains with random crystal orientations were successfully fabricated, and it was revealed that their magneto-optical performances were equal to or higher than those of conventional single crystal counterpart materials.

In paramagnetic materials that do not contain iron (Fe), terbium (Tb^{3+}) was paid attention in order to improve the magneto-optical performance because it is a magnetically active ion. By controlling the occupancy of Tb^{3+} ion at cation site of the host materials, it was successful to further improve the Faraday rotation characteristics. In addition, the insertion loss, which is an important parameter for the magneto-optical characteristics, was found to be comparable to that of the TGG ($Tb_3Ga_5O_{12}$, the current main material) single crystal on the market. With optimized synthesis conditions, the insertion loss could be reduced to nearly 1/5 that of a single crystal, achieving a very low insertion loss (0.01 dB). As described in Chapter 1, since polycrystalline ceramic is an aggregate of micro crystallites with random crystal orientations, the resulting polarization characteristics (inaccurate polarization due to the difference in Verdet constant for each orientation) have been a major concern. However, their characteristics were found as analogous to those of single crystals and there was no problem at all. It was also proved that the extinction ratio (the ability to shut down the laser beam using a polarizer) completely exceeds that of a single crystal. In actual, extinction ratio (over 38 dB) higher than the characteristic value required for practical application (over 30 dB) has been obtained from all the developed magneto-optical ceramic elements.

In ferrimagnetic materials that contain iron (Fe), fabrication of additive-free YIG ($Y_3Fe_5O_{12}$) polycrystalline ceramics with very high transmittance was successful for the first time in the world. Successively, it was achieved to make the Bi-substituted iron garnet ceramics transparent. Furthermore, it was confirmed that the magneto-optical characteristics of these polycrystalline ceramics are comparable to those of the single crystal counterparts. By further material exploratory research from academic and industrial perspectives, the development of Ce-substituted iron garnet polycrystalline ceramics has become possible, and remarkably its magneto-optical properties were confirmed as far exceeding the performance of the conventional materials that have been industrially applied until now. The detailed results of each magneto-optical ceramic material developed in this study were summarized in the following.

In Chapter 2, development of optical grade $(Tb_xY_{1-x})_3Al_5O_{12}$ ceramics was investigated as Faraday rotator material. Excellent optical characteristics were obtained from the synthesized $(Y_{1-x}Tb_x)_3Al_5O_{12}$ （x=0.5~1.0) ceramics. Specifically, the transmission characteristics of all of the $(Y_{1-x}Tb_x)_3Al_5O_{12}$ ceramics at a wavelength of 1064 nm reached the theoretical limit, and the optical loss was estimated to be less than 0.1 % cm^{-1}. In

particular, the optical loss of TAG (x = 1.0, $Tb_3Al_5O_{12}$) ceramics was about 1/100 of the single crystal of the same composition produced by the floating zone (FZ) method in the past. It is also clarified that the Verdet constant of TAG ceramics at the measurement wavelength of 1064 nm is 60 rad T^{-1} m^{-1}, which is about 1.5 times larger than that of the TGG single crystal (39 rad T^{-1} m^{-1}). Furthermore, as for the isolation characteristics, the extinction ratio was as large as 39 to 42 dB, and the insertion loss was as small as 0.01 to 0.06 dB, which exceeded the characteristics of the commercially available TGG single crystal. Since this material can be produced by the ceramic synthesis method, it can be produced in large size. Based on the above research results, the technical problems of conventional TAG single crystals were completely defeated.

In Chapter 3, improved optical properties of developed $Tb_2Hf_2O_7$ (THO) pyrochlore ceramics were examined. Super-high density and optical grade THO ceramics could be synthesized by reactive sintering of Tb_4O_7 and HfO_2 followed by HIP treatment. There are no residual pores in the obtained ceramic material. It is an optically isotropic body observed under a transmitted polarized light. Very low optical scattering characteristic (< 0.1 % cm^{-1}) was confirmed. After the HIP treatment, annealing at 1700 °C in hydrogen atmosphere allowed further improving the optical homogeneity. As a result, it was demonstrated that the input high-quality laser beam can maintain high quality with almost no deterioration even after passing through the THO medium. Specifically, the Verdet constant, insertion loss, and extinction ratio of the newly developed material were 50 rad T^{-1} m^{-1}, 0.03 dB and 38 dB at 1064 nm, respectively. These characteristic values were exceeding those of commercially available TGG single crystals.

In Chapter 4, total performance of terbium oxide ceramics with a bixbyite structure was extensively studied. When terbium oxide (Tb_4O_7) powder was used as the starting material, oxygen gas was released during sintering by the reaction of $Tb_4O_7 \rightarrow 2Tb_2O_3 + 1/2\ O_2$, and the sample was ended with cracking. Also, even when Tb_2O_3 (obtained by hydrogen reduction of Tb_4O_7) powder was used as a starting material, the crystal structure and volume changed with temperature fluctuations because a phase transition point exists near 1400 °C. Therefore, there were problems such as generation of mechanical stress in the sintered body and induction of crack formation. Nevertheless, when a small amount of nano-sized ZrO_2 was added as a sintering aid, all of these problems could be solved. The composition analysis of the inside grain and the grain boundary of this sintered ceramics was performed by high-resolution microstructure observation and TEM-EDS (Electron Dispersive Spectroscopy) analysis. Segregation of ZrO_2 added as a sintering aid was not detected. In conclusion, the properties obtained by the development of $(Tb_xY_{1-x})_2O_3$ (x=0.5~1.0), TYO materials overturned the conventional understanding in materials science. The synthesis of optical grade TYO ceramics was successful for the first time. Its basic characteristics greatly exceeded those of commercially available TGG ($Tb_3Ga_5O_{12}$) single crystals. The Faraday rotation angle increased with increasing Tb concentration. Until now, it has been considered that only single crystals or glass can be used for Faraday elements. (Polycrystalline ceramics have been considered unsuitable because they are composed of fine grains with random crystal orientations and different Verdet

constants of each grain). However, it was shown that even with the polycrystalline ceramics that were successfully developed in this study, an insertion loss (0.04 dB) equivalent to that of a commercially available high-quality TGG single crystal can be obtained, and especially, the maximum extinction ratio was 47 dB, which far exceeded the TGG value (35 dB). Since the Verdet constant of TYO ceramics at 1064 nm can be increased approximately 2.1 (x=0.5, 82 rad T^{-1} m^{-1}) to 3.8 (x=1.0, 154 rad T^{-1} m^{-1}) times compared to the TGG single crystal (39 rad T^{-1} m^{-1}), the medium length or magnet can be minimized. This fact is an extremely useful merit for practical use in optical isolator.

In Chapter 5, development of high performance magneto-optical Dy_2O_3 ceramics was performed. Optical grade Dy_2O_3 ceramics could be synthesized by HIP sintering using a small amount of ZrO_2 as a sintering aid in Dy_2O_3 powder. No residual pores were detected inside the material, and there was no grain boundary phase or secondary phase. Since birefringence does not exist in polarized light observation, the produced Dy_2O_3 ceramics are optically isotropic. It was shown that there was almost no beam distortion during laser irradiation test, and the optical loss was extremely small (< 0.1 % cm^{-1}). Moreover, very high Verdet constant of 422 rad T^{-1} m^{-1} at a wavelength of 633 nm was confirmed, and the extinction ratio also reached 34 dB.

In Chapter 6, development of transparent polycrystalline YIG ceramics was discussed for application as Faraday rotator materials for infra-red wavelength regions. It was shown that super-dense and transparent YIG ($Y_3Fe_5O_{12}$) ceramics can be synthesized by solid-state reactive sintering of Y_2O_3 and Fe_2O_3. The relative density reached almost 100 % (5.17 g cm^{-3}) by HIP treatment after densification by sintering at 1400 °C. The obtained material became transparent at wavelengths above 1100 nm and it showed in-line transmittance (~ 77 %) comparable to that of commercially available YIG single crystals at wavelengths above 2000 nm. Although the magnetic domain pattern of the ceramic material was different from that of the commercially available YIG single crystal, the Faraday rotation angle at 1.5 μm was 220 deg cm^{-1}. The wavelength dependence of the Verdet constant at 1100-2500 nm was similar to that of the YIG single crystal. The extinction ratio of the obtained YIG ceramics was 35 dB, and the insertion loss at 45 ^{o} polarization was 0.3 dB. From the above results, it was proved that the Faraday characteristics of a polycrystalline ceramic, which has a large number of grain boundaries in an aggregate of random crystal orientations, were analogous to a single crystal. This research work is the first for the successful production of a polycrystalline iron garnet transparent material, and it is expected that it will be applied to optical isolators in the field of optical communication in the future.

In Chapter 7, fabrication of $Tb_3Fe_5O_{12}$ ceramics was investigated. Transparent TIG ($Tb_3Fe_5O_{12}$) ceramics could be synthesized for the first time by solid-state reactive sintering of Tb_4O_7 and Fe_2O_3 powders. It is a promising isolator for mid-IR (1.3~1.5 μm) wavelength. Although there were no grain boundary phase nor impurity phase observed in the material, a small number of residual pores was observed in the depth direction. This material is transparent in the infrared region of 1.1 to 2.0 μm, and the Faraday rotation angle at 1300 nm was 350 deg cm^{-1}, which was nearly 1.5 times larger than that of the YIG ($Y_3Fe_5O_{12}$) single crystal. The magnetic

domain structure of the polycrystalline material was different from that of the single crystal material, but a uniform refractive index distribution was confirmed in the infrared schlieren image. In the future, if the residual pores can be eliminated, it is highly expected that the optical properties of this material can be significantly improved.

In Chapter 8, development of Bi substituted YIG ceramics was examined for isolator to be applied in optical communication. It was the first to synthesize transparent $(Bi_xY_{3-x})Fe_5O_{12}$ [x=0~1.1] ceramics by the reactive sintering method. The transmission characteristics of Bi-substituted YIG ceramics was comparable to those of the Bi:$Gd_3Fe_5O_{12}$ single crystal prepared by the LPE method. When observed using a scanning electron microscope (SEM), the obtained Bi:YIG ceramics had a uniform polycrystalline microstructure composed of fine grains of approximately 5 μm. Residual pores, heterogeneous phase, or grain boundary phase were not detected. In addition, elemental mapping analysis of Bi, Y, Fe, and O by EDS analysis and backscattered electron image (BEI) analysis were performed. It was confirmed that the distribution of composition is uniform in this material. Moreover, segregation of Bi was not detected in the local structural analysis by high-resolution transmission electron microscope (HR-TEM). The Faraday rotation angle increased linearly with respect to the amount of Bi substitution. The Faraday rotation angle at 1550 nm per 1 at.% Bi was -26.3 deg cm^{-1}, which was similar to the LPE-grown $(Bi_{1.2}\ Gd_{1.8})\ Fe_5O_{12}$ single crystal. Accordingly, this study enabled the synthesis of Bi-substituted iron garnets in additional to the LPE method, which requires a seed substrate ($Gd_3Ga_5O_{12}$) and a steep temperature gradient during crystal growth. Also, it was demonstrated that the magneto-optical performance equivalent to that of a single crystal can be obtained even with a polycrystalline ceramic form.

In Chapter 9, development of heavily Ce-doped YIG bulk ceramics aimed for giant Faraday rotation was described. Homogeneous and transparent Ce:YIG ceramics was achieved for the first time in the world by reactive sintering and post HIP process using Y_2O_3, Fe_2O_3 and CeO_2 as starting materials. The absorption coefficient of Ce:YIG ceramics obtained by the sintering method was as low as 0.3 cm^{-1}. The Faraday rotation performance at 1550 nm was extremely high at -144 deg cm^{-1} per 1 at.% Ce. This corresponded to 5 times of the rotation angle per 1 at.% Bi of the Bi:GIG single crystal produced by the LPE method reported previously. Based on the results of this study, the polycrystalline Ce:YIG ceramics that can be produced by the sintering method exceeded the performance of Bi-substituted iron garnet, which is the main commercial material of existing optical isolators for optical communication. In addition, the sintering method does not require an expensive GGG single crystal substrate, and is expected to have an excellent productivity, and is also expected to become a promising Faraday rotator material for optical communication in the future 5G network. Through the above development and promotion to practical applications, it can be said that the magneto-optical material is now approaching the time of generational change from “single crystal” to “polycrystalline ceramics”.

In particular, the magneto-optical characteristics of TO and TYO ceramics with the bixbyite structure described in Chapter 4 are very excellent, and their Verdet constant is about 2 to 4 times larger than that of the

commercially available TGG single crystals. Thus, the length required to rotate the laser beam to 45 degrees can be shortened to about 1/4 (approx. 5 mm) at the minimum, compared to L=20 mm for the TGG. Utilizing this feature, a prototype of a very compact isolator device equipped with these ceramics was fabricated. Currently, it has been commercialized for high-power lasers. This achievement was featured in CTT (Ceramic Tech Today) News (July 14, 2020) by the American Ceramic Society as "Isolating a better option — ceramic Faraday rotators improve optical isolator performance". (https://ceramics.org/ceramic-tech-today/optics/ceramic-faraday-rotators-improve-optical-isolator-performance)

(a)

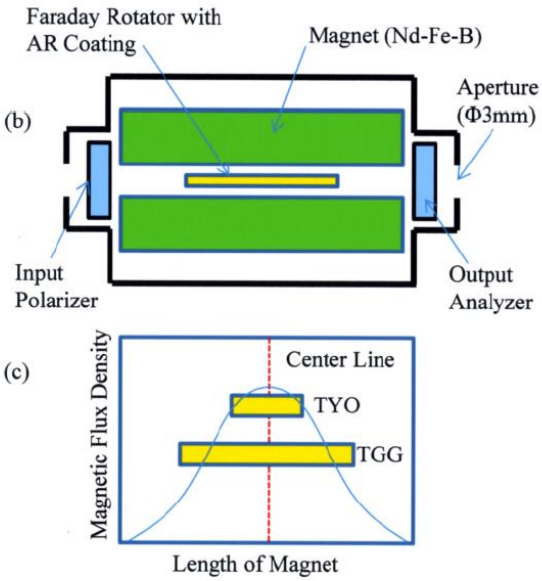

(d)

	(1) Conventional	(2) This Work I	This Work II
Material	TGG Single Crystal	TYO (Tb-60%) Ceramics	Tb_2O_3 Ceramics
Length of Media for 45 deg. Rotation	20.0 mm	8.0 mm	5.1 mm
Normalized Ratio of Magnet Volume	100%	49%	<35%

Figure 10.1 Prototype of optical isolator using TYO (Tb-60%) ceramic in comparison with commercial TGG optical isolator. (b) Schematic diagram of the optical isolator. (c) Magnetic flux distribution inside the magnet house of optical isolator and the position of Faraday rotator sample influenced by the magnetic field. (d) Comparison of features of each Faraday rotator material.

Demonstration of ceramic isolators with large aperture size suitable for high power laser were also demonstrated in this work. Good reproducibility and productivity were achieved in this work, which are better than the case of single crystal, with advanced ceramic fabrication technology. For example, in the case of sample with Φ6 x 10 mm^2 dimension, it is possible to produce more than several thousands of pieces per batch. Samples

with 5 mm diameter described above are normally usable for laser power up to 100 W class. For kW class high-power laser operations, Faraday rotator element with large aperture (Φ10 ~ 15 mm) are required. For application in nuclear fusion and high energy physics in the future, samples with larger aperture (Φ20~50 mm) will become indispensable. With the invention from this work, it was successful to produce large size samples with good transparency as presented in Figure 10.2. The work on the development of large-scaled samples with improved optical quality is in progress, and it is still necessary to achieve good laser damage performance of large samples higher than the TGG reference material. It was also confirmed that the laser damage property of the TYO ceramics significantly exceeded the value of TGG. Production technique of ceramic is different from that of single crystal. In the case of single crystal, at first a relatively large size crystal is produced and then it is cut and machined down to obtain required smaller size elements. In the case of ceramics, they can be produced in near net shaping to the required size and in large quantity. Therefore, ceramic production technique is more favorable than that of the conventional single crystal production.

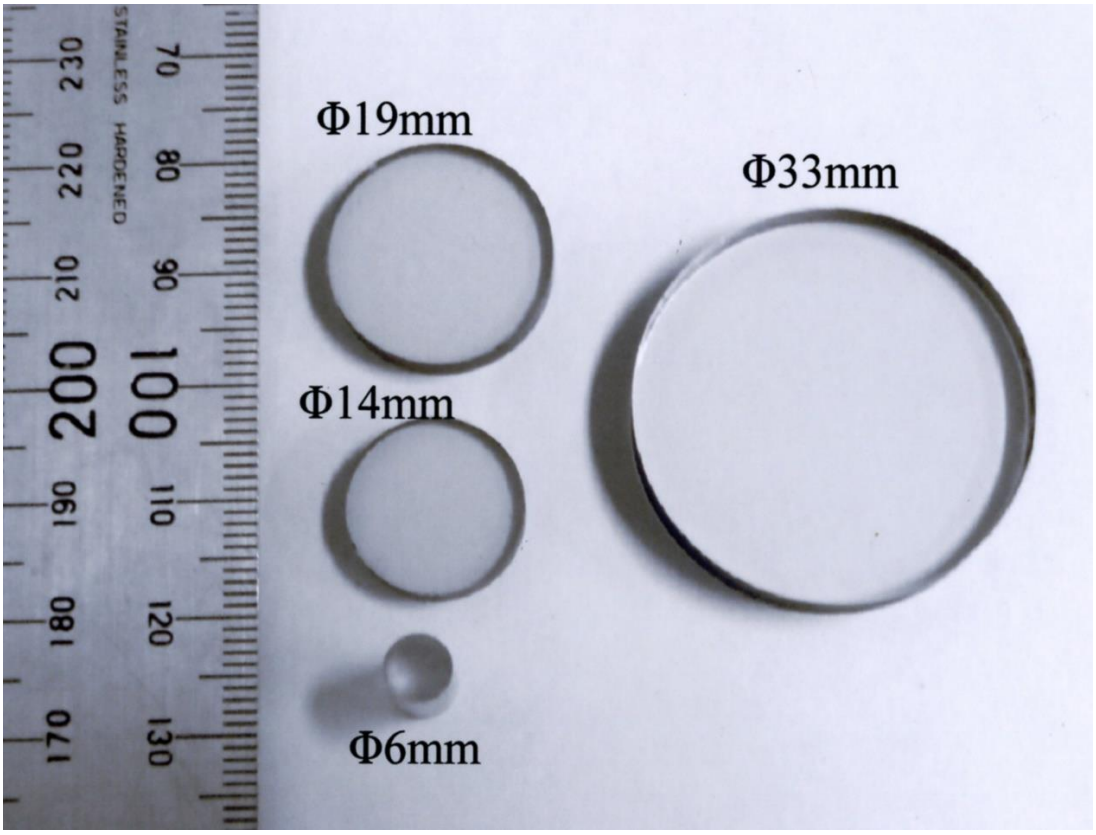

Figure 10.2 Appearance of large scaled TYO ceramic samples demonstrated with various aperture sizes.

Acknowledgments

First of all, the author would like to express sincere gratitude to supervisor, Professor Dr. Yuji Iwamoto of Nagoya Institute of Technology, for providing helpful advice and warm encouragement in preparing the manuscript and presentation of the doctoral thesis. The author is also thankful to Professor Dr. Tomokatsu Hayakawa, Professor Dr. Shinobu Hashimoto, and Professor Dr. Hiromi Nakano for sharing their valuable times as deputy examiners to this doctoral thesis.

Especially Dr. Akio Ikesue, the founder of World Lab Co., Ltd. and also the pioneer of the "laser ceramics" has given the author a place to be involved in the development of various types of transparent ceramics since after leaving the Kyushu Institute of Technology, and the author is very indebted to him for a fruitful research and carrier life also for the completion of this doctoral thesis.

The author is thankful to associate professor Dr. Ryo Yasuhara of National Institute of Fusion Science, and Mr. Shinji Makikawa, Mr. Akira Yahagi and Mr. Toshiaki Watanabe of Shin-etsu Chemical Industry Ltd., (*Precise functional material laboratory, Advanced Functional Materials Research Center*) cooperated for the measurements on the performances of magneto-optical ceramics developed in this work.

Last but not least, the author would like to thank benefactors, friends, family (wife: Yamin Zarchi Soe, and daughter: Yun Shweyi Aung), and specially to late parents, for their long-term supports behind the scenes for the completion of the doctoral thesis.

January 2021

YAN LIN AUNG

List of publications

I. List of publications related to this research

Chapter 2
Y. L. Aung, A. Ikesue, Development of Optical Grade $(Tb_xY_{1-x})_3Al_5O_{12}$ Ceramics as Faraday Rotator Material, *J. Am. Ceram. Soc*., **100**, No.9, 4081-4087 (2017)
doi.org/10.1111/jace.14961.

Chapter 3
Y. L. Aung, A. Ikesue, R. Yasuhara, Y. Iwamoto, Optical Properties of Improved $Tb_2Hf_2O_7$ Pyrochlore Ceramics, *J. Alloy and Compounds*, **822**, 153564 (2020)
doi.org/10.1016/j.jallcom.2019.153564.

Chapter 4
A. Ikesue, **Y. L. Aung**, S. Makikawa, A. Yahagi, Polycrystalline $(Tb_xY_{1-x})_2O_3$ Faraday Rotator, *Opt. Lett*., **42**, No.21, 4399-4401 (2017)
doi.org/10.1364/OL.42.004399.

Chapter 4
A. Ikesue, **Y. L. Aung**, S. Makikawa, A. Yahagi, Total Performance of Magneto-Optical Ceramics with a Bixbyite Structure, *Materials*, **12,** No.3, 421 (2019)
doi.org/103390/ma12030421.

Chapter 5
Y. L. Aung, A. Ikesue, R. Yasuhara, Y. Iwamoto, Magneto-Optical Dy_2O_3 Ceramics with Optical Grade, *Opt. Lett*., **45**, No.16, 4615-4617 (2020)
doi.org/10.1364/OL.396397.

Chapter 6
A. Ikesue, **Y. L. Aung**, Development of Optical Grade Polycrystalline YIG Ceramics for Faraday Rotator, *J. Am. Ceram. Soc*., **101**, No.11, 5120-5126 (2018)
doi.org/10.1111/jace.15772.

Chapter 7
Y. L. Aung, A. Ikesue, Transparent $Tb_3Fe_5O_{12}$ Ceramics as Mid-IR isolator, *J. Alloys and Compounds*, **773**, 739-742 (2018)
doi.org/10.1016/j.jallcom.2018.09.299.

Chapter 8
Y. L. Aung, A. Ikesue, T. Watanabe, S. Makikawa, Y. Iwamoto, Bi substituted YIG Ceramics Isolator for Optical Communication, *J. Alloy and Compounds*, **811**, 152059 (2019)
doi.org/10.1016/j.jallcom.2019.152059.

Chapter 9
A. Ikesue, **Y. L. Aung**, R. Yasuhara, Y. Iwamoto, Giant Faraday Rotation in Heavily Ce-doped YIG Bulk Ceramics, *J. Euro. Ceram. Soc*., **40**, No.15, 6073-6078 (2020)
doi.org/10.1016/j.jeurceramsoc.2020.05.062.

II. General list of publications

1. ○**Y. L. Aung**, A. Ikesue, R. Yasuhara, Y. Iwamoto, "Magneto-Optical Dy_2O_3 Ceramics with Optical Grade", Opt. Lett., **45**, No.16, 4615-4617 (2020).
   doi.org/10.1364/OL.396397
2. A. Ikesue, ○**Y. L. Aung**, R. Yasuhara, Y. Iwamoto, "Giant Faraday Rotation in Heavily Ce-doped YIG Bulk Ceramics", J. Euro. Ceram. Soc., **40**, No.15, 6073-6078 (2020).
   doi.org/10.1016/j.jeurceramsoc.2020.05.062
3. A. Ikesue, **Y. L. Aung**, "Advanced Spinel Ceramics with Highest VUV-vis Transparency", J. Euro. Ceram. Soc., **40**, No.6, 2432-2438 (2020).
   doi.org/10.1016/j.jeurceramsoc.2020.01.062
4. A. Ikesue, **Y. L. Aung**, "High Quality Sapphire Crystal by Advanced Chemical Transport Process", J. Euro. Ceram. Soc., **40**, No.13, 4536-4538 (2020).
   doi.org/10.1016/j.jeurceramsoc.2020.05.069
5. ○**Y. L. Aung**, A. Ikesue, T. Watanabe, S. Makikawa, Y. Iwamoto, "Bi substituted YIG Ceramics Isolator for Optical Communication", J. Alloy and Compounds, **811**, 152059 (2019).
   doi.org/10.1016/j.jallcom.2019.152059
6. ○**Y. L. Aung**, A. Ikesue, R. Yasuhara, Y. Iwamoto, "Optical Properties of Improved $Tb_2Hf_2O_7$ Pyrochlore Ceramics", J. Alloy and Compounds, **822**, 153564 (2020).
   doi.org/10.1016/j.jallcom.2019.153564
7. A. Ikesue, ○**Y. L. Aung**, S. Makikawa, A. Yahagi, "Total Performance of Magneto-Optical Ceramics with a Bixbyite Structure", Materials, **12(3)**, 421 (2019).
   doi.org/103390/ma12030421
8. A. Ikesue, ○**Y. L. Aung**, "Development of Optical Grade Polycrystalline YIG Ceramics for Faraday Rotator", J. Am. Ceram. Soc., **101**, No.11, 5120-5126 (2018).
   doi.org/10.1111/jace.15772
9. ○**Y. L. Aung**, A. Ikesue, "Transparent $Tb_3Fe_5O_{12}$ ceramics as Mid-IR isolator", J. Alloys and Compounds, **773**, 739-742 (2018).
   doi.org/10.1016/j.jallcom.2018.09.299
10. A. Ikesue, **Y. L. Aung**, "Origin and Future of Polycrystalline Ceramic Laser", IEEE, J. Selected Topics in Quantum Electronics, **24**, No.5, Sept./ Oct. (2018).
    doi.org/10.1109/JSTQE.2018.2811901
11. A. Ikesue, **Y. L. Aung**, T. Kamimura, S. Honda, Y. Iwamoto, "Composite Laser Ceramics by Advanced Bonding Technology", Materials. **11(2)**, 271 (2018).
    doi.org/10.3390/ma11020271
12. A. Ikesue, ○**Y. L. Aung**, S. Makikawa, A. Yahagi, "Polycrystalline $(Tb_xY_{1-x})_2O_3$ Faraday Rotator", Opt. Lett., **42**, No.21, 4399-4401 (2017).
    doi.org/10.1364/OL.42.004399.
13. ○**Y. L. Aung**, A. Ikesue, "Development of Optical Grade $(Tb_xY_{1-x})_3Al_5O_{12}$ Ceramics as Faraday Rotator Material", J. Am. Ceram. Soc., **100**, No.9, 4081-4087 (2017).
    doi.org/10.1111/jace.14961.

14. S. Sattayaporn, G. Aka, P. Loiseau, A. Ikesue, **Y. L. Aung**, "Optical spectroscopic properties, 0.946 and 1.074 μm laser performances of Nd^{3+} - doped Y_2O_3 transparent ceramics", J. Alloys and Compounds, **711**, 15, 446-454 (2017).
doi.org/10.1016/j.jallcom.2017.03.343
15. A. Ikesue, **Y. L. Aung**, "Synthesis of Yb:YAG Ceramics without Sintering Additives and their Performance", J. Am. Ceram. Soc., **100**, No.1, 26-30, (2016).
doi.org/10.1111/jace.14588
16. S. Nakayama, T. Watanabe, T. Asahi, H. Kiyono, **Y. L. Aung**, M. Sakamoto, "Influence of rare earth additives and boron component on electrical conductivity of sodium rare earth borate glasses", Ceramics International, **36**, No.8, 2323-2327, (2010).
doi.org/10.1016/j.ceramint.2010.07.026
17. E. Pawlowski, M. Kluge, Y. Menke-Berg, U. Peuchert, A. Engel, **Y. L. Aung**, A. Ikesue, K. Beil, R. Peters, H. Kuehn, K. Petermann, P. Heist. "Yb:YAG composite ceramic laser". Proc. SPIE **7578**, Solid State Lasers XIX: Technology and Devices, 757815, (2010).
doi.org/10.1117/12.842071
18. S. Nakayama, K. Onishi, T. Asahi, **Y. L. Aung**, S. Kuwata, "Response characteristics of all-solid-state pH sensor using $Li_5YSi_4O_{12}$ glass", Ceramics International, **35**, No.8, 3057-3060, (2009).
doi.org/10.1016/j.ceramint.2009.04.020
19. A. Ikesue, **Y. L. Aung**, "Ceramic Laser Materials", Nature Photonics, **2**, 721-727 (2008).
doi.org/10.1038/nphoton.2008.243
20. **Y. L. Aung**, K. Itani, T. Asahi, H. Kiyono, M. Sakamoto and S. Nakayama, "Electrical Properties of $(Na_2O)_{35.7}(RE_2O_3)_{7.2}(GeO_2)_{57.1}$ (RE= Sm, Gd, Dy, Y, Ho, Er and Yb) Glasses", Materials Chemistry and Physics, **109**, No.1, 30-33 (2008).
doi.org/10.1016/j.matchemphys.2007.10.026
21. M.O. Ramirez, J. Wisdom, H. Li., **Y.L. Aung**, J. Stitt, G. L. Messing, V. Dierolf, Z. Liu, A. Ikesue, R. L. Byer, V. Goplan, "Three-Dimensional Grain Boundary Spectroscopy in Transparent High Power Ceramic Laser Materials", Opt. Express, **16**, No.9, 5965-5973 (2008).
doi.org/10.1364/OE.16.005965
22. A. Ikesue, **Y. L. Aung**, T. Yoda, S. Nakayama, T. Kamimura, "Fabrication and Laser Performance of Polycrystal and Single Crystal Nd:YAG by Advanced Ceramic Processing", Optical Materials, **29**, No.10, 1289-1294 (2007).
doi.org/10.1016/j.optmat.2005.12.013
23. S. Nakayama, T. Asahi, H. Kiyono, **Y. L. Aung** and M. Sakamoto, "Electrical properties of $(Na_2O)_{35.7}(RE_2O_3)_{7.2}(SiO_2)_{57.1}$ (RE=Y, Sm, Gd, Dy, Ho,Er and Yb) glasses and ceramics", J. Euro. Ceram. Soc., **26**, No.9, 1605-1610 (2006).
doi.org/10.1016/j.jeurceramsoc.2005.03.245
24. A. Ikesue, **Y. L. Aung**, "Synthesis and Performance of Advanced Ceramic Lasers", J. Am. Ceram. Soc., **89**, No.6, 1936-1944 (2006).
doi.org/10.1111/j.1551-2916.2006.01043.x
25. A. Ikesue, **Y. L. Aung**, T. Taira, T. Kamimura, K. Yoshida, G. L. Messing. "Progress in Ceramic Lasers", Annual Rev. Mat. Res., **36**, 397-429 (2006).

doi.org/10.1146/annurev.matsci.36.011205.152926

26. M. Yoshida, N. B. Ibrahim, **Y. L. Aung**, S. Takase, Y. Shimizu, "A Hydrogen-Phosphate Ion Sensor Using Solid Electrolyte Impedance Transducer and Perovskite-Type Oxide Receptor", Electrochemistry, **74**, No.2, 163-165, (2006).
doi.org/10.5796/electrochemistry.74.163
27. I. B. Mukhin, O. V. Palashov, E. A. Khazanov, A. Ikesue, and **Y. L. Aung**. "Experimental study of thermally induced depolarization in Nd:YAG ceramics", Optics Express, **13**, No.16, 5983-5987, (2005).
doi.org/10.1364/OPEX.13.005983
28. **Y. L. Aung**, S. Nakayama and M. Sakamoto, "Electrical properties of $MREGeO_4$ (M=Li, Na, K; RE=rare earth) ceramics", Journal of Materials Science, **40**, 129-133 (2005).
doi.org/10.1007/s10853-005-5697-y
29. S. Nakayama, T. Asahi, **Y. L. Aung**, R. Ohhara and M. Sakamoto, "Electrical Properties of $(K_2O)_{35.7}(RE_2O_3)_{7.2}(SiO_2)_{57.1}$ (RE=Sm, Gd, Dy, Y, Ho, Er, Yb) Glasses", J. Ceram. Soc. Jap., **112**, No.1304, 238-241 (2004).
doi.org/10.2109/jcersj.112.238
30. S. Nakayama, M. Okazaki, **Y. L. Aung** and M. Sakamoto, "Preparations of perovskite-type oxides $LaCoO_3$ from three different methods and their evaluation by homogeneity, sinterability and conductivity", Solid State Ionics, **158**, No.1-2, 133-139 (2003).
doi.org/10.1016/S0167-2738(02)00767-1
31. T. Asahi, **Y. L. Aung**, M. Saito, S. Imai, M. Sakamoto and S. Nakayama, "Preparation of $(Li_2O)_{35.7}(RE_2O_3)_{7.2}(SiO_2)_{57.1}$ (RE=Sm, Gd, Dy, Y, Ho, Er and Yb) Glasses and Their Electrical Properties", J. Ceram. Soc. Jap., **110**, No.1279, 200-203 (2002).
doi.org/10.2109/jcersj.110.200

Books

1. A. Ikesue, **Y. L. Aung**, V. Lupei, "Ceramic Lasers". Cambridge University Press, 2010: pp.1-445. ISBN: 9780511978043.

2. A. Ikesue, **Y. L. Aung**, T. Mikami, J. Li, J. Xu, "tentative title: Latest Ceramic Optics". Wiley-American Ceramic Society, New York, 2021: 432 pages. (Now under review process and scheduled to be published in April 2021). ISBN-13 : 978-1119538707